Topology-Dependent Complexation of Cyclic Poly (Ethylene Glycol) with Nanoparticles and Proteins

A Dissertation for the Degree of Doctor of Philosophy

Onyinyechukwu Justina Oziri Nee Chioke

Hokkaido University

March 24, 2022

ACKNOWLEDGEMENTS

Special thanks to almighty God for seeing me through this journey. I am forever grateful.

To my Supervisor, Associate Professor Takuya Yamamoto, thank you for your kindness, supervision with love, listening ears, and gently allowing me grow. This thesis wouldn't have been possible without you. I cannot thank you enough. A shout out to Associate Professor Kenji Tajima for allowing use his laboratory, reagents, instruments, and always offering a helping hand anytime, any day. I cannot thank you enough for your kindness.

I want to also thank Professor Manabu Tokeshi, and Associate Professor Masatoshi Maeki for allowing me use their instruments, laboratory, and collaborations. Thank you, Professor Toshifumi Satoh, and Associate Professor Shin-ichiro Sato for your inputs and corrections. Thank you, Associate Professor Takuya Isono, for the few times we talked.

Many thanks to all the wonderful people I met along the line: Shuya Uno, Yubo Wang, Yuto Miyata, Minato Nakamura, Atsuo Utagawa, Shotaro Yoshitomi, Tomohisa Watanabe, Ryohei Sato, Kodai Watanabe, Bono Aoshima, Hiroko Ninoyu, Akira Takatsuka, Yuna Kinoshita, Masato Yamasaki, Yuto Okuma, and Tomoko Ono. Thank you, Kudo Rika for the many toy gifts you gave my daughter Desire, it made her busy while I write my papers.

To my parents, Late Supol, Mr. and Mrs., Aniedo Chioke, may your souls rest on. I know you must be proud wherever you are. You gave me your wings and foundation which I am utmost grateful. To my lovely husband, Mr. Chidiebere Oliver Oziri, and daughter Desire, I lack what to say. Best gift ever. God bless you plenty for me. I love you all.

Onyinyechukwu Justina Oziri

CONTENTS

Chapter 1

General Introduction

1.1 POLYMER TOPOLOGY

Polymer scientist has reported that various polymer properties depend to a large extent on the primary structure[1] among others. Topology could be defined as the shape and connectedness of the polymer backbone taking into considerations as polymer segments. Polymer topologies include linear, mono cyclic, star shaped, randomly branched, graft, dendritic, helical, multicyclic, comb, branched, 8-shaped, tadpole etc. [2] Branched polymer topologies include 'star' polymers, 'H-shaped' polymers, 'super H-shaped' polymers, 'pom–pom shaped' polymers. In the new era, attention have been drawn to polymer properties such as melting, diffusion, rheology, crystallization, and phase separation because of distinct topological differences[3]. Of the various polymer topologies, cyclic polymers without polymer termini and steric constraints introduced by their cyclization strongly influence polymer dynamics and diffusion within solutions and melts, shown potential in various applications resulting from their physical and chemical properties in bulk and solution states[4], such as increased glass transition temperature[5], higher refractive index[6], less entanglement[7], slow hydrolytic degradation[8], , smaller hydrodynamic volume[9, 10] and radius of gyration [11], lower intrinsic viscosity[12] , high critical solution temperature, accelerated rate of crystallization, high refractive indices and self-assembling behaviors [13]etc. which are

different from their linear counterparts with the same molecular weight[14]. On the other hand, in the fabrication of self-assembled core–shell micelles by cyclic block copolymers, structural properties of the assemblies were altered by the topology of the cyclic constituents when compared to similar micelles prepared from linear analogs[15]. In nature, the cyclic biopolymers such as DNAs, peptides, and polysaccharides, have attracted attention due to their topology-based functions, and have been invaluable for designing functions and properties in synthetic polymer materials[16]. Decades ago, in the case of extremophile archaea, it was found that common linear fatty esters used within cell walls are most often replaced with more exotic isoprenoid ethers, for stability at extreme temperature and pH[17]. In addition to swapping linear esters for linear ethers, many archaea incorporate into their cell walls cyclic ethers that span either the length of the lipid monolayer or in some cases the entire bilayer. In biomedical applications, cyclic polymers have gained attention and usage because of their distinct superior properties as well[7]. The work of Giulia reported reduced friction between surfaces by cyclic poly(-2-ethyl-2-oxazoline) by not interaction of the cyclic moieties when compared to its linear counterpart of the same composition at an applied force.[18] Guiying *et al*., 2020 reported dumbbell-shaped amphiphilic copolymers with cyclic moieties as enhanced performance for controlled drug release[19]. Maria *et al*., 2018 reported

a topology-controlled particle disassembly for the controlled release of an anti-cancer drug *in vitro*[20]. Cyclic poly(2-methyl-2-oxazoline) (PMOXA) films have also been applied on cartilage, to recover the lubrication properties of tissue after degradation, and protection from osteoarthritis (OA)-correlated enzymatic digestion.[21] Topology of poly(ethylenimine)s (PEIs) has been reported to influence polymer-DNA complex formation and subsequent transfection to fibroblast and endothelial cells.[22] Cyclic PEI was reported to complex DNA effectively than its linear counterpart because of it higher charge density. Significant higher transfection efficiency and reduced toxicity was reported compared to linear PEI. Reports of cyclic polycations as effective synthetic vector for delivery abound in recent literature. [23] investigated the effect of polycation topology on the delivery of DNA and reported highly efficient gene delivery and lower toxicity with respect to linear polycations. In drug delivery systems, the application of cyclic polymers has been recently explored with an effect on pharmacokinetics and biodistribution seen with the works of Nasongkla et al[24]. Longer time of circulation and higher accumulation within organs have been reported for cyclic macromolecules when comparing the in vivo applications. This is a result of more hindered reptation through nanopores in kidney. An interesting effect of polymer topology has been reported in hydrolysis. In hydrolysis of PCL, initial degradation of cyclic polyesters

encompasses the formation of linear chains with the same mass, leading to a lag in the reduction of molecular weight with respect to that observed for linear PCL counterparts[23]. Of recent time cyclized PEG (c-PEG) without any chemical inhomogeneity was found to endow gold nanoparticles (AuNPs) with high dispersion stability by physisorption[25].

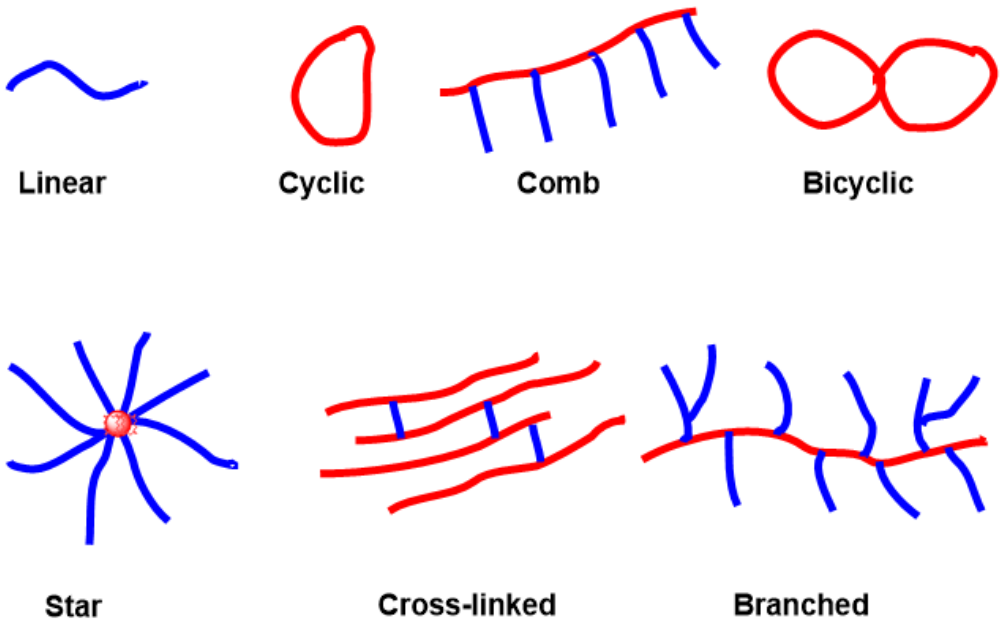

Fig 1.1. Examples of polymer topology

On the other hand, acceptability of polyethylene glycol (PEG) by United States Food and Drug Association as a biocompatible, non-ionic polymer with a flexible structure, ability to attach a variety of reactive functional groups to the terminal sites has basically increased its various applications in medical, food, drug delivery, agriculture, manufacturing industries. PEGylation, defined as covalent grafting of a PEG derivative onto molecules, improves the water solubility, stability and biocompatibility and has made poly(ethylene glycol) (PEG) an indispensable polymer in biomedical science[26], liposome[27], hydrogel in cell and tissue culture[28], nanoparticle functionalization[29, 30], dendrimers, micelles, drug delivery[31]. AgNPs and AuNPs has been reported functionalized of their surface by PEG namely PEGylation to improve their biocompatibility, stability, *in vivo* interactions among other. Mei et al. reported a multistage liposome drug delivery system co-modified with RGD, TAT, a specific ligand and a penetrating peptide, containing a cleavable PEG that increased the stability and circulation time of the liposomes.[32] Bioactivity of PEGylated molecules are influenced by length of the PEG chain, the PEGylation site, the linker chemistry, and the temperature for the PEGylation reaction among others. Example, PEGylation of proteins is greatly influenced by the solvent used during the conjugation to the PEG.[33] Reports by Peng et al. stated that organic solvents such as DMSO increase the degree of PEGylation, minimize the PEG

hydrolysis, and decrease the PEGylation time for hydrophobic proteins such as G-CSF, when compared to PEGylation in water phase.[34] PEGylation on AuNPs by thiol coordination stabilize the AuNPs but forms a AgCl surface on AgNPs., and further formation of AgCl salts under certain conditions.[35] A steady method of PEGylation is needed for AgNPs.

1.2 Nanoscience and nanotechnology

Nanoscience and nanotechnologies are currently researched on because of the huge potential and benefit it brings to various areas of research and application. Nanotechnology which is the design and application of components at nanoscale encompasses the study of structural properties of nanostructures at the molecular and sub-molecular level along with their electrical, biological, optical and magnetic properties[36]. The discovery of ruby gold nanoparticles (AuNPs) by Michael Faraday in 1857 began the modern nanotechnology which has been since the Mesopotamian era[37]. Nanoscience and many nanotechnologies are concerned with producing new or enhanced materials by 'top down' techniques, producing very small structures from larger pieces of material, 'bottom up' techniques, atom by atom or molecule by molecule and other methods. The general definition of ‘nanotechnology’ now reads: science, engineering, and technology conducted at nanoscale, which is about 1–

100 nm. Nanoscience is applied almost in everyday life and recently, applications of nanotechnology have expanded into various fields with emerging importance that cannot be overemphasized. Nanoscience applications ranges in medical imaging[38], drug delivery[39], cell electrode[40], biosensors[41], cancer diagnosis[42, 43], oil and gas sectors[44-46], catalysis[47, 48], cosmetic and treatment.[49, 50] Nanostructure such as carbon nanotubes, nanoparticles, quantum dots, nano diamond, liposomes, and paramagnetic nanostructures among others are currently been utilized in various applications. Examples: carbon nanotubes have been used in water treatment, biomedicine, energy, capacitors etc., nano diamonds for tissue engineering. The immediate nano environment of nanomaterial in its various applications has a notable effect on its response/activity. Severally, transformations occur leading to aggregation, dissolution, change in structure, activity loss, shape etc[51]. The utmost crucial factor of stability has been desirable and sought after in the application of nanoparticles.

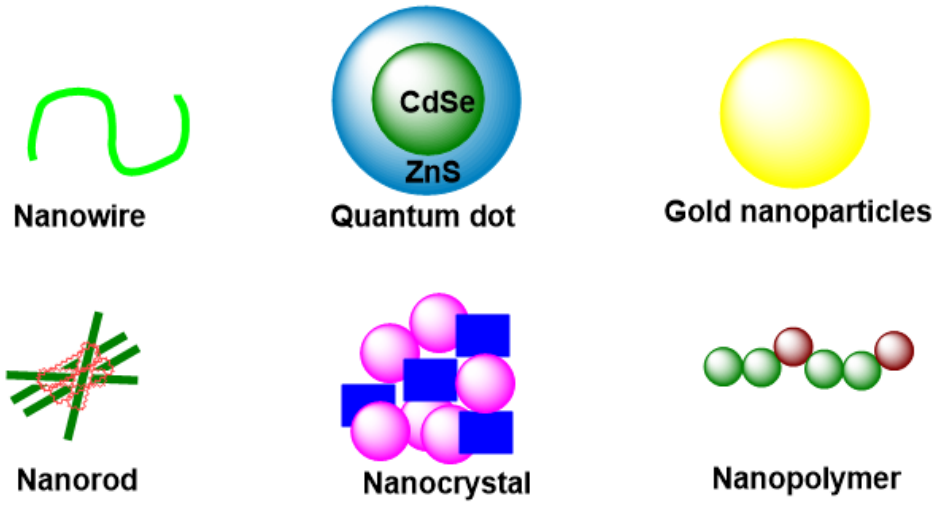

Figure 1.2. Examples of nanostructure being utilized in various applications

1.3 METAL NANOPARTICLES: GOLD AND SILVER.

Metal nanoparticles which include the silver, copper, gold, titanium, platinum, zinc, magnesium, and iron nanoparticles have a metal core composed of inorganic metal that is usually covered with a shell made up of organic or inorganic material with diverse application in our daily life. Their properties are found to be size dependent which contributes to valuable chemical and physical properties. These properties have resulted in modeling and designing of different medical and biological tools and applications. especially due to their small size-

to-volume ratio. They offer diagnostic and therapeutic possibilities as anticancer, radiotherapy enhancement, drug delivery, thermal ablation, antibacterial, diagnostic assays, antifungal, gene delivery, and many others. Metal nanoparticles can be functionalized with a variety of functional groups, such as peptides, antibodies, RNA, and DNA, to target different cells along with potential biocompatible polymers, for example, polyethylene glycol. Nobel metals "Gold and silver" are consistently used in various applications because of their stability, and functionalization, low toxicity, and ease of detection. They posse unique properties that makes it more valuable. They are considered as more specific and multipurpose agents with a diversity of biomedical applications considering their use in extremely sensitive investigative assays, radiotherapy enhancement, gene delivery, thermal ablation, and drug delivery Silver (AgNPs) and gold nanoparticles (AuNP) are attractive nanomaterials because of their unique optical[52], surface plasmon resonance (SPR)[53], physiochemical, chemical, quantum size effect[54], assembly of various sizes[55], stability, and strong antimicrobial properties[56]. They are used in biomedicines[57], functional textiles[58], cosmetics[59], probes[60], food packaging[61], sensor[62], electronics[63], water disinfectants[64], paints[65], diagnostic and therapeutic purpose[66]. Mohammed *et* al., 2018 reported stable AuNPs loaded with two anticancer therapeutics improved anticancer activities, cytotoxicity, uptake

and intracellular localization in HeLa cells. Therapeutic efficacy of the nanohybrid drug was strongly enhanced with a significant decrease of the half-maximal effective drug concentration, through blockage of HeLa cancer cell cycle. On the other hand, AuNPs as an attractive and applicable scaffold for delivery of nucleic acids has been reported. Rezvan 2021 stated catalytic properties of AuNPs for the development of optical aptasensor.[67] AgNPs on the other hand has been used in therapeutics as in trauma and orthopedics[68], water disinfection[69] as antimicrobial, antioxidant agent as well as catalyst[70] etc. As a result of increasing demand, rise in production and application have been reported in recent years.

AuNPs **AgNPs**

Fig 1.3 Pictorial representation of AuNPs and AgNPs.

1.4. FACTORS AFFECTING APPLICATIONS OF NANOPARTICLES

The physical and chemical properties of the NPs can be modified by their environment which affect their final form, fate and transformation. On exposure to certain environment, NPs may

undergo different changes in their state, surface charge and morphology which affect their applications. Various factors affect the application of nanoparticles which causes aggregation, dissolution, and instability having an adverse effect on its size, form, surface charge, shape and coating and invariably affect their fate, transport *in vivo,* and bioavailability. In various cases, these factors have hindered their application or optimum potential. Factors such as pH, dissolved oxygen concentration, temperature, salts, light, incubation time, etc. are critical for optimum usage and applications of NPs. Studies has reported that size, chemical composition, crystal structure, surface area as well as the release rate of ionic silver determines, AgNPs toxicity to organs such as lungs, liver, brain, vascular system, immune system, and reproductive organ[71]. Factors such as pH[72], ionic strength[73], temperature[74], and light[75] among other are factors[76] that affect and determines the fate of nanoparticles in their various applications. pH influences the surface charge of NPs, which is a dominant factor in determining their fate. Carbonate-coated AgNPs becomes positive below pH 4, and agglomeration occurs[77]. This shows the dependence in the oxidation of AgNPs on both protons and dissolved O_2. Jutaek 2009 also reported pH induced aggregation of AuNPs. The ionic strength affect NPs as studies has reported that chloride concentration affects particle stability and dissolution. Study on AgNPs, [78] reported AgNPs dissolution in the presence of

high chloride concentration and further formation of AgCl layer on the surface of AgNPs. Dissolution is enhanced by the formation of more soluble Ag−Cl complexes. Jutaek 2015 reported irreversible aggregation of AuNPs at salt concentration higher than 50 mM. Photoirradiation(light) has been reported as a critical factor that affects the stability of nanoparticles causing several transformational changes. AgNPs are broken into fragments by light exposure as the photo ejection of electrons induces a positive charge on the AgNPs that results in their disintegration into smaller-sized particles.[79] Size reduction or transformation of capping layers upon exposure to light can alter surface properties leading to aggregation and dissolution. On the other hand, temperature has a notable effect on the stability of nanoparticles. Above storage temperature of 4ºC, slight transformation of nanoparticles occurs and at extreme temperatures, aggregation, and dissolution

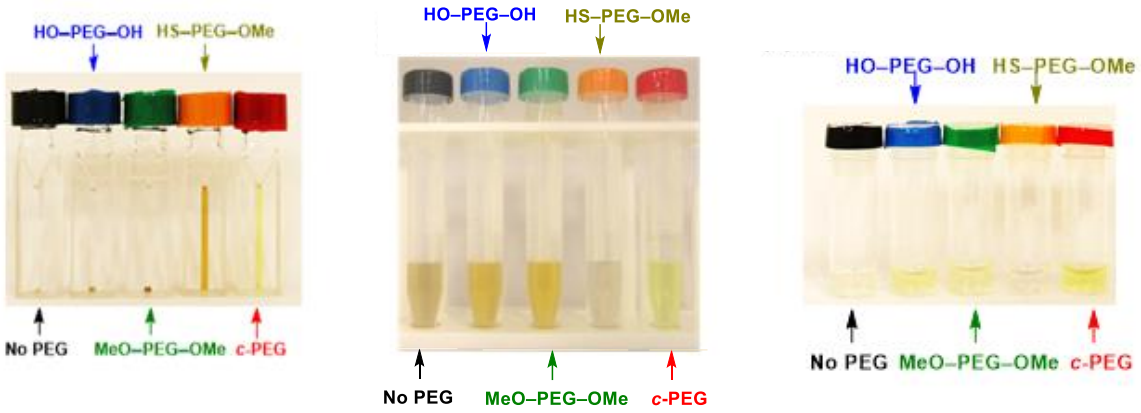

(a) Salt stability (b) White light stability (c) High temperature stability

Fig 1.4. AgNPs stability against salt (NaCl 150 mM), white light (860-990 lux), and high temperature (95°C).

1.5. POLYMER-PROTEINS INTERACTIONS.

The interaction of polymers with various molecules and surfaces[80-82] is critical in determining the properties and usage of a particular polymers in various fields including biosensor[83], biomedical[84], among others. Among various polymer interactions, polymer -protein interactions have remained active research over several decades owing to its various applications such as tissue engineering[85], implant materials[86], food packaging,[87] etc. Determination of the driving force and exact process of interaction is necessary for the development of useful products and applications. Polymers used in protein applications have evolved to serve multiple functions through intricate and complex interfaces. Poly(ethylene

glycol), a biocompatible polymer has been reported to interact with specific proteins[88] improving their stability for bio applications[89], protection in hostile environment[90], delivery[91], and prevention of non-specific interaction with other biomolecules. An important approach to investigating protein–PEG interactions is to characterize the structure and shape of the bioconjugate.[92] A shroud-like conformation indicates a strong favorable interaction whereas a dumbbell-like conformation indicates an unfavorable interaction.[93] Report by Pai et al.,[94] on small-angle neutron scattering (SANS) studies on mono-PEGylated lysozyme and mono-PEGylated human growth hormone stated that conjugated PEG with a molecular weight of 20 kDa acts as a random coil adjacent to the protein. Of the protein–polymer conjugates, serum albumins have been increasingly assessed as viable targets for PEGylation for unique applications. Serum albumin is a 67 kDa transport protein and one of the most abundant proteins in mammalian plasma, thereby serving as an appropriate protein to model potential bioconjugates.

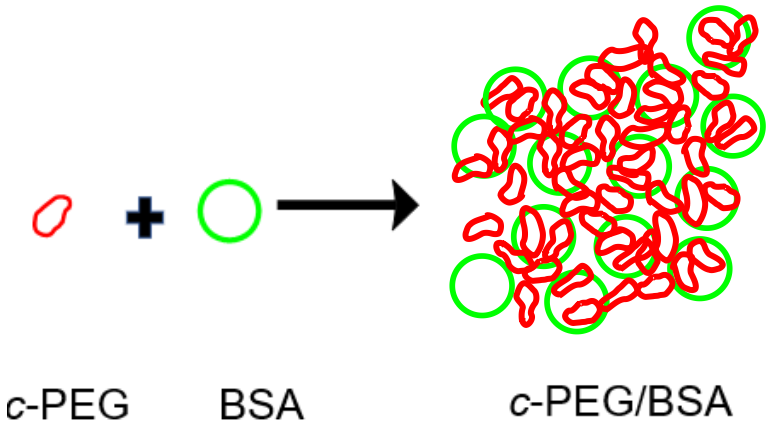

Fig 1.5. Example of polymer (*c*-PEG) -protein (BSA) interaction

1.6. Objectives of dissertations

Having discussed the above aspects, the aim of this study is to further probe the physisorption phenomenon of cyclic topology of poly(ethylene glycol) on other nanostructure such as silver nanoparticles (AgNPs.) and bovine serum albumin (BSA). Bearing in mind previous report on suppression of thermal aggregation of lysozyme by triangular PEG, dispersion stability of AuNPs by c-PEG and impossible thiol coordination to AgNPs, studies on physisorption of *c*-PEG to AgNPs was investigated. Factors such as; (i) stability against white light, high temperature, ionic strength, (ii) PEG molecular weight, PEG concentration and AgNPs size dependence , (iii) antimicrobial efficacy of AgNPs against *Escherichia coli*, (iv) cytotoxicity against HeLa cells were reported in this thesis. On the other hand, interactions of *c*-PEG

and BSA and further complexation to AuNPs for a colorimetric change was investigated with factors such as; (i) polymer topology (ii) BSA concentration (iii) Incubation time (iv) c-PEG concentration (v) AuNPs concentration (vi) AuNPs sizes. In achieving these objectives, an effective approach was to synthesize cyclic poly(ethylene glycol) from it linear counterpart (HO-PEG-OH) by williamson etherification in dilute solution. Characterization of product synthesized to authentic cyclization was obtained with a pure product. In this thesis, the author reported a comprehensive investigation of the effect of topology of cyclic poly(ethylene glycol) by physisorption to AgNPs and BSA. First, *c*-PEG physiorbed to AgNPs and stability against a physiological condition, white light, high temperature and it biological properties including antimicrobial and cytotoxicity were evaluated. The results were compared with its linear counterparts of the same molecular weight and composition. On the other hand, I also investigated linear and *c*-PEG interactions with BSA and further complexation with AuNPs at different PEG, AuNPs, and BSA concentrations. The *c*-PEG significantly enhanced the dispersion stability of AgNPs at PEG concentration of 0.25wt% and further showed persistent antimicrobial and cytotoxic effect against *E.*coli and HeLa cells respectively. Dispersion stability was not obtainable with other linear PEG nor biological properties retained. Thiol terminated poly(ethylene glycol) sulfidated the surface of AgNPs

to form AgS shell which further formed AgCl in the presence of salt. Dissolution and reduction in size of AgNPs was evident. Result of BSA interaction with *c*-PEG showed a shouldering effect on the fluorescence spectra of BSA by *c*-PEG, significant increase in hydrodynamic size of BSA and appearance of new peak in the proton NMR. Complex formation was seen between *c*-PEG and BSA whereas no complex was formed between the linear and BSA. Further complexation to AuNPs, resulted to aggregation of AuNPs and release of BSA molecules with an increase in incubation time. In the case of linear PEG, no complex was formed neither aggregation of AuNPs. The sensitivity of *c*-PEG towards BSA was found to be concentration dependent as high concentration of *c*-PEG lead to equilibrium in interaction between *c*-PEG/BSA and *c*-PEG/AuNPs with no aggregation of AuNPs. Increase in BSA and AuNPs concentration lead more obvious effect and aggregation of AuNPs. *c*-PEG was seen as the driving force by it ability to interact with both BSA and AuNPs.

Scheme 1a. Synthesis of *c*-PEG

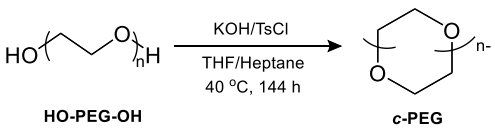

HO-PEG-OH **c-PEG**

Scheme 1b. Synthesis of MeO-PEG-OMe

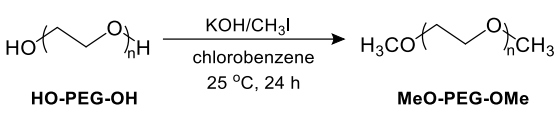

HO-PEG-OH **MeO-PEG-OMe**

An outline of this dissertations is as follows:

Chapter two describes the physisorption of *c*-PEG to AgNPs and further enhancement of the dispersion stability, antimicrobial and cytotoxicity effect of AgNPs which was not obtainable with the linear counterparts (HO-PEG-OH, MeO-PEG-OMe and HS-PEG-OMe). *c*-PEG with linear PEGs were synthesized and purified by the Williamson etherification methods. Then, respective PEGs were mixed with AgNPs and further exposed to conditions of physiological conditions (150 mM NaCl), high temperature, and white light. Thereafter, the biological properties including antimicrobial against *E. coli* and cytotoxicity against HeLa cells were evaluated. Enhanced dispersion stability of AgNPs against the various conditions was obtained in the presence of *c*-PEG which also maintained the antimicrobial and cytotoxic effect of AgNPs. On the other hand, other linear PEGs could not stabilize AgNPs and resulted to aggregation, dissolution, and various transformational changes on the surface of AgNPs evident by the colour change and Uv-Vis spectra changes.

Chapter three describes the unique interaction between *c*-PEG and BSA. First, *c*-PEG was synthesized along with other linear PEGs as previously explained. Thereafter, *c*-PEG was mixed with BSA at PEG concentration of o.15 and 0.25 wt. PEG. Evaluated by NMR, florescence and DLS showed complex formation which was not obtainable with linear PEGs.

On further complexation with AuNPs, aggregation of AuNPs was evident in *c*-PEG/BSA/AuNPs system. *c*-PEG was found to sensitively interact with BSA without any significant conformational changes and subsequent aggregation of AuNPs. Incubation time was reported as a major factor for this interaction as more BSA molecules become release from the AuNPs into the solution with an increase in time. *c*-PEG concentration was also found as a major factor for interaction as high concentration of *c*-PEG drive the system and prevents further aggregation. Interaction between *c*-PEG and BSA was reported to be slow and stronger than interaction between *c*-PEG and AuNPs. BSA and AuNPs concentration were seen to cause an effect on the aggregation of AuNPs as more BSA or AuNPs concentration leds to more obvious effect of *c*-PEG by aggregation of AuNPs. A new ability of *c*-PEG towards BSA and other proteins was discovered.

Chapter four Chapter 4 summarizes the results. This dissertation has shown a new method of AgNPs stabilization by physisorption of c-PEG while maintaining its biological properties. This was not attainable by HS–PEG–OMe or any other linear PEGs. Usage of *c*-PEG in biomedical fields is underway in tandem with concerns of biocompatibility. On the other hand, a new effect of *c*-PEG on proteins is reported in this dissertation. Sensitivity of *c*-PEG towards BSA and further aggregation of AuNPs when complexed has given insight to the

possibility of biosensing ability of *c*-PEG in biomedical fields. When corona formation is important, *c*-PEG could be useful in further studies.

REFERENCES

1. Takata, T. Aoki, D. *Polym. J.* 2018, **50**, 127-147.

2. Tezuka, Y. Oike, H. *Prog. Polym. Sci.* 2002, **27**, 1069-1122.

3. Takeshita, H., Shiomi, T., Takenaka, K. & Arai, F. *Polymer* 2013,**54**, 4776-4789.

4. Yamamoto, T. *React. Funct. Polym.* 2018, **132**, 43-50.

5. Zhang, L.H., Elupula, R., Grayson, S.M. & Torkelson, J.M. *Macromolecules* 2016,**49**, 257-268.

6. Yoon, K.B., Choi, J.S., Lee, D.H., Hur, Y. & Noh, S.K. *Mol. Cryst. Liq.* 2006, **459**, 27-34.

7. Lienard, R., De Winter, J. & Coulembier, O. *J Polym Sci.,* 2020, **58**, 1481-1502.

8. Haque, F.M. & Grayson, S.M. *Nat. Chem.*, 2020, 433-444.

9. Kricheldorf, H.R. *J. Polym. Sci., Part A: Polym. Chem.* 2010, **48**, 251-284.

10. Jia, Z.F. Monteiro, M.J. *J Polym Sci Part A:Polym Chem* 2012, **50**, 2085-2097.

11. Deguchi, T. *Kobunshi Ronbunshu* 2011, **68**, 767-772.

12. Jeong, Y., Jin, Y., Chang, T., Uhlik, F. & Roovers, J. *Macromolecules* 2017, **50**, 7770-7776.

13. Muramatsu, Y. Takasu, A. *Polym. J.*

14. Yamamoto, T. Tezuka, Y. Topological Polymer Chemistry:. *Kobunshi Ronbunshu* 2011, **68**, 782-794.

15. Ree, B.J., Satoh, T. Yamamoto, T. *Polymers* 2019, **11** .

16. Semlyen, J.A. (ed.) Edn. 2nd. (Kluwer Academic Publishers, New York; 2002).

17. Semlyen, J.A. *Pure Appl. Chem.,* 1981, **53**, 1797-1804 .

18. Morgese, G. *Angew. Chem., Int. Ed.,* 2016, **55**, 15583-15588.

19. Kang, G.Y. *Che Comm.,.* 2020, **56**, 3003-3006.

20. Arno, M.C. *Biomaterials* 2018, **180**, 184-192.

21. Morgese, G., Cavalli, E., Rosenboom, J.G., Zenobi-Wong, M. & Benetti, E.M. *Angew. Chem., Int. Ed.,* 2018, **57**, 1621-1626.

22. Cortez, M.A. *J. Am. Chem. Soc.*, 2015, **137**, 6541-6549.

23. Tan, Z. *J. Am. Chem. Soc.,* 2009, **141**, 15804-15817.

24. Nasongkla, N. *Angew. Chem., Int. Ed.,* 2004, **43**, 6323-6327.

25. Wang, Y.B. *Nat. Commun.* 2020, **11**.

26. Harris, J.M. *Acs Symposium Series* 1991, **467**, 418-429.

27. Narainpersad, N., Singh, M. & Ariatti, M. *Hum. Gene Ther.,* 2009, **20**, 1542-1542.

28. Whitehead, A.K., Barnett, H.H., Caldorera-Moore, M.E. & Newman, J.J.

Regen. Biomater. 2018, **5**, 167-175.

29. del Pino, P. *Angew. Chem., Int. Ed.* , 2016, **55**, 5483-5487.

30. Pelaz, B. *Acs Nano* 2015, **9**, 6996-7008.

31. Knop, K., Hoogenboom, R., Fischer, D. & Schubert, U.S. *Angew. Chem., Int. Ed.* 2010, **49**, 6288-6308.

32. Mei, L. *Intl J Pharm*2014, **468**, 26-38.

33. Zhang, F., Liu, M.R. Wan, H.T. 2014, **37**, 335-339

34. Peng, F. *J Biotechnol.,* 2014, **170**, 42-49.

35. Marchioni, M. *J. Phys. Chem. C.,* 2020, **124**, 13467-13478.

36. Aziz, Z.A.A. *Front. Chem.,* 2019,**7**.

37. Thompson, D. *Gold Bulletin* 2007, **40**, 267-269.

38. Ekpenyong-Akiba, A.E. *et al.*. *Nanoscale Horiz* 2019, **4**, 757-768.

39. Moosa, B. *J. Nanosci. Nanotechnol* 2019,**14**, 332-343.

40. Yadav, S., Hassan, M.S., Verma, P. & Sapra, S. *J. Nanosci. Nanotechnol* 2019,**19**, 375-382.

41. Dimcheva, N. *Curr. Opin. Electrochem.*, 2020, **19**, 35-41.

42. Pandey, A.P.. *J. Nanosci. Nanotechnol.* 2014, **14**, 828-840.

43. Laurent, S. Mahmoudi, M. S. *Int. J. of Molec. Epidemiol. Genet* 2011,**2**, 367-390.

44. Alvim, R.S., Suxo, V., Babilonia, O.A., Celaschi, Y.M. & Miranda, C.R. *Mrs Advances* 2017, **2**, 477-482.

45. Aziz, H. Tunio, S.Q. *Advances in Natural Sciences-Nanoscience and Nanotechnology* 2019,**10**.

46. Mirshahghassemi, S., Ebner, A.D., Cai, B. & Lead, J.R. *Sep. Purif. Technol.* 2017, **179**, 328-334.

47. Bell, A.T. *Science* 2003, **299**, 1688-1691.

48. Grunes, J., Zhu, A. & Somorjai, G.A. *Chem Comm*, 2003, 2257-2260.

49. Kumari, H., Kang, X., Mirzamani, M. & Dawn, A. *Abstracts of Papers of the American Chemical Society* 2019, **257**.

50. Morganti, P.. *Clinical Cosmetic and Investigational Dermatology* 2010, **3**, 5-13.

51. Sperling, R.A. Parak, W.J. *Philosophical Transactions of the Royal Society a-Mathematical Physical and Engineering Sciences* 2010, **68**, 1333-1383.

52. Sabela, M., Balme, S., Bechelany, M., Janot, J.M. & Bisetty, K. *Adv. Eng. Mater.,* 2017, **19**.

53. Liang, A.H., Liu, Q.Y., Wen, G.Q. & Jiang, Z.L. *TrAC - Trends Anal. Chem.* 2012, **37**,

32-47.

54. Bagheri, Z., Allameh, Z. & Massudi, R. *Photonics and Nanostructures-Fundamentals and Applications* 2015,**15**, 24-31.

55. Scarabelli, L., Coronado-Puchau, M., Giner-Casares, J.J., Langer, J. & Liz-Marzan, L.M. *Acs Nano* 2014,**8**, 5833-5842.

56. Banach, M. Pulit, J. *Przemysl Chem.,* 2013, **92**, 1056-1060.

57. Dreaden, E.C., Alkilany, A.M., Huang, X.H., Murphy, C.J. & El-Sayed, M.A.. *Chem. Soc. Rev* 2012, **41**, 2740-2779.

58. Abou Elmaaty, T. *Rsc Advances* 2018, **8**, 25546-25557.

59. Pulit-Prociak, J., Grabowska, A., Chwastowski, J., Majka, T.M. & Banach, M. *Colloids Surf. B***,** 2019,**183**.

60. Modrzejewska-Sikorska, A. & Konowal, E. *Journal of Molecular Liquids* **302** (2020).

61. Kumar, A., Choudhary, A., Kaur, H., Mehta, S. & Husen, A. *J. Nanobiotechnology* 2021,**19**.

62. Bindhu, M.R. & Umadevi, M. *Spectrochim. Acta A Mol. Biomol. Spectrosc.,* 2014,**128**, 37-45 .

63. Tai, Y.L. & Yangt, Z.G. *Acs Appl. Mater. Interfaces,* 2015,**7**, 17104-17111.

64. Vilela, D., Stanton, M.M., Parmar, J. & Sanchez, S. *Acs Appl. Mater. Interfaces,* 2017. **9**, 22093-22100.

65. Kumar, A., Vemula, P.K., Ajayan, P.M. & John, G. *Nat. Mater.* 2008, **7**, 236-241.

66. Lopes, T.S., Alves, G.G., Pereira, M.R., Granjeiro, J.M. & Leite, P.E.C. *J. Cell. Biochem.* 2019, **120**, 16370-16378.

67. Yazdian-Robati, R. *l. Anal. Biochem.*, 2021,**629**.

68. Brennan, S.A. *Bone Jt. J* , **97B**, 2015, 582-589.

69. Deshmukh, S.P., Patil, S.M., Mullani, S.B. & Delekar, S.D. *Mater. Sci. Eng. C*, 2019, **97**, 954-965.

70. Dong, X.Y., Gao, Z.W., Yang, K.F., Zhang, W.Q. & Xu, L.W. *Catal. Sci. Technol.,* 2015, **5**, 2554-2574.

71. Xu, L.. *Theranostics* , 2020, **10**, 8996-9031.

72. Chutrakulwong, F., Thamaphat, K. & Limsuwan, P. *J. Phys. Commun***.** 2020, **4** .

73. Burns, C., Spendel, W.U., Puckett, S. & Pacey, G.E. *Talanta* 2006, **69**, 873-876.

74. Khan, I. & Saeed, K. *Arab. J. Chem.,* 2009, **12**, 908-931.

75. Korshed, P., Li, L., Ngo, D.T. & Wang, T. *Nanomaterials* 2018, **8**.

76. El Badawy, A.M. *Environ. Sci. Technol.* , 2010, **44**, 1260-1266.

77. Piccapietra, F., Sigg, L. & Behra, R. *Environ. Sci. Technol.*, 2012, **46**, 818-825.

78. Levard, C. *Environ. Sci. Technol.*, 2013, **47**, 5738-5745.

79. Cheng, Y.W. *J. Phys. Chem. C* . , 2011, **115**, 4425-4432.

80. Milinchuk, V.K., Taraban, V.B., Bol'bit, N.M., Klinshpont, E.R. & Shelukhov, I.P. *Nuclear Instruments & Methods in Physics Research Section B-Beam Interactions with Materials and Atoms* , 2001, **185**, 123-128.

81. Li, S.F., Wei, X.N., Ju, W.L., Su, Y.L. & Wang, D.J. *Acta Polym. Sin.* , 2021, **52**, 146-157.

82. Liu, Z.H., Jiao, Y.P., Wang, T., Zhang, Y.M. & Xue, W. *J Control Release* , 2012, **160**, 14-24.

83. Ramakrishna, S., Lala, N.L., Garudadhwaj, H., Ramaseshan, R. & Ganesh, V.K. *Molecular Building Blocks for Nanotechnology: from Diamondoids to Nanoscale Materials and Applications* , 2007, **109**, 377-392.

84. Wilson, V.R. *Mol. Pharm* , 2021,**18**, 836-849.

85. Cho, C.S. *Biomaterials* , 2006, **27**, 576-585.

86. Bakker, D., Vanblitterswijk, C.A., Hesseling, S.C., Grote, J.J. & Daems, W.T. *Biomaterials*,, 1988, **9**, 14-23.

87. Silvestre, C., Duraccio, D. & Cimmino, S. *Prog. Polym. Sci.*, 2011, **36**, 1766-1782.

88. Katre, N.V. *Adv. Drug Deliv. Rev.*, 1993, **10**, 91-114.

89. Lee, L.L.Y. & Lee, J.C. T. *Biochemistry* **26**, 1987, 7813-7819.

90. Novaes, L.C.D., Jozala, A.F., Mazzola, P.G. & Pessoa, A. *Braz. J. Pharm. Sci,* 2014, **50**, 371-380.

91. Chao, S.H.. *J. Phys. Chem* , 2014, **118**, 8388-8395 .

92. Caliceti, P. & Veronese, F.M. *Adv. Drug Deliv. Rev.*, 2003, **55**, 1261-1277 .

93. Lam, C.N., Chang, D., Wang, M.Z., Chen, W.R. Olsen, B.D. *J. Polym. Sci. A Polym. Chem.* , 2016, **54**, 292-302.

94. Pai, S.S. *Bioconjug. Chem,* 2011*,* **22**, 2317-2323.

Chapter 2

Cyclic Poly(ethylene glycol) Interaction with Silver Nanoparticles for Enhanced Dispersion Stability, Antimicrobial Activity, and Cytotoxicity

2.1. Introduction

The emerging importance of nano science cannot be overemphasized, and the field of nanotechnology has drawn special worldwide attention especially in cases of noble metals such as gold and silver.[1] The distinct properties of silver nanoparticles (AgNPs) have led to its broad applications in medical imaging,[2] drug delivery,[3] cell electrode,[4] biosensors,[5] cancer diagnosis and treatment,[6] and cytotoxic agents[7] as well as antimicrobial agents against broad spectrum of gram-negative and gram-positive bacteria.[8] The nano environment of AgNPs has notable effects on its response/activity in many applications. However, unlike gold nanoparticles (AuNPs), AgNPs are not a stable material and susceptible to light, dissolved electrolytes, and various chemical species, and transformations occur leading to aggregation, dissolution, change in structure, activity loss, etc.[9] In diverse fields of nanoscience, the instability of AgNPs often hinders their applications and commercialization. Although, several capping agents have been explored for AgNPs, transformations, dissolution and agglomerations in various environments still remain a significant issue.

The use of stabilizers such as cetyltrimethylammonium bromide (CTAB),[10, 11] sodium dodecyl sulfate (SDS),[10, 12] and other surfactants are well reviewed with limitations of non-biocompatibility and instability. The utmost crucial factor of stability and

biocompatibility has been desirable and sought after in the application of nanoparticles. In this regard, poly(ethylene glycol) (PEG), a non-ionic polymer with a flexible structure, is the most commonly used biocompatible polymer accepted by United States Food and Drug Association and increased its applications including food, commodity, and drug as well as uses in agriculture and manufacturing industries.[13-16] In order to use PEG as a stabilizer for metal nanoparticles, especially AuNPs, thiol-functionalized PEG (HS–PEG–OMe) is often employed through the chemisorption between the sulfur atom and metal surface.[17] However, the use of HS–PEG–OMe for AgNPs forms a silver sulfide (Ag_2S) layer on the surface to drastically disturbs the nanoparticles' properties[18] and leads to dissolution,[19, 20] inhibiting PEGylation of AgNPs by the thiol chemisorption. A few reports show that $AgNO_3$ is reduced by hydroxy-terminated PEG (HO–PEG–OH), and the resulting nanoparticles were capped by the same polymer in the process.[21-23] However, the number of reports using this method is quite limited, and thus the capping structure and properties of the formed nanoparticles are not well studied. For these reasons, polyvinylpyrrolidone (PVP) is an alternative polymer often used for AgNPs but has limited biocompatibility compared to PEG.[24-26] Therefore, stable PEGylation of AgNPs to curb the various restrictions is utmost needed.

In recent years, attention has been drawn to interesting polymer properties such as

melting, diffusion, rheology, crystallization, and phase separation as a result of distinct topological differences.[27, 28] Of the various polymer topologies, cyclic polymers has shown unique physical and chemical properties such as increased glass transition temperature, higher refractive index, less entanglement, slow hydrolytic degradation, and self-assembling behaviors etc. different from their linear counterparts with the same molecular weight.[29-35] In biomedical applications, cyclic polymers have promising potentials due to their superior properties such as higher efficacy of gene delivery,[36] higher cancer cell take up,[37] longer circulation time *in vivo*,[38 39] and controlled release of drugs.[40] It has been reported that cyclic amphiphilic block copolymers form micelles with strong salt and thermal stabilities.[41, 42] Recently, cyclized PEG (*c*-PEG) without any chemical inhomogeneity was found to endow AuNPs with high dispersion stability by physisorption.[43] Moreover, AuNPs PEGylated by *c*-PEG can be used for the colorimetric detection of bovine serum albumin through unique complexation.[44] The strong physisorption of *c*-PEG likely arises from the less entropic penalty upon adsorption to the surface compared to the linear counterparts,[45, 46] which is also suggested by theoretical and computational studies.[47-51] Bearing this in mind, the physisorption of *c*-PEG is considered suitable for PEGylation and dispersion stabilization of AgNPs because AgNPs are much less chemically stable than AuNPs, and the thiol

chemisorption is essentially inapplicable. The present work provides a new approach for the stabilization of AgNPs in the presence of *c*-PEG against a physiological condition, white light, and high temperature, as well as to examine the antimicrobial activity and cytotoxicity of AgNPs. In the result, in contrast to HS–PEG–OMe and other linear PEG, *c*-PEG readily

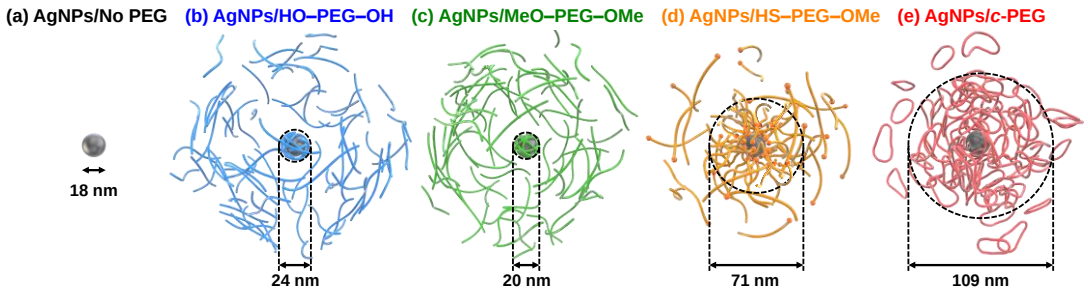

Fig. 2.1 Schematic illustrations of (a) AgNPs/No PEG, (b) AgNPs/HO–PEG–OH, (c) AgNPs/MeO–PEG–OMe, (d) AgNPs/HS–PEG–OMe, and (e) AgNPs/*c*-PEG. The indicated sizes were determined by DLS.

stabilized AgNPs against the various harsh conditions and persisted the biological activities (Fig. 2.1). This knowledge is important as the first stable PEGylation method for AgNPs owing to their potential biomedical applications.

2.2 Experimental

2.2.1 Materials

Citrate-capped AgNPs with a size of 10, 20, and 30 nm ($AgNPs_{10}$, $AgNPs_{20}$, and $AgNPs_{30}$, respectively) dispersed in a 2 mM sodium citrate solution with a silver mass concentration of 0.02 mg/mL were purchased from nanoComposix, USA and used as received. AgNPs with a size of 80 nm functionalized by methoxy polyethylene glycol sulfhydryl with a molecular weight of 5 kDa ($HS–PEG_{5k}–OMe$) in milli-Q water with a silver mass concentration of 0.02 mg/mL were also purchased from nanoComposix, USA and used as received. Poly(ethylene glycol) 2,000 ($HO–PEG_{2k}–OH$) (Sigma–Aldrich, Japan), poly(ethylene glycol) 4,000 ($HO–PEG_{3k}–OH$) (Kanto Chemical Co., Inc., Japan), poly(ethylene glycol) 6,000 ($HO–PEG_{9k}–OH$) were purified by passing through a silica gel column using chloroform/methanol (90/10, v/v) as an eluent. mPEG-SH, 10K ($HS–PEG_{9k}–OMe$) (Funakoshi Co., Ltd., Japan) was purified by recycling preparative SEC. The AgNPs' and PEGs' names in the parentheses above are the ones used in the paper. The molecular weights of PEG in the catalogs deviated from my measurement to some extent, and the measurement values are used. Tetrahydrofuran (THF), dehydrated stabilizer free (>99.0%, Kanto Chemicals Co., Japan), anthralin (≥95.0%, Nacalai Co., Japan), silver trifluoroacetate

(98%, Sigma–Aldrich, Japan), *n*-heptane (>99.0%, Kanto Chemicals Co., Japan), potassium hydroxide (>99.0%, Kanto Chemicals Co., Japan), iodomethane (>99.0%, Kanto Chemicals Co., Japan), chlorobenzene (>99.0%, Kanto Chemicals Co., Japan), chloroform (>99.0%, Kanto Chemicals Co., Japan), tosyl chloride (>99.0 %, Sigma–Aldrich, Japan), acetone (>99.0%, Kanto Chemicals Co., Japan), methanol (>99.6%, Kanto Chemicals Co., Japan), dichloromethane (>99.0 %, Kanto Chemicals Co., Japan), magnesium sulfate (>96.0 %, Kanto Chemicals Co., Japan), sodium dihydrogen phosphate (>99.0 %, FUJIFILM Wako Pure Chemical Co., Japan), disodium hydrogen phosphate (>99.0%, FUJIFILM Wako Pure Chemical Co., Japan), sodium chloride (>99.0%, Kanto Chemicals Co., Japan), chloroform-d (99.6 atom%D, Tokyo Chemical Industry Co., Ltd., Japan), Wakosil C-300 (FUJIFILM Wako Pure Chemical Co., Japan), *E. coli* JM 109 (NIPPON GENE Co., Ltd., Japan), Muller Hinton Broth (Sigma–Aldrich, Japan), ampicillin (Fujita Pharmaceutical. Co., Ltd., Japan), HeLa cells (KAC Co., Ltd., Japan), fetal bovine serum (FBS) (Thermo Fisher Scientific, USA), penicillin–streptomycin, and trypsin (2.5%) (Thermo Fisher Scientific, USA), Dulbecco's modified Eagle's medium (DMEM) with low glucose (Sigma–Aldrich, USA), and D-PBS (–) (FUJIFILM Wako Pure Chemical Co., Japan) were used as received.

2.2.2 Synthesis of *c*-PEG

Cyclization of HO–PEG–OH was carried out by the previously reported method.[52] Thus, a solution of vacuum dried HO–PEG–OH (5.0 g) and tosyl chloride (190 mg) in 100 mL of dry THF was added over 144 h to a dispersion of powdered potassium hydroxide (3.3 g) in 100 mL of a mixture of dry THF and *n*-heptane (75/25 v/v) at 40 °C using a syringe pump under dry nitrogen atmosphere. Additional 24 h of stirring was allowed for complete cyclization. The reaction mixture was filtered, and the solvent was removed under reduced pressure. Chloroform was added to the filtrate, washed with brine followed by deionized water. The organic phase was dried with magnesium sulfate, and the solvent was removed under reduced pressure. Silica gel column chromatography was carried out with a mixture of chloroform/acetone (9/1 v/v) to elute intermolecularly reacted polymeric products, followed by a mixture of chloroform/methanol (9/1 v/v) to elute a crude containing *c*-PEG. The crude was dissolved in dichloromethane, and *n*-heptane was slowly added until the solution turns cloudy. The cloudy solution was heated to 40 °C and cooled to 25 °C with resultant two layers. The upper clear layer containing a relatively large proportion of *c*-PEG was collected, and this procedure was repeated several times to obtain pure *c*-PEG as white solid. The yield for *c*-PEG_{2k}, *c*-PEG_{3k}, and *c*-PEG_{9k} was 303 (6.1 %), 247 (4.9 %), and 145 mg (2.9 %),

respectively. Concerning the very low isolated yields, the purity was prioritized over the yield, resulting in major loss during the isolation.

2.2.3 Synthesis of MeO–PEG–OMe

Methylation of HO–PEG–OH was carried out according to the previous method.[52] Typically, under dry nitrogen atmosphere, chlorobenzene (20 mL) was added to finely powdered potassium hydroxide (2.3 g), and the mixture was stirred at 25 °C. Iodomethane (0.35 g) was added to the mixture, followed by slow addition of HO–PEG_{2k}–OH (5.0 g) dissolved in chlorobenzene (50 mL) over 25 min. The mixture was stirred for 24 h. Filtration was carried out, and the filtrate was reduced to a small volume under reduced pressure, followed by washing with distilled water and deionized water. The organic phase was dried with magnesium sulfate and concentrated under reduced pressure. The residue was applied to a silica gel column with a mixture of chloroform/acetone (9/1 v/v), and the product was eluted by a mixture of chloroform/methanol (9/1 v/v). The solvent was removed and vacuum dried to obtain dimethylated poly(ethylene glycol) (MeO–PEG_{2k}–OMe) (3.6 g, 72%) as white solid.

2.2.4 NMR

^{1}H NMR (400 MHz) and ^{13}C NMR (100 MHz) were recorded on a JEOL JNM-

ESC400 instrument at room temperature at a polymer concentration of 20 mg/mL. Deuterated chloroform was used as a solvent.

2.2.5 SEC

Size exclusion chromatography measurements were performed on a Shodex GPC-101 gel permeation chromatography system (Shodex DU-2130 dual pump, Shodex RI-71 reflective index detector, and Shodex ERC-3125SN degasser) equipped with a Shodex KF-G guard column (4.6 mm × 10 mm; pore size, 8 μm) and two Shodex KF-804L columns (8 mm × 300 mm) in series. THF was used as an eluent at a flow rate of 1.0 mL/min. Calibration was performed with PEG standard samples.

2.2.6 MALDI-TOF MS

Matrix-assisted laser desorption/ionization time-of-flight mass spectrometry (MALDI-TOF MS) was performed at the Open Facility, Hokkaido University using a an ABSCIEX TOF/TOF 5800 mass spectrometer. PEG (1.5 mg) dissolved in THF (10 μL) was mixed with a matrix (anthralin, 40 mg/mL, 25 μL) and an ionization agent (silver trifluoroacetate, 40 mg/mL, 10 μL). The mixture (0.4 μL) was dropped cast on an opti-TOF 384-Well Insert (123 × 81 mm) plate for the measurement.

2.2.7 Recycling Preparative SEC

A Japan Analytical Industry LC-908 recycling preparative HPLC system (Hitachi L-7110 pump and JAI RI detector RI-5) was used. JAIGEL-2H and 3H columns and a pre-column were connected in series. Chloroform was used as a solvent, and the flow rate was set at 3.5 mL/min.

2.2.8 UV–Vis Spectroscopy

UV–Vis absorption spectra were recorded using a JASCO Ubset V-670 Spectrophotometer at 25 °C in a micro quartz cuvette (M25-UV2, GL Science Inc, Japan) with a path length of 10 mm. Deionized water was used a blank. Spectra were acquired at a wavelength range of 300–800 nm. Optical density at 600 nm (OD_{600}) in the antimicrobial activity experiment was determined by the intensity of an incubated specimen at 600 nm subtracted by that of the medium.

2.2.9 DLS and ζ-Potential

DLS and ζ-potential measurements were carried out by a Zetasizer Nano ZS instrument (He–Ne laser, 633 nm, Max 4 mW, Malvern Panalytical Ltd.). Micro quartz cuvette (ZEN2112, Hellma Analtytics) and Zetasizer nano cell (DTS1060, Malvern Instruments, Ltd) were used. Measurements were carried out at 25 °C with a 120 s equilibration time. A cumulants analysis provided in software built into the instrument was

used to determine the *z*-average size.

2.2.10 Preparation of AgNPs/HO–PEG–OH, AgNPs/MeO–PEG–OMe, AgNPs/HS–PEG–OMe, and AgNPs/*c*-PEG

Typically, an aqueous dispersion of $AgNPs_{10}$ (0.54 mL) was added to HO–PEG_{9k}–OH, MeO–PEG_{9k}–OMe, HS–PEG_{9k}–OMe, or *c*-PEG_{9k} (1.5 mg) in a 1.5 mL Eppendorf tube, and the mixture was vortexed for 1 min to form $AgNPs_{10}$/HO–PEG_{9k}–OH, $AgNPs_{10}$/MeO–PEG_{9k}–OMe, $AgNPs_{10}$/HS–PEG_{9k}–OMe, or $AgNPs_{10}$/*c*-PEG_{9k}, respectively. The PEG concentration was varied by changing the amount of PEG. $AgNPs_{10}$/No PEG was prepared by vortex mixing an aqueous dispersion of $AgNPs_{10}$ (0.54 mL).

2.2.11 Stability in a PBS Buffer

A tenfold-concentrated phosphate-buffered saline (PBS) solution (pH 7.4, NaCl 1500 mM, Na_2HPO_4 81 mM, NaH_2PO_4 14.7 mM) was prepared in advance. $AgNPs_{10}$/No PEG, $AgNPs_{10}$/HO–PEG_{9k}–OH, $AgNPs_{10}$/MeO–PEG_{9k}–OMe, $AgNPs_{10}$/HS–PEG_{9k}–OMe, or $AgNPs_{10}$/*c*-PEG_{9k} (0.54 mL) prepared above was placed in a micro quartz cuvette. Subsequently, the tenfold-concentrated PBS solution (0.06 mL) was added to the cuvette, and the resulting mixture was 0.6 mL with pH 7.4 and a NaCl concertation of 150 mM with a PEG concentration of 0.25 wt%. A time-course UV–Vis measurement was performed for

1000 min.

For ESI Movie 1, an aqueous dispersion of $AgNPs_{10}$ (0.54 mL) was added to HO–PEG_{9k}–OH, MeO–PEG_{9k}–OMe, HS–PEG_{9k}–OMe, or *c*-PEG_{9k} (1.5 mg) in a glass vail and mixed by pipetting to dissolve PEG to form $AgNPs_{10}$/HO–PEG_{9k}–OH, $AgNPs_{10}$/MeO–PEG_{9k}–OMe, $AgNPs_{10}$/HS–PEG_{9k}–OMe, or $AgNPs_{10}$/*c*-PEG_{9k}, respectively. $AgNPs_{10}$/No PEG was prepared by pipetting an aqueous dispersion of $AgNPs_{10}$ (0.54 mL). Subsequently, the tenfold-concentrated PBS solution (0.06 mL) was added to the glass vail and mixed by pipetting. The resulting mixture was 0.6 mL with pH 7.4 and a NaCl concertation of 150 mM with a PEG concentration of 0.25 wt%. The color change was observed.

2.2.12 *c*-PEG's Molecular Weight-Dependent Stability

An aqueous dispersion of $AgNPs_{10}$ (0.54 mL) was added to *c*-PEG_{2k}, *c*-PEG_{3k}, or *c*-PEG_{9k} (0.15 mg) in a 1.5 mL Eppendorf tube, and the mixture was vortexed for 1 min to form $AgNPs_{10}$/*c*-PEG_{2k}, $AgNPs_{10}$/*c*-PEG_{3k}, or $AgNPs_{10}$/*c*-PEG_{9k}, respectively. Subsequently, the tenfold-concentrated PBS solution (0.06 mL) was added to the cuvette, and the resulting mixture was 0.6 mL with pH 7.4 and a NaCl concertation of 150 mM with a PEG concentration of 0.25 wt%. A time-course UV–Vis measurement was performed for 1000 min.

2.2.13 *c*-PEG's Concentration-Dependent Stability

An aqueous dispersion of $AgNPs_{10}$ (0.54 mL) was added to *c*-PEG_{9k} (0.3, 1.5, 3.0, or 7.5 mg) in a 1.5 mL Eppendorf tube, the mixture was vortexed for 1 min to form $AgNPs_{10}$/*c*-PEG_{9k}. Subsequently, the tenfold-concentrated PBS solution (0.06 mL) was added to the cuvette, and the resulting mixture was 0.6 mL with pH 7.4 and a NaCl concertation of 150 mM with a PEG concentration of 0.05, 0.25, 0.40, or 1.25 wt%, respectively. A time-course UV–Vis measurement was performed for 1000 min.

2.2.14 AgNPs' Size-Dependent Stability

c-PEG_{9k} (1.5 mg) was added to an aqueous dispersion of $AgNPs_{10}$, $AgNPs_{20}$, or $AgNPs_{30}$ (0.54 mL), and the mixture was vortexed for 1 min. Subsequently, the tenfold-concentrated PBS solution (0.06 mL) was added to the cuvette, and the resulting mixture was 0.6 mL with pH 7.4 and a NaCl concertation of 150 mM with a PEG concentration of 0.25 wt%. A time-course UV–Vis measurement was performed for 1000 min.

2.2.15 Stability in a $CaCl_2$ Solution

A tenfold-concentrated calcium chloride solution ($CaCl_2$ 100 mM, pH unadjusted) was prepared in advance. $AgNPs_{10}$/No PEG, $AgNPs_{10}$/HO–PEG_{9k}–OH, $AgNPs_{10}$/MeO–PEG_{9k}–OMe, $AgNPs_{10}$/HS–PEG_{9k}–OMe, or $AgNPs_{10}$/*c*-PEG_{9k} (0.54 mL) prepared above

was placed in a micro quartz cuvette. Subsequently, the tenfold-concentrated $CaCl_2$ solution (0.06 mL) was added to the cuvette, and the resulting mixture was 0.6 mL with 10 mM of $CaCl_2$ with a PEG concentration of 0.25 wt%. A time-course UV–Vis measurement was performed for 1000 min.

2.2.16 Stability Against White Light

An aqueous dispersion of $AgNPs_{10}$ (2.1 mL) was two times diluted with deionized water (2.1 mL) and added to HO–PEG_{9k}–OH, MeO–PEG_{9k}–OMe, HS–PEG_{9k}–OMe, or *c*-PEG_{9k} (10.5 mg) in a 50 mL Falcon tube. The mixture was vortexed for 1 min to form $AgNPs_{10}$/HO–PEG_{9k}–OH, $AgNPs_{10}$/MeO–PEG_{9k}–OMe, $AgNPs_{10}$/HS–PEG_{9k}–OMe, or $AgNPs_{10}$/*c*-PEG_{9k}, respectively, where the PEG concentration was 0.25 wt%. $AgNPs_{10}$/No PEG was prepared by diluting AgNPs (2.1 mL) with deionized water (2.1 mL) and vortexed for 1 min. The mixtures were kept under 860–990 lux light intensity using a white light emitting tube at 25 °C for 35 d. 0.60 mL of the mixtures was withdrawn from the falcon tubes immediately after mixing (day 0) and subsequently at a 7-day interval for an absorption measurement and did not return to the tubes.

2.2.17 Stability Against Various Temperatures

An aqueous dispersion of $AgNPs_{10}$ (0.30 mL) was two times diluted with deionized

water (0.30 mL) and added to HO–PEG$_{9k}$–OH, MeO–PEG$_{9k}$–OMe, HS–PEG$_{9k}$–OMe, or *c*-PEG$_{9k}$ (1.5 mg) in a 1.5 mL Eppendorf tube. The mixture was vortexed for 1 min to form AgNPs$_{10}$/HO–PEG$_{9k}$–OH, AgNPs$_{10}$/MeO–PEG$_{9k}$–OMe, AgNPs$_{10}$/HS–PEG$_{9k}$–OMe, or AgNPs$_{10}$/*c*-PEG$_{9k}$, respectively, where the PEG concentration was 0.25 wt%. AgNPs$_{10}$/No PEG was prepared by diluting AgNPs (0.30 mL) with deionized water (0.30 mL) and vortexed for 1 min. The mixtures were incubated for 4 h at 4, 37, or 95 °C, and UV–Vis absorption spectra were recorded.

2.2.18 TEM

A few drops from above AgNPs$_{10}$/No PEG, AgNPs$_{10}$/HS–PEG$_{9k}$–OMe, or AgNPs$_{10}$/*c*-PEG$_{9k}$ heated at 95 °C for 4 h were paced on a carbon coated Formvar TEM grid and blown away with a blower. Measurements were performed with a Japan Electron Optics Laboratory JEM-2010 operated at 200 kV.

2.2.19 Antimicrobial Activity

E. coli was grown in a Muller Hinton Broth (MHB) medium containing ampicillin (100 μg/mL) at 37 °C for 24 h and standardized using 0.5 McFarland standard (10^8 CFU/mL). A tenfold-concentrated PBS solution (300 μL, pH 7.4, NaCl 1500 mM) was added to AgNPs$_{10}$/No PEG, AgNPs$_{10}$/HO–PEG$_{9k}$–OH, AgNPs$_{10}$/MeO–PEG$_{9k}$–OMe, AgNPs$_{10}$/HS–

PEG$_{9k}$–OMe, or AgNPs$_{10}$/*c*-PEG$_{9k}$ (2.7 mL) with a PEG concentration of 0.25 wt% and incubated for 24 h. The resulting mixture was centrifuged at 3000 rpm for 20 min, and the supernatant or dispersion was ultrafiltrated to reduce the volume to 100 μL and mixed with 10 μL of 10^5 CFU/mL *E. coli* in a 1.5 mL Eppendorf tube. The mixture was added to a test tube containing a MHB medium (2.9 mL) and incubated at 37 °C and 200 rpm for 24 h. UV–Vis absorption spectra were recorded.

2.2.20 Cytotoxicity

HO–PEG$_{9k}$–OH, MeO–PEG$_{9k}$–OMe, HS–PEG$_{9k}$–OMe, or *c*-PEG$_{9k}$ was dissolved into DMEM (FBS (–)) at a concentration of 5 mg/mL. The PEG solution was mixed with an aqueous dispersion of AgNPs (20 μg/mL) at a 1:1 volume ratio. The mixture was diluted with DMEM (FBS (–)) by 10-fold for the final concentrations of AgNPs (1.0 μg/mL) and of PEG (0.25 mg/mL). For AgNPs/No PEG, AgNPs (20 μg/mL) was diluted with DMEM (FBS (–)) to form AgNPs (1.0 μg/mL). HeLa cells were cultured in cell culture dishes (Eppendorf) containing DMEM with 10% FBS, 100 U/mL penicillin, and 100 μg/mL streptomycin at 37 °C in 5% CO_2. For the cell viability assay, the cells were seeded at a concentration of 6×10^3 per well in a 96 well microplate (Thermo scientific) and grown for 24 h. The cells were treated with 100 μL of AgNPs$_{10}$/No PEG, AgNPs$_{10}$/HO–PEG$_{9k}$–OH, AgNPs$_{10}$/MeO–PEG$_{9k}$–

OMe, AgNPs$_{10}$/HS–PEG$_{9k}$–OMe, or AgNPs$_{10}$/*c*-PEG$_{9k}$ followed by incubation for 2 h at 37 °C in 5% CO_2. After the incubation, the cells were washed with D-PBS (–), and the medium was replaced with 100 μL of fresh DMEM (FBS (+)). The cells were additionally incubated for 24 h at 37 °C in 5% CO_2. The cell viability was measured using CellTiter-Glo 2.0 Cell Viability Assay kit (Promega) according to the manufacture's protocol.

2.2.21 Cell scratch assay

AgNPs$_{10}$/No PEG, AgNPs$_{10}$/HO–PEG$_{9k}$–OH, AgNPs$_{10}$/MeO–PEG$_{9k}$–OMe, AgNPs$_{10}$/HS–PEG$_{9k}$–OMe, and AgNPs$_{10}$/*c*-PEG$_{9k}$ were prepared in the same manner as the cell viability assay with the final concentrations of AgNPs (1.0 μg/mL) and of PEG (0.25 mg/mL) in DMEM (FBS (–)). HeLa cells were seeded at a concentration of 8×10^4 per well in a 24 well microplate (Corning) and grown for 24 h. The cells were treated with 250 μL of AgNPs$_{10}$/No PEG, AgNPs$_{10}$/HO–PEG$_{9k}$–OH, AgNPs$_{10}$/MeO–PEG$_{9k}$–OMe, AgNPs$_{10}$/HS–PEG$_{9k}$–OMe, or AgNPs$_{10}$/*c*-PEG$_{9k}$ followed by incubation for 2 h at 37 °C in 5% CO_2. After incubation, the cells were washed with D-PBS (–) and scratched using a pipette tip followed by washing with D-PBS (–). The medium was replaced with 100 μL of fresh DMEM (FBS (+)). The scratched regions were observed using a microscope (BZ-X800, Keyence). Subsequently, the cells were incubated for 22 h at 37 °C in 5% CO_2, and the scratched regions

were measured again.

2.3. Results and Discussion

2.3.1 Synthesis of *c*-PEG and MeO–PEG–OMe

HO–PEG–OH with a molecular weight of 2, 3, and 9 kDa (HO–PEG_{2k}–OH, HO–PEG_{3k}–OH, and HO–PEG_{9k}–OH, respectively) was successfully cyclized by etherification. Thus, the chain ends of HO–PEG–OH were intramolecularly connected in the presence of tosyl chloride and potassium hydroxide in dilution. Highly pure *c*-PEG_{2k}, *c*-PEG_{3k}, and *c*-PEG_{9k} were obtained after column chromatography and repeated separation using dichloromethane and *n*-heptane. SEC of *c*-PEG showed a unimodal trace with a peak shift to the lower molecular weight region compared to the prepolymer HO–PEG–OH (Fig. 2.2). The decrease in the hydrodynamic volume resulting from cyclization caused the shift in the apparent molecular weight. For example, $M_{p,SEC}$ decreased from 9640 of HO–PEG_{9k}–OH to 6040 of *c*-PEG_{9k} (Table 2.1, Fig. 2.2c).

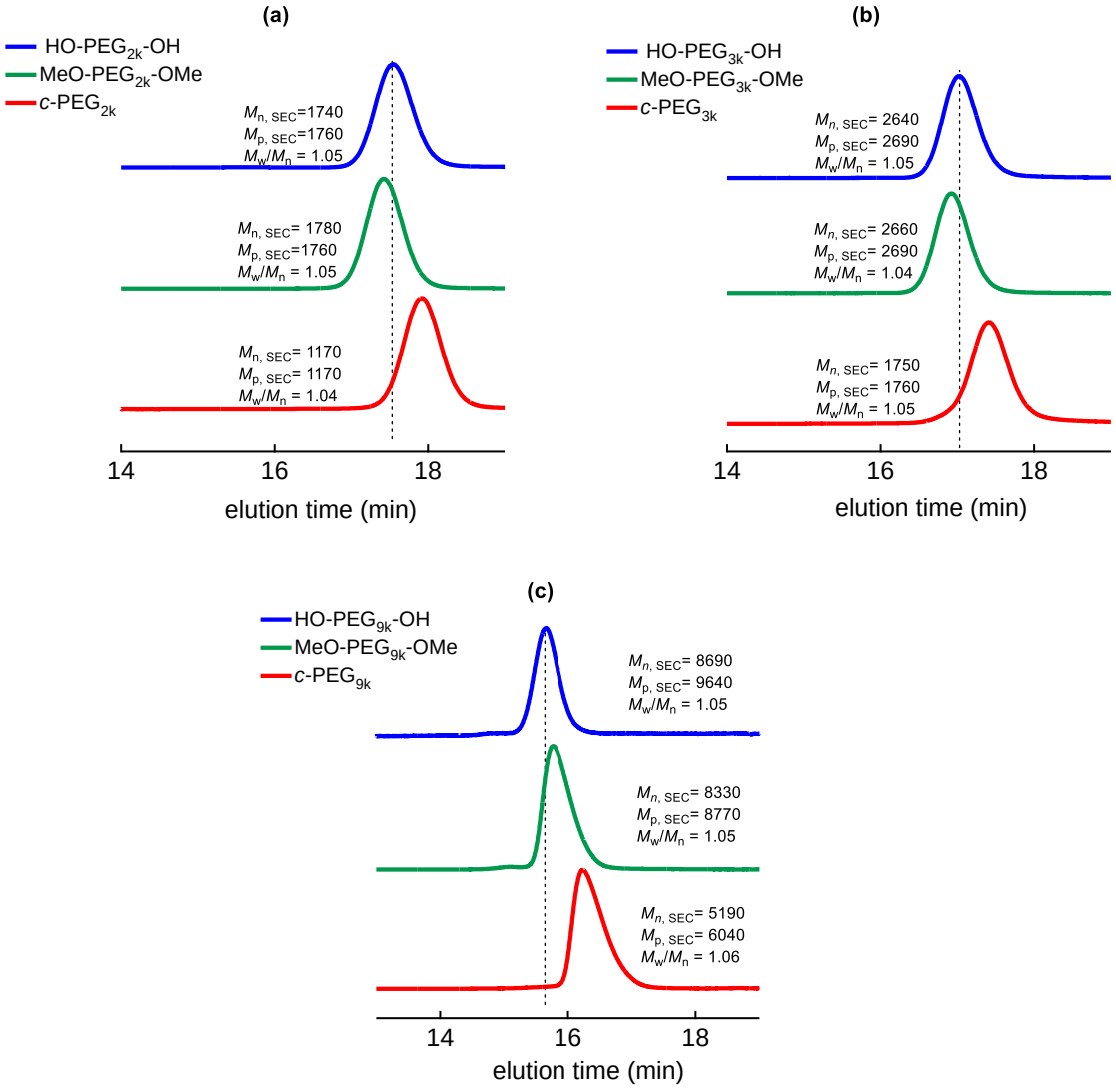

Fig 2.2 SEC traces of HO–PEG–OH (blue), MeO–PEG–OMe (green) and *c*-PEG (red) with a molecular weight of (a) 2, (b) 3, and (c) 9 kDa.

^{13}C NMR spectra showed a complete disappearance of the peaks at 61.8 and 72.5 ppm from the carbon atoms adjacent to the hydroxyl end groups of HO–PEG–OH, thus confirming the elimination of the chain ends (Fig. 2.3).

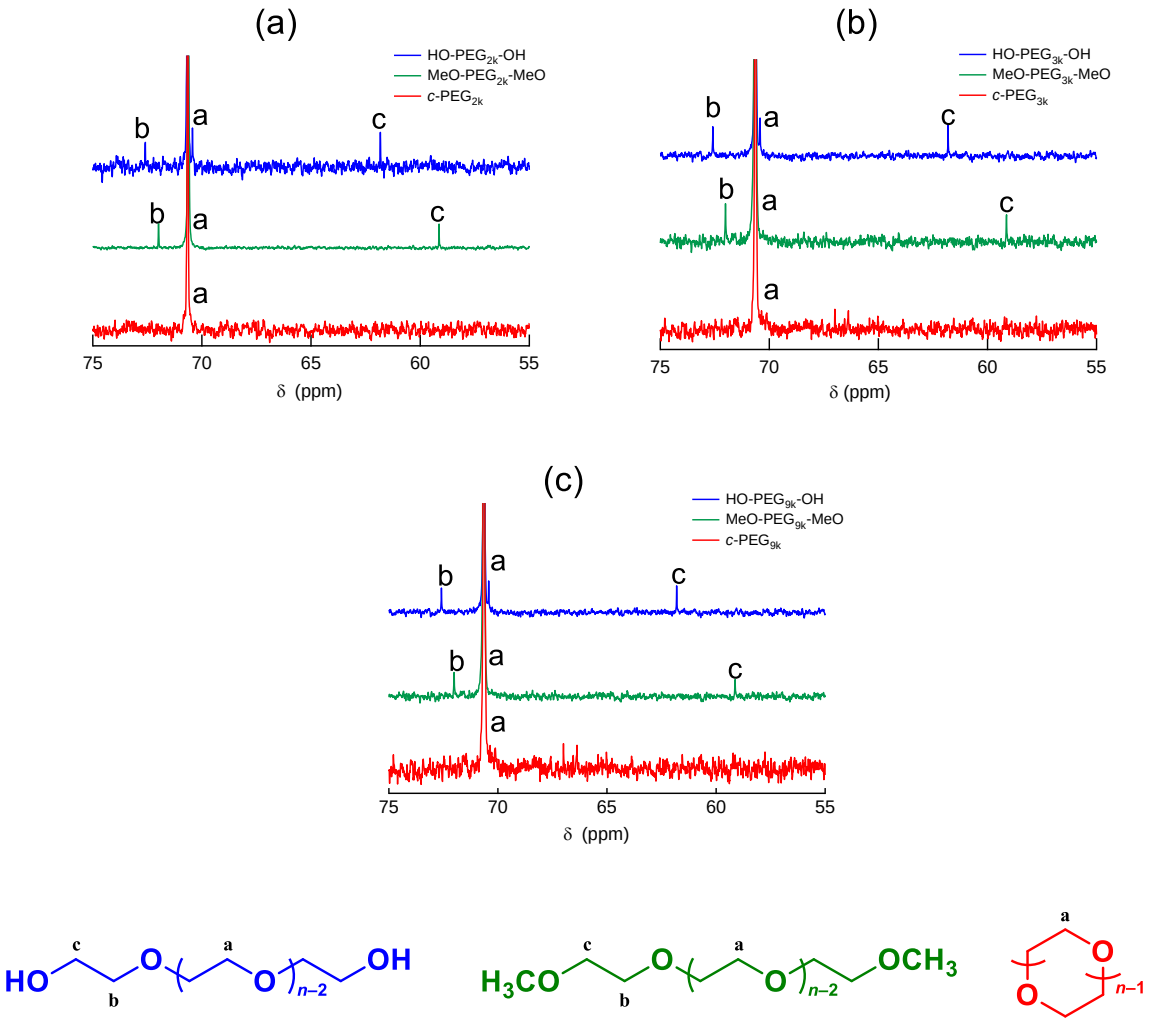

Fig. 2.3 ^{13}C NMR spectra of HO–PEG–OH (blue), MeO–PEG–OMe (green), and *c*-PEG (red) with a molecular weight of (a) 2, (b) 3, and (c) 9 kDa.

^{1}H NMR of *c*-PEG also gave a single peak unlike that of HO–PEG–OH, which showed the distinguishable signals from the methylene protons close to the chain ends (Fig. 2.4).

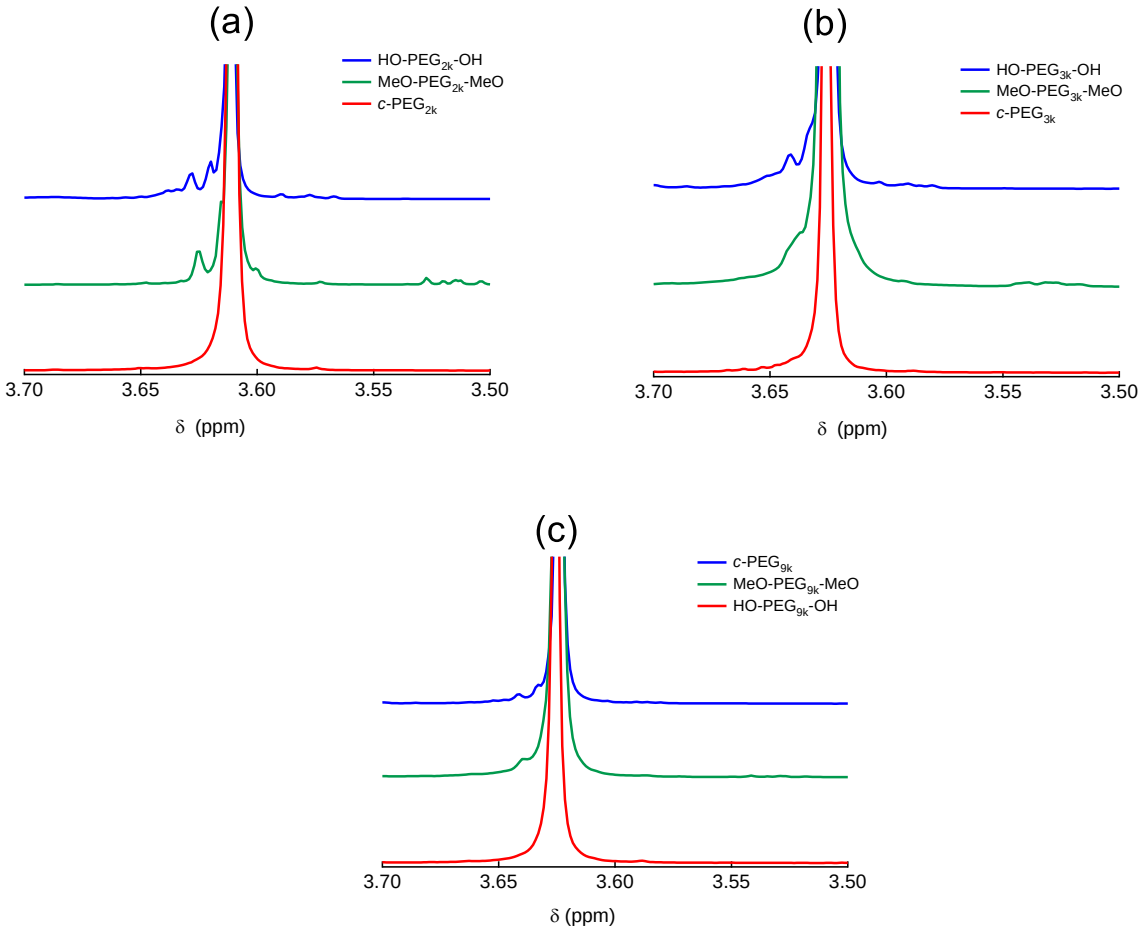

Fig. 2.4 ^{1}H NMR spectra of HO–PEG–OH (blue), MeO–PEG–OMe (green), and *c*-PEG (red) with a molecular weight of (a) 2, (b) 3, and (c) 9 kDa.

MALDI-TOF mass spectrometry of *c*-PEG and HO–PEG–OH further gave a striking difference in their isotopic distributions (Fig. 2.5). For example, HO–PEG_{2k}–OH gave a peak at m/z = 2062.13 for $[HO(C_2H_4O)_{44}H + Ag]^+$, where Ag^+ was from silver trifluoroacetate, an ionization agent, whereas *c*-PEG_{2k} had a peak at m/z = 2044.26 for $[(C_2H_4O)_{44} + Ag]^+$ with a difference arising from the elimination of a water molecule. However, a MALDI-TOF mass spectrum for PEG_{9k} was not obtainable due to its large molecular weight.

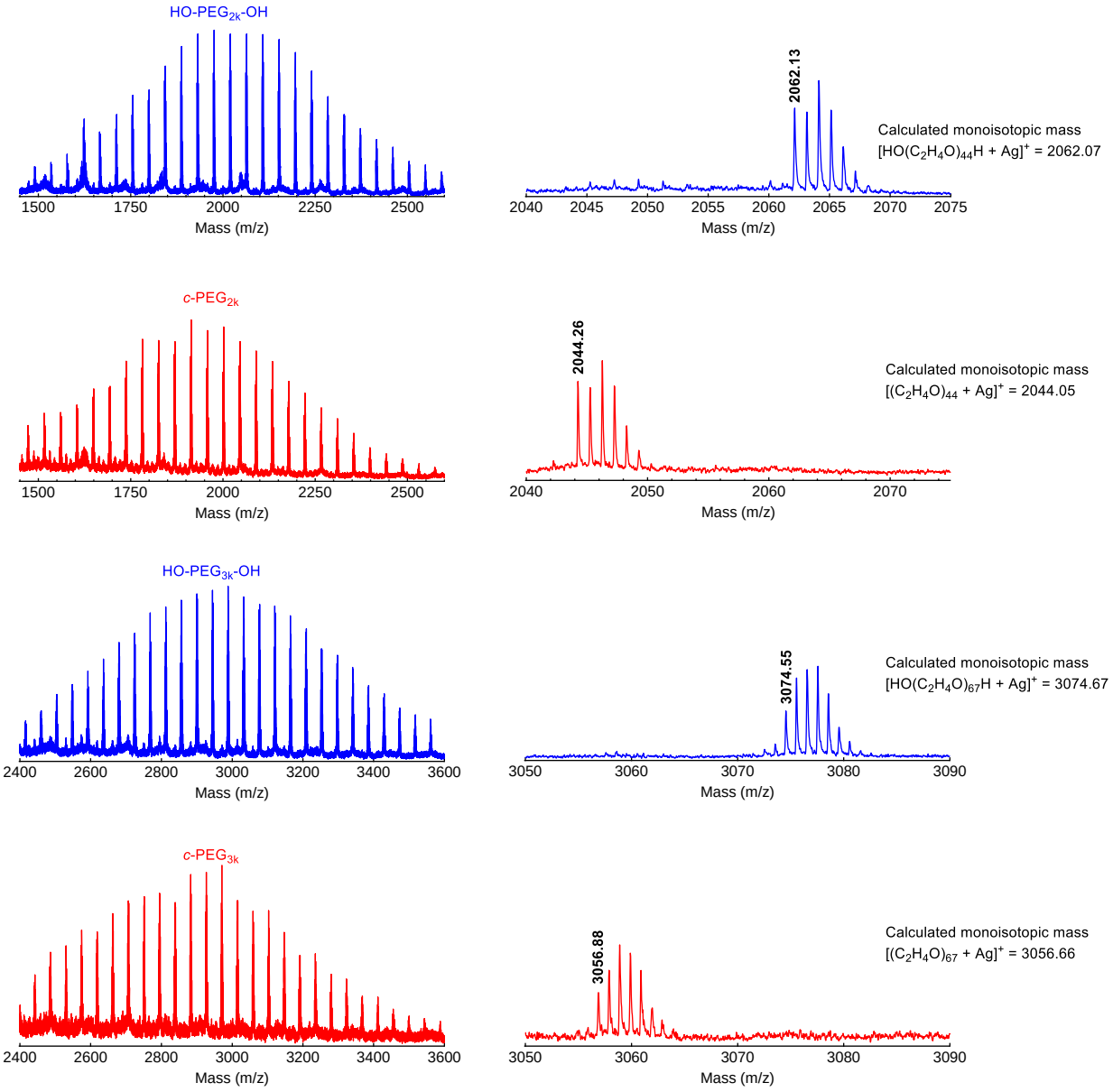

Fig. 2.5 MALDI-TOF mass spectra of HO–PEG–OH (blue) and *c*-PEG (red) with a molecular weight of (a) 2 and (b) 3kDa.

The expected diameter of *c*-PEG$_{2k}$, *c*-PEG$_{3k}$, and *c*-PEG$_{9k}$ was 4.5, 6.8, and 22 nm, respectively, when they form an ideal right circular conformation. Furthermore, methylation of HO–PEG–OH resulted in successful synthesis of MeO–PEG–OMe with features similar to its precursor HO–PEG–OH in term of the appearance of the carbon atoms adjacent to the methoxy ends group (Fig. 2.3). UV–Vis spectroscopy showed no absorbance from any of these PEG at 300–800 nm in wavelength (Fig. 2.6), suggesting the PEG samples are free of impurity and suitable for optical investigations of AgNPs.

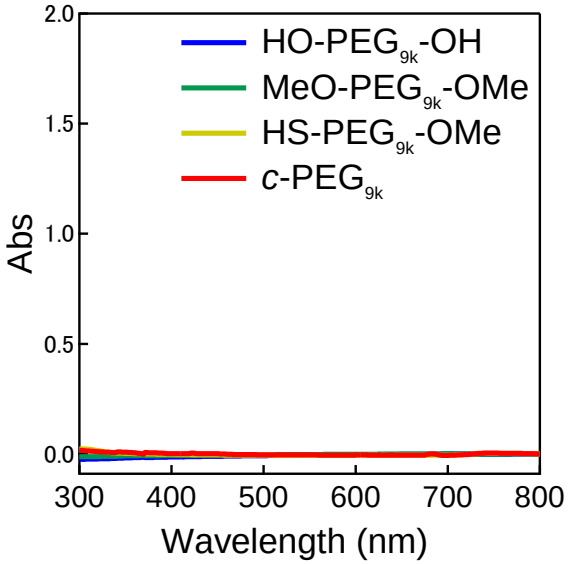

Fig. 2.6 UV–Vis spectra of HO–PEG$_{9k}$–OH (blue), MeO–PEG$_{9k}$–OMe (green), HS–PEG$_{9k}$–OMe (yellow), and *c*-PEG$_{9k}$ (red).

Table 2.1. Properties of PEG by SEC

	$M_{n,SEC}$[a] (g mol^{-1})	$M_{p,SEC}$[a] (g mol^{-1})	M_w/M_n	Ideal diameter of *c*-PEG (nm)
HO–PEG$_{2k}$–OH	1740	1760	1.05	–
MeO–PEG$_{2k}$–OMe	1780	1760	1.05	–
HS–PEG$_{2k}$–OMe	1690	1760	1.05	–
c-PEG$_{2k}$	1170	1170	1.04	4.5
HO–PEG$_{3k}$–OH	2640	2690	1.05	–
MeO–PEG$_{3k}$–OMe	2660	2690	1.04	–
c-PEG$_{3k}$	1750	1760	1.05	6.8
HO–PEG$_{9k}$–OH	8690	9640	1.05	–
MeO–PEG$_{9k}$–OMe	8330	8770	1.05	–
HS–PEG$_{9k}$–OMe	9480	9640	1.04	–
c-PEG$_{9k}$	5190	6040	1.06	22

[a]Determined by SEC in THF using PEG standards.

2.3.2 Physisorption of c-PEG to AgNPs

According to the procedure previously established,[43] HO–PEG–OH, MeO–PEG–OMe, HS–PEG–OMe, or *c*-PEG with a molecular weight of 2, 3, or 9 kDa, (PEG$_{2k}$, PEG$_{3k}$, or PEG$_{9k}$, respectively), was simply mixed with an aqueous dispersion of AgNPs with a size of 10, 20, or 30 nm (AgNPs$_{10}$, AgNPs$_{20}$, or AgNPs$_{30}$, respectively). The addition of HO–

PEG–OH, MeO–PEG–OMe, or *c*-PEG to AgNPs had no effect on the surface plasmon resonance (SPR) shown in Fig. 2.7a. The UV–Vis absorption spectra and visual color were almost identical to an AgNPs dispersion without PEG, and λ_{max} remained at 398 nm. On the other hand, the addition of HS–PEG$_{9k}$–OMe abruptly reduced the absorption, broaden the peak, and deepen the yellow color of the AgNPs dispersion to yellowish brown. This change in SPR is explained as a result of increase in the local dielectric environment upon thiol coordination to the Ag surface.[19]

DLS and ζ-potential measurements proved distinct formation of a *c*-PEG layer on the surface of AgNPs as in the case of AuNPs.[43] Thus, by DLS, AgNPs$_{10}$/No PEG had a size of 18 nm, which on addition of HO–PEG$_{9k}$–OH and MeO–PEG$_{9k}$–OMe sightly enlarged to 24 and 20 nm, respectively (Fig. 2.1, Table 2.1). On the other hand, a significant increase was seen for AgNPs$_{10}$/HS–PEG$_{9k}$–OMe with 71 nm and AgNPs$_{10}$/*c*-PEG$_{9k}$ with 109 nm. Moreover, an increase in the size with increase in molecular weight of *c*-PEG was evident. In the case of AgNPs$_{10}$, complexation with *c*-PEG$_{2k}$, *c*-PEG$_{3k}$, and *c*-PEG$_{9k}$ resulted in 35, 77, and 109 nm in size, respectively. This molecular weight dependence is consistent with the previously reported adsorption of cyclic PEG and cyclic poly(dimethylsiloxane) on silica.[45, 46] When AgNPs$_{20}$ and AgNPs$_{30}$ were used with *c*-PEG$_{9k}$ (73 and 71 nm, respectively),

the increase in size was less intense compared to $AgNPs_{10}$ (109 nm). Thus, *c*-PEG_{9k} with a diameter of 22 nm in the ideal right circular conformation exhibited the strongest interaction to $AgNPs_{10}$ with a size of 18 nm.

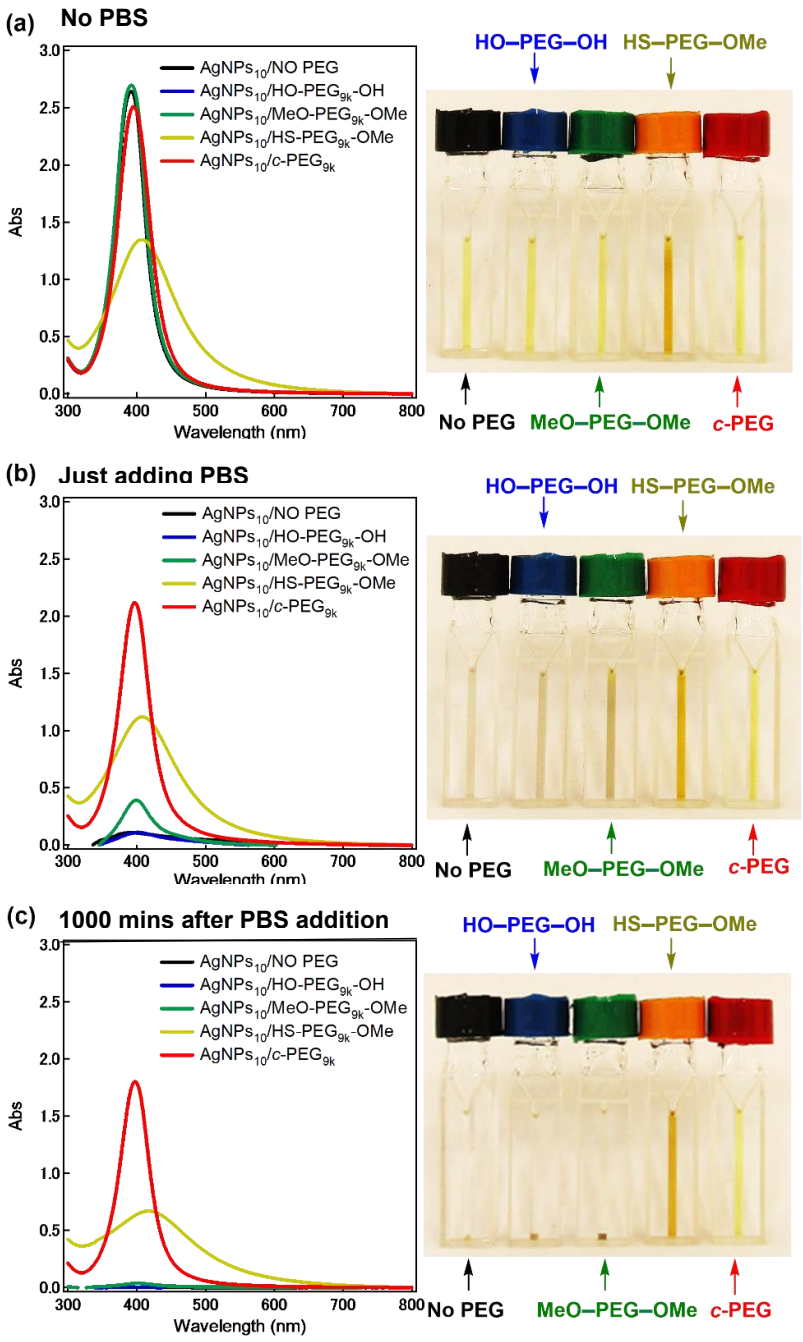

Fig. 2.7 Stability test of AgNPs/PEG against a physiological condition (PBS with pH 7.4 and a NaCl concertation of 150 mM). UV–Vis spectra and photographs of $AgNPs_{10}$/No PEG (black), $AgNPs_{10}$/HO–PEG_{9k}–OH (blue), $AgNPs_{10}$/MeO–PEG_{9k}–OMe (green), $AgNPs_{10}$/HS–PEG_{9k}–OMe (yellow/orange), and $AgNPs_{10}$/*c*-PEG_{9k} (red) with a PEG concentration of 0.25 wt% (a) before (b) immediately after and (c) 1000 min after the addition of a concentrated PBS solution. The resulting dispersions were pH 7.4 and 150 mM of NaCl.

Table 2.2. DLS size of AgNPs/No PEG, AgNPs/HO–PEG–OH, AgNPs/MeO–PEG–OMe, AgNPs/HS–PEG–OMe, and AgNPs/*c*-PEG with various AgNPs sizes and PEG molecular weights[a]

	$AgNPs_{10}$	$AgNPs_{20}$	$AgNPs_{30}$
AgNP/No PEG	18	26	35
HO–PEG_{2k}–OH	19	30	36
HO–PEG_{3k}–OH	23	35	41
HO–PEG_{9k}–OH	24	33	38
MeO–PEG_{2k}–OMe	32	36	40
MeO–PEG_{3k}–OMe	32	34	38
MeO–PEG_{9k}–OMe	20	32	41
HS–PEG_{2k}–OMe	43	51	49
HS–PEG_{9k}–OMe	71	59	59
c-PEG_{2k}	35	35	45
c-PEG_{3k}	77	45	49
c-PEG_{9k}	109	73	71

[a]Units are in nm.

Due to citrate anions existing at the surface of AgNPs, the ζ-potential of $AgNPs_{10}$/No PEG showed a negative value of –31 mV, which on addition of non-ionic PEG reduced to –25 mV for $AgNPs_{10}$/HO–PEG_{9k}–OH and –16 mV for $AgNPs_{10}$/MeO–PEG_{9k}–OMe (Table 2.3). A neutral PEG layer on the surface was reported to shield the negative charges of citrate

to decrease in the magnitude of the ζ-potential.[53] A near zero potential was seen for AgNPs$_{10}$/HS–PEG$_{9k}$–OMe and AgNPs$_{10}$/*c*-PEG$_{9k}$ with –2 mV. This suggests that chemisorption of HS–PEG$_{9k}$–OMe and physisorption of *c*-PEG to the surface of AgNPs shield the charge more efficiently. A significant decrease in magnitude of the ζ-potential by the addition of *c*-PEG was also previously observed in AuNPs.[43] Furthermore, an increase in molecular weight led to a reduction in the ζ-potential: AgNPs$_{10}$/*c*-PEG$_{2k}$ gave –12 mV, AgNPs$_{10}$/*c*-PEG$_{3k}$ was –6 mV, and a further reduction to –2 mV in AgNPs$_{10}$/*c*-PEG$_{9k}$. Thus, a thicker layer formed by *c*-PEG with a higher molecular weight shielded the charge more effectively.

The adsorption of *c*-PEG on AgNPs is probably an enthalpically favorable and entropically unfavorable process. Because the number of the conformations of *c*-PEG in the unadsorbed state is limited compared to that of HO–PEG–OH and MeO–PEG–OMe, the entropic loss upon the adsorption of *c*-PEG is expected to be smaller.[45-51] On the other hand, the adsorption enthalpy would be similar for both *c*-PEG and the linear counterparts because they have the same chemical structure of the repeating units and the same molecular weight. Based on these, the total adsorption free energy change is likely larger in negative value for *c*-PEG.

Table 2.3. ζ-potential of AgNPs/No PEG, AgNPs/HO–PEG–OH, AgNPs/MeO–PEG–OMe, AgNPs/HS–PEG–OMe, and AgNPs/*c*-PEG with various AgNPs sizes and PEG molecular weights[a]

	$AgNPs_{10}$	$AgNPs_{20}$	$AgNPs_{30}$
AgNP/No PEG	–31	–33	–40
HO–PEG_{2k}–OH	–23	–27	–31
HO–PEG_{3k}–OH	–24	–24	–26
HO–PEG_{9k}–OH	–25	–29	–33
MeO–PEG_{2k}–OMe	–26	–34	–35
MeO–PEG_{3k}–OMe	–28	–36	–33
MeO–PEG_{9k}–OMe	–16	–20	–22
HS–PEG_{2k}–OMe	–18	–17	–18
HS–PEG_{9k}–OMe	–2	–1	–1
c-PEG_{2k}	–12	–13	–15
c-PEG_{3k}	–6	–10	–9
c-PEG_{9k}	–2	–2	–2

[a]Units are in mV.

2.3.3 Enhancement of the Dispersion Stability

Subsequently, dispersion stability of $AgNPs_{10}$/No PEG, $AgNPs_{10}$/HO–PEG_{9k}–OH, $AgNPs_{10}$/MeO–PEG_{9k}–OMe, $AgNPs_{10}$/HS–PEG_{9k}–OMe, and $AgNPs_{10}$/*c*-PEG_{9k} with a PEG

concentration of 0.25 wt% under a physiological condition was investigated. On addition of a tenfold-concentrated PBS solution (0.06 mL) to each AgNPs dispersion (0.54 mL) to form an intended physiological condition (pH 7.4 and a NaCl concentration of 150 mM), there was an immediate color change from yellow to light brown by $AgNPs_{10}$/No PEG and $AgNPs_{10}$/HO–PEG_{9k}–OH or to dark brown by $AgNPs_{10}$/MeO–PEG_{9k}–OMe (Fig. 2.7b), which was followed by precipitation. The dark yellow color by $AgNPs_{10}$/HS–PEG_{9k}–OMe remained unchanged. Remarkably, $AgNPs_{10}$/*c*-PEG_{9k} exhibited only a slight color change and nearly preserved the initial yellow color even after 1000 min. UV–Vis spectroscopy showed only a minor decrease in absorption of $AgNPs_{10}$/*c*-PEG_{9k} on addition and after 1000 min, whereas there was essentially no absorption from $AgNPs_{10}$/No PEG, $AgNPs_{10}$/HO–PEG_{9k}–OH, or $AgNPs_{10}$/MeO–PEG_{9k}–OMe due to precipitation (Fig. 2.7c). The relative absorption intensity (Rel. Abs) calculated by dividing the absorption value at λ_{max} after 1000 min by that before the addition of PBS was 75% for $AgNPs_{10}$/*c*-PEG_{9k}. The presence of NaCl in PBS has been well reviewed as a causative factor of aggregation of metal nanoparticles, but properly performed PEGylation can avoid aggregation.[54] Thus, *c*-PEG_{9k} protected AgNPs by physiosorbed to the surface thereby preventing agglomeration in the presence of increased ionic strength. In the meantime, a significant reduction in the UV–Vis absorption spectra of

$AgNPs_{10}$/HS–PEG_{9k}–OMe was evident after 1000 min (Rel. Abs = 48%), which was likely caused by dissolution of AgNPs in the presence of thiol.[18]

Subsequently, the stabilization effect depending on the molecular weight of *c*-PEG was investigated. Fig. 2.8a shows Rel. Abs versus time for $AgNPs_{10}$/*c*-PEG_{2k}, $AgNPs_{10}$/*c*-PEG_{3k}, and $AgNPs_{10}$/*c*-PEG_{9k} in a PBS buffer solution with pH 7.4 and a NaCl concentration of 150 mM. A significant increase in the dispersion stability was observed with an increase in the molecular weight. Rel. Abs after 1000 min for $AgNPs_{10}$/*c*-PEG_{9k} retains 74%, while $AgNPs_{10}$/*c*-PEG_{3k} was only 39%, and $AgNPs_{10}$/*c*-PEG_{2k} also showed a weak stabilization with Rel. Abs of 37%. Moreover, the concentration of *c*-PEG_{9k} was varied from 0.05 to 1.25 wt% (Fig. 2.8b). At 0.05 wt%, a continuous decrease in absorbance was seen, and Rel. Abs was 19% after 1000 min. In the meantime, at 0.25 wt% and higher concentrations, there was a much smaller change in time course (Rel. Abs $\geq$ 76% after 1000 min). At a *c*-PEG concentration of 0.05 wt%, an insufficient amount of *c*-PEG existed in the dispersion as the surface of AgNPs was scarcely covered. At the concentration of 0.25 wt% and higher, the amount of *c*-PEG was satisfactory to form a thick enough layer on the surface of AgNPs, thereby enhancing the dispersion stability. The *c*-PEG layer thickness was likely saturated at 0.25 wt%, and this phenomenon was previously observed for AuNPs.[43] Furthermore, the

stability in relation to the size of AgNPs was also examined. Fig. 2.8c shows that *c*-PEG$_{9k}$ can stabilize AgNPs$_{10}$, AgNPs$_{20}$, and AgNPs$_{30}$, which have a size of 10, 20 and 30 nm, respectively. However, stability was best conferred in AgNPs$_{10}$/*c*-PEG$_{9k}$ with Rel. Abs of 82% after 1000 min compared to AgNPs$_{20}$/*c*-PEG$_{9k}$ (Rel. Abs = 60%) and AgNPs$_{30}$/*c*-PEG$_{9k}$ (Rel. Abs = 57%). I showed above that the DLS size and ζ-potential depending on the molecular weight and AgNPs size (Tables 2.2 and 2.3); *c*-PEG$_{9k}$ formed a thicker layer than *c*-PEG$_{2k}$ and *c*-PEG$_{3k}$, on AgNPs$_{10}$ compared to AgNPs$_{20}$ and AgNPs$_{30}$. The dispersion stability against the physiological condition was in accord with the DLS size and ζ-potential; the thicker the PEG layer forms on AgNPs, the better the dispersion stability is. In accordance with these results, the following experiments were mainly performed with AgNPs$_{10}$/PEG$_{9k}$ with a polymer concentration of 0.25 wt%.

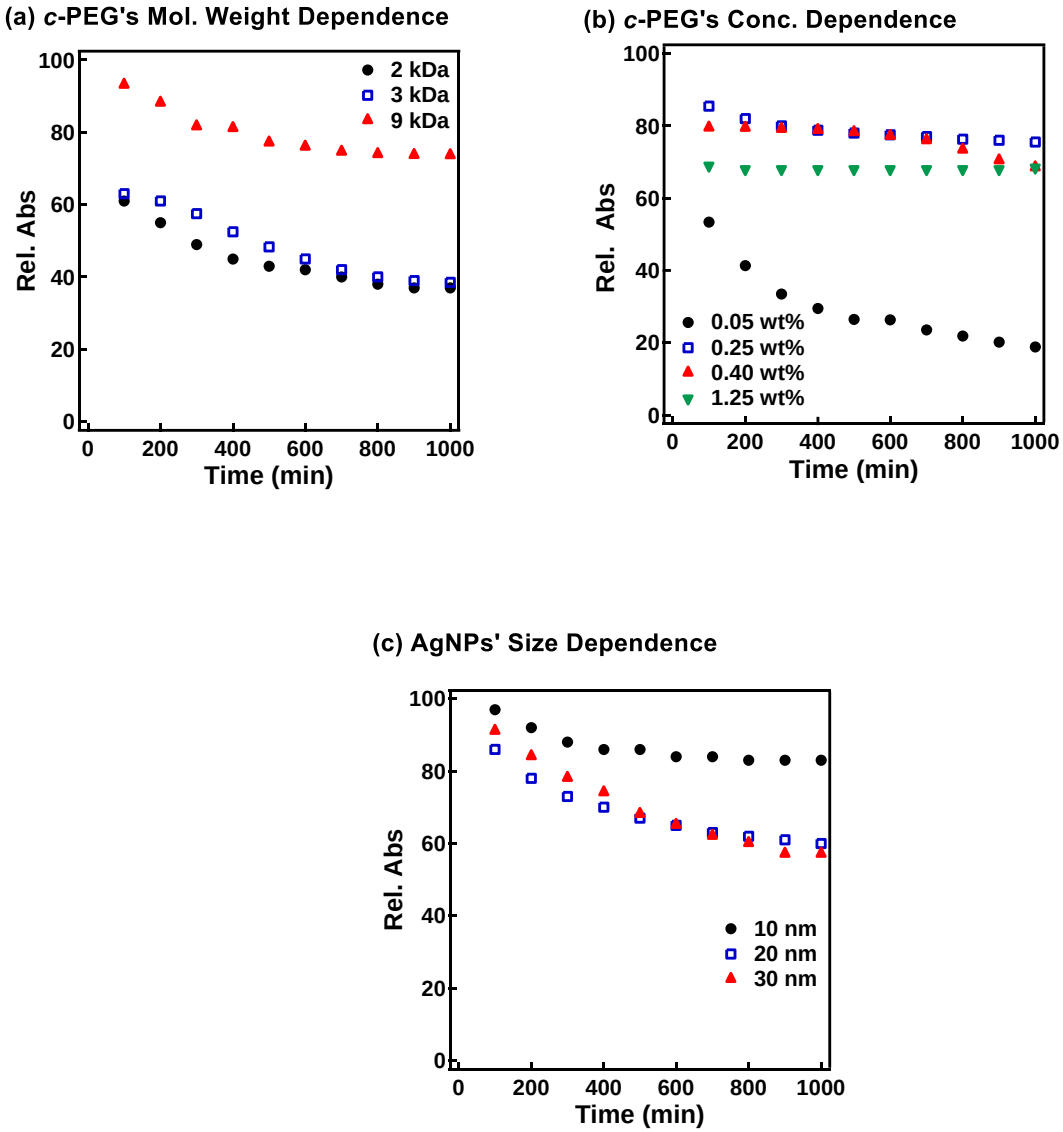

Fig. 2.8. Time course of the relative absorption intensity (Rel. Abs) of AgNPs/*c*-PEG in a physiological condition (PBS with pH 7.4 and a NaCl concertation of 150 mM). Rel. Abs was calculated by dividing the λ_{max} absorption value at given time by that before the addition of PBS. (a) *c*-PEG's molecular weight dependence tested by $AgNPs_{10}$/*c*-PEG_{2k}, $AgNPs_{10}$/*c*-PEG_{3k}, and $AgNPs_{10}$/*c*-PEG_{9k} with a PEG concentration of 0.25 wt%. (b) *c*-PEG_{9k}'s concentration dependence tested by $AgNPs_{10}$/*c*-PEG_{9k} with a PEG concentration of 0.05, 0.25, 0.40, and 1.25 wt%. (c) AgNPs' size dependence tested by $AgNPs_{10}$/*c*-PEG_{9k}, $AgNPs_{20}$/*c*-PEG_{9k}, and $AgNPs_{30}$/*c*-PEG_{9k} with a PEG concentration of 0.25 wt%.

Moreover, divalent ionic salts have been reported to exert stronger dissolution and agglomeration effects on nanoparticles than the monovalent counterparts.[55-57] On account of stabilization conferred to AgNPs by *c*-PEG$_{9k}$ against PBS with its main constituent as NaCl, I investigated the dispersion stability of AgNPs$_{10}$/No PEG, AgNPs$_{10}$/HO–PEG$_{9k}$–OH, AgNPs$_{10}$/MeO–PEG$_{9k}$–OMe, AgNPs$_{10}$/HS–PEG$_{9k}$–OMe, and AgNPs$_{10}$/*c*-PEG$_{9k}$ with a PEG concentration of 0.25 wt% against a 10 mM $CaCl_2$ solution. Similar to the case of the PBS experiment, *c*-PEG conferred stability to AgNPs after 1000 min with Rel. Abs of 78% (Fig. 2.9). On the other hand, AgNPs$_{10}$/No PEG, AgNPs$_{10}$/HO–PEG$_{9k}$–OH, and AgNPs$_{10}$/MeO–PEG$_{9k}$–OMe precipitated with Rel. Abs ~0%, while AgNPs$_{10}$/HS–PEG$_{9k}$–OMe with a shifted and broaden spectrum caused decrease in the absorption (Rel. Abs = 45%). This further proved strong dispersion stability endowed by *c*-PEG.

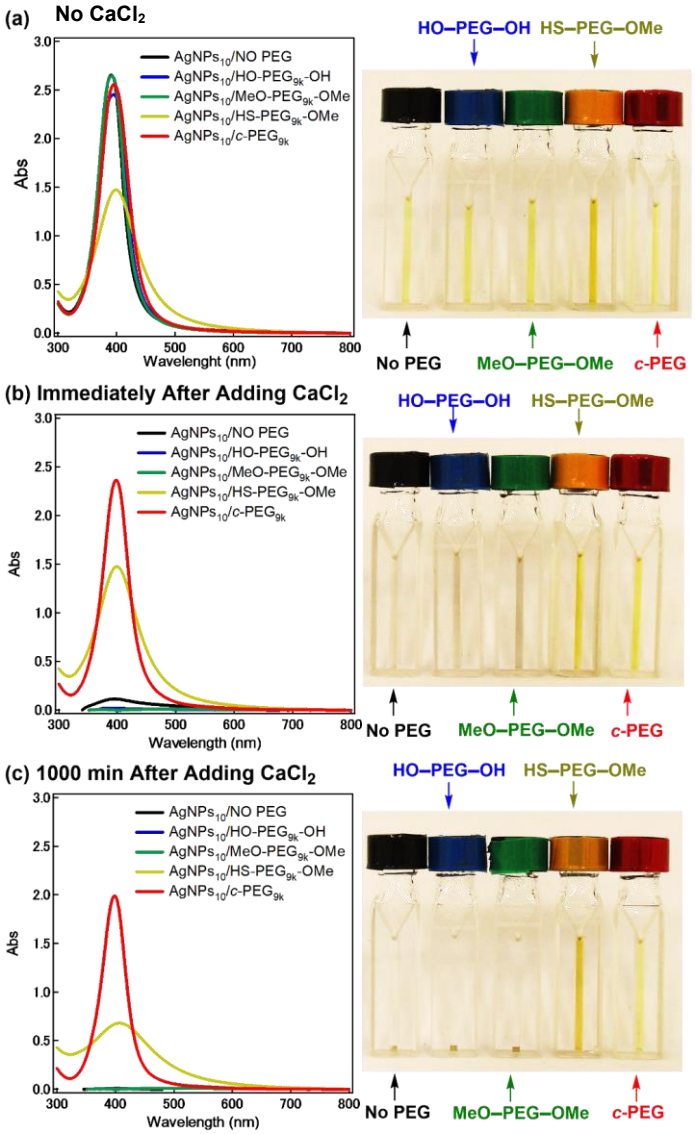

Fig. 2.9 Stability test of AgNPs/PEG against $CaCl_2$. UV–Vis spectra and photographs of $AgNPs_{10}$/No PEG (black), $AgNPs_{10}$/HO–PEG_{9k}–OH (blue), $AgNPs_{10}$/MeO–PEG_{9k}–OMe (green), $AgNPs_{10}$/HS–PEG_{9k}–OMe (yellow/orange), and $AgNPs_{10}$/*c*-PEG_{9k} (red) with a PEG concentration of 0.25 wt% (a) before (b) immediately after and (c) 1000 min after the addition of a concentrated $CaCl_2$ solution. The resulting dispersions had 10 mM of $CaCl_2$.

It was reported that the dissolution, aggregation, and secondary phase precipitation of AgNPs are caused by photoirradiation.[58] Thus, in production, storage, and applications, light is a well-known limiting factor which causes transformational changes of AgNPs.[59, 60] Also, emphasis is always made in the safety data sheets with respect to light. Thus, I tested the stability endowed by *c*-PEG against photoirradiation. $AgNPs_{10}$/No PEG, $AgNPs_{10}$/HO–PEG_{9k}–OH, $AgNPs_{10}$/MeO–PEG_{9k}–OMe, $AgNPs_{10}$/HS–PEG_{9k}–OMe, and $AgNPs_{10}$/*c*-PEG_{9k} with a PEG concentration of 0.25 wt% were exposed to white light at 860–990 lux (Fig. 2.10). $AgNPs_{10}$/No PEG (Fig. 2.10a), $AgNPs_{10}$/HO–PEG_{9k}–OH (Fig.2.10b), and $AgNPs_{10}$/MeO–PEG_{9k}–OMe (Fig. 2.10c) showed an initial reduction in absorbance at 398 nm, followed by an appearance of a new peak at 550 nm for AgNPs/No PEG and 460–495 nm for $AgNPs_{10}$/HO–PEG_{9k}–OH and $AgNP_{10}$/MeO–PEG_{9k}–OMe, which intensified with time. The appearance of $AgNPs_{10}$/No PEG (black-marked tube), $AgNPs_{10}$/HO–PEG_{9k}–OH (blue-marked tube), and $AgNPs_{10}$/MeO–PEG_{9k}–OMe (green-marked tube) changed from light yellow to deep yellow, which intensified as the days progressed via the aggregation of AgNPs (Fig. 2.10f, 2.10g, and 2.10h). The strong oscillating dipole–dipole interaction by photoirradiation reportedly causes aggregation.[61] On the other hand, no obvious change in the UV–Vis spectra in Fig. 4e suggests a superior protection of AgNPs by *c*-PEG_{9k} even after

35 d of exposure to white light, and there was no color change as it remained yellow (red-marked tube in Fig. 2.10f, 2.10g, and 2.10h). This was likely by that the thick *c*-PEG layer on the surface inhibited the contact of AgNPs to aggregate. In the meantime, AgNPs$_{10}$/HS–PEG$_{9k}$–OMe resulted in a reduced absorption of AgNPs immediately after mixing with HS–PEG$_{9k}$–OMe as seen above,[19] and subsequently gave nearly no absorption from the SPR on the day 7 and later (Fig. 2.10d). The apparent color changed from brownish yellow (orange-marked tube in Fig. 2.10f) to gray (Fig. 2.10g and 2.10h), which eventually turned to colorless. Moreover, it was also reported that AgNPs coated by PVP cannot withstand against photoirradiation, resulting in aggregation.[61] That is to say, the unique topology of *c*-PEG allows for physisorption to protect AgNPs from degrative reactions taken place at the surface caused by white light exposure.

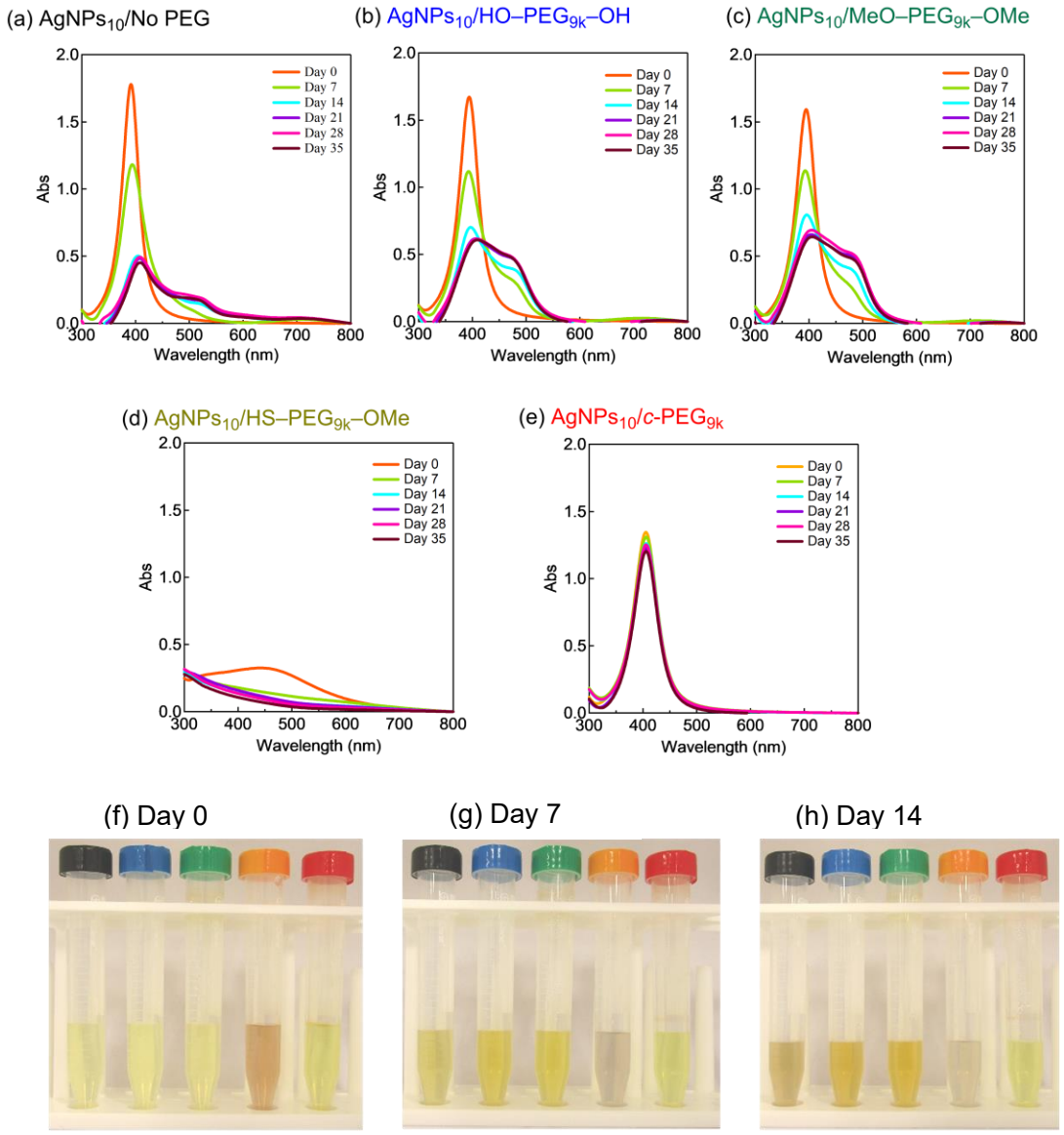

Fig. 2.10 Stability test of AgNPs/PEG against white light of 860–990 lux. UV–Vis spectra of (a) $AgNPs_{10}$/No PEG, (b) $AgNPs_{10}$/HO–PEG_{9k}–OH, (c) $AgNPs_{10}$/MeO–PEG_{9k}–OMe, (d) $AgNPs_{10}$/HS–PEG_{9k}–OMe, and (e) $AgNPs_{10}$/*c*-PEG_{9k} with a PEG concentration of 0.25 wt%. Photographs taken at (f) day 0, (g) day 7, and (h) day 14. In each photograph from left to right: $AgNP_{10}$/No PEG (black); $AgNP_{10}$/HO–PEG_{9k}–OH (blue); $AgNP_{10}$/MeO–PEG_{9k}–OMe (green); $AgNP_{10}$/HS–PEG_{9k}–OMe (orange); $AgNP_{10}$/*c*-PEG_{9k} (red).

It is also known that temperature is another important factor for the aggregation of AgNPs,[61] and stability against temperature would offer opportunities in various applications such as photothermal therapy.[62, 63] Thus, I furthermore tested the stabilization by *c*-PEG against heating. Keeping $AgNPs_{10}$/No PEG (Fig. 2.11a), $AgNPs_{10}$/HO–PEG_{9k}–OH (Fig. 2.11b), $AgNPs_{10}$/MeO–PEG_{9k}–OMe (Fig. 2.11c), or $AgNPs_{10}$/*c*-PEG_{9k} (Fig. 2.11e) at 4 and 37 °C for 4 h gave no change in the absorption spectra. On the other hand, $AgNPs_{10}$/HS–PEG_{9k}–OMe (Fig. 2.11d) showed a red shift and reduced absorption intensity at 4 °C as in the cases of the stability tests against PBS and $CaCl_2$.[18] Further decrease in the absorption spectra of $AgNPs_{10}$/HS–PEG_{9k}–OMe was seen when keep at 37 °C with a brownish color appearance (orange-marked tube in Fig. 2.11g). When the temperature was raised to 95 °C, $AgNPs_{10}$/No PEG, $AgNPs_{10}$/HO–PEG_{9k}–OH, and $AgNPs_{10}$/MeO–PEG_{9k}–OMe after 4 h resulted in Rel. Abs of 42%, 76%, and 72%, respectively, while $AgNPs_{10}$/HS–PEG_{9k}–OMe was only 5% (Fig. 2.11a–d). In contrast, $AgNPs_{10}$/*c*-PEG_{9k} had an insignificant change with Rel. Abs of 98% through the same condition (Fig. 2.11e). After heating at 95 °C for 4 h, $AgNPs_{10}$/No PEG and $AgNPs_{10}$/HS–PEG_{9k}–OMe turned colorless, $AgNPs_{10}$/HO–PEG_{9k}–OH and $AgNPs_{10}$/MeO–PEG_{9k}–OMe gave a slight faint yellow color, whereas $AgNPs_{10}$/*c*-PEG_{9k} remained the original yellow color (Fig. 2.11h).

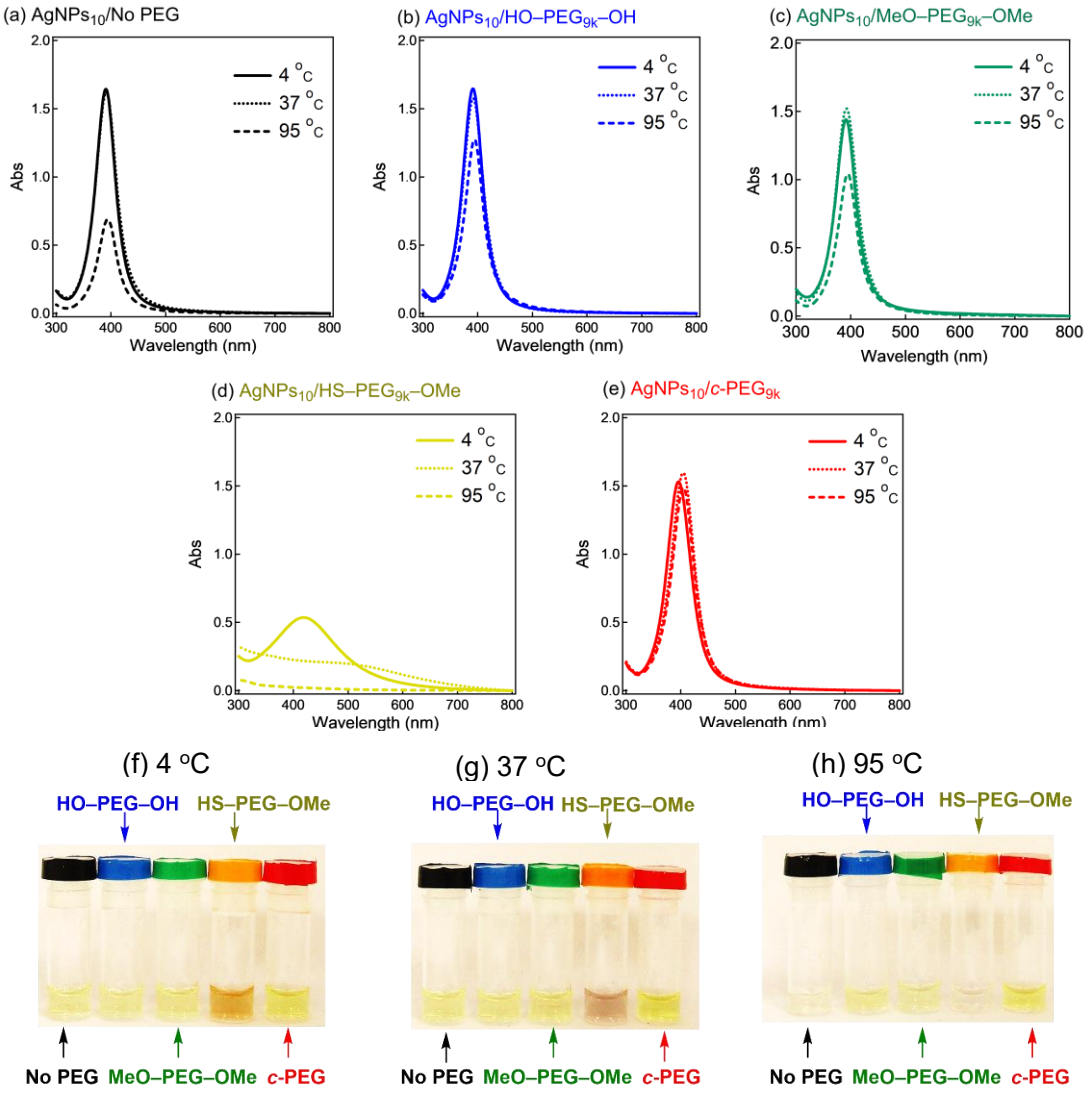

Fig. 2.11 Stability test of AgNPs/PEG against various temperatures. UV–Vis spectra of (a) $AgNPs_{10}$/No PEG, (b) $AgNPs_{10}$/HO–PEG_{9k}–OH, (c) $AgNPs_{10}$/MeO–PEG_{9k}–OMe, (d) $AgNPs_{10}$/HS–PEG_{9k}–OMe, and (e) $AgNPs_{10}$/*c*-PEG_{9k} with a PEG concentration of 0.25 wt% kept at 4, 37, and 95 °C for 4 h. Photographs of the experiments at (f) 4, (g) 37, and (h) 95 °C. In each photograph from left to right: $AgNP_{10}$/No PEG (black); $AgNP_{10}$/HO–PEG_{9k}–OH (blue); $AgNP_{10}$/MeO–PEG_{9k}–OMe (green); $AgNP_{10}$/HS–PEG_{9k}–OMe (yellow/orange); $AgNP_{10}$/*c*-PEG_{9k} (red).

Moreover, commercial $AgNPs_{80}$/HS–PEG_{5k}–OMe was also heated at 95 °C for 4 h, and there was no conferment of stability to AgNPs as reduction in absorption intensity with disappearance of the yellow color of AgNPs was seen (Fig. 2.12). This was in tandem with the above result of $AgNPs_{10}$/HS–PEG_{9k}–OMe and further proved the inability of HS–PEG in stabilization of AgNPs.

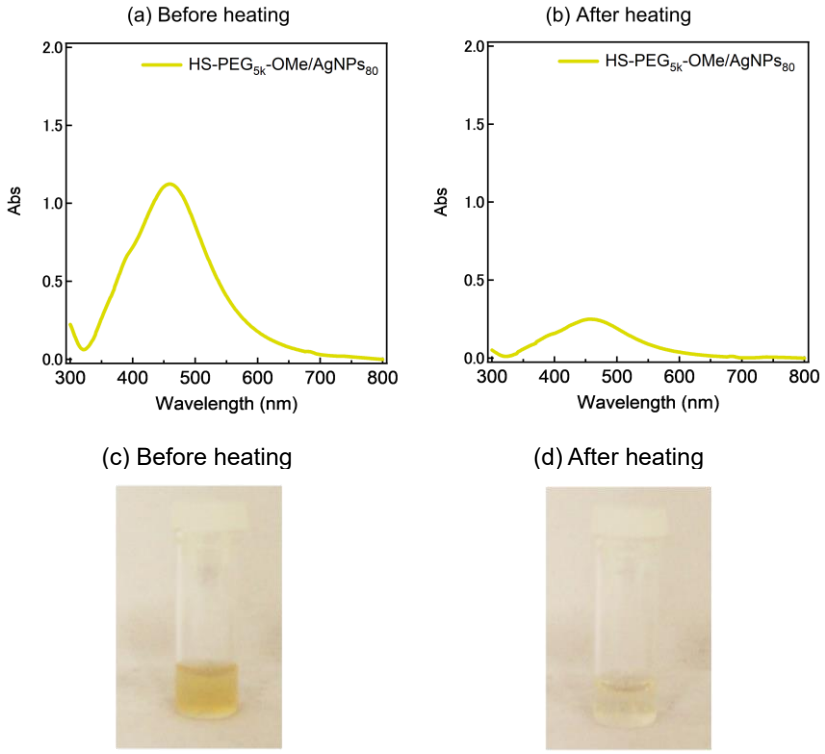

Fig. 2.12 Stability test of commercial $AgNPs_{80}$/HS–PEG_{5k}–OMe against heating. UV–Vis spectra of $AgNPs_{80}$/HS–PEG_{5k}–OMe (a) before heating and (b) after heating at 95 °C for 4 h. Photographs of $AgNPs_{80}$/HS–PEG_{5k}–OMe (c) before heating and (d) after heating at 95 °C for 4 h.

A TEM measurement of AgNPs$_{10}$/No PEG, AgNPs$_{10}$/HS–PEG$_{9k}$–OMe, and AgNPs$_{10}$/*c*-PEG$_{9k}$ kept at 95 °C for 4 h explained the effect of heating (Fig. 2.13). TEM photographs of AgNPs$_{10}$/No PEG showed aggregated AgNPs likely caused by the dipole–dipole interaction enhanced at the high temperature (Fig. 2.13d).[61] AgNPs$_{10}$/HS–PEG$_{9k}$–OMe after heating drastically also changed the form; particles with reduced size (≤5 nm) along with stain-like objects with a few hundred nanometer in size were observed. The coordination of thiol to AgNPs surface gives a Ag_2S layer.[18, 19] At high temperature, dissociation of Ag_2S from AgNPs was stimulated to reduce the median particle size shown in Fig. 2.13e. Moreover, the large stain-like objects were likely Ag_2S aggregated upon drying. What needs to be emphasized here is AgNPs$_{10}$/*c*-PEG$_{9k}$ after heating. These were intact with no significant change in size, and the particles were still well dispersed (Fig. 2.13f). Because each nanoparticle was isolated by the *c*-PEG layer formed on the surface, aggregation of AgNPs did not take place to keep the original size and shape. Concerning this, the nanoparticles of AgNPs$_{10}$/*c*-PEG$_{9k}$ observed in Fig. 2.13c and 2.13f were separated from each other likely by the *c*-PEG layer, compared to those of AgNPs/No PEG in contact with each other shown in Fig. 2.13a. These experiments demonstrate how AgNPs/No PEG and AgNPs/HS–PEG–OMe are degraded at high temperature, and *c*-PEG serves as an effective protection for AgNPs.

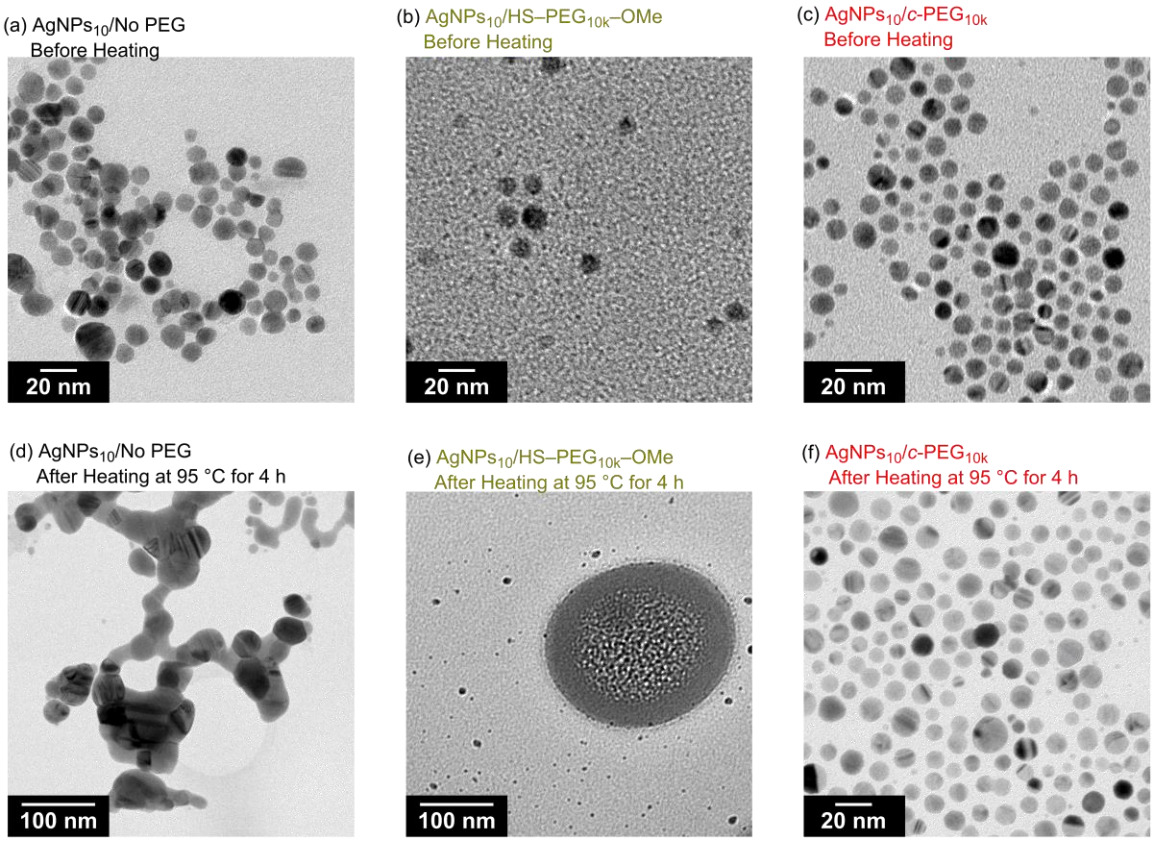

Fig. 2.13 TEM photographs of (a) $AgNP_{10}$/No PEG (scale bar: 20 nm), (b) $AgNP_{10}$/HS–PEG_{9k}–OMe (scale bar: 20 nm), and (c) $AgNP_{10}$/*c*-PEG_{9k} (scale bar: 20 nm) before heating. Those of (d) $AgNP_{10}$/No PEG (scale bar: 100 nm), (e) $AgNP_{10}$/HS–PEG_{9k}–OMe (scale bar: 100 nm), and (f) $AgNP_{10}$/*c*-PEG_{9k} (scale bar: 20 nm) after heating at 95 °C for 4 h.

2.3.4 Biological Applications

Antimicrobial activity is inherent and one of the most important properties of AgNPs, and that against Gram-negative *Escherichia coli* (JM 109) in a Muller Hinton Broth (MHB) medium was evaluated. Thus, $AgNPs_{10}$/No PEG, $AgNPs_{10}$/HO–PEG_{9k}–OH, and

AgNPs$_{10}$/MeO–PEG$_{9k}$–OMe, AgNPs$_{10}$/HS–PEG$_{9k}$–OMe, and AgNPs$_{10}$/*c*-PEG in PBS (pH 7.4, NaCl 150 mM) was added to an *E. coli*-containing medium. Upon addition of AgNPs$_{10}$/*c*-PEG to *E. coli*, immediate change in the color to brownish was observed, while the other mixtures did not cause the change. After 24 h of incubation, the *E. coli*-containing medium with AgNPs$_{10}$/No PEG, AgNPs$_{10}$/HO–PEG$_{9k}$–OH, and AgNPs$_{10}$/MeO–PEG$_{9k}$–OMe became cloudy, suggesting the growth of *E. coli* (Fig. 2.14a). For AgNPs$_{10}$/HS–PEG$_{9k}$–OMe, a gradual disappearance of the transparent yellow color of AgNPs to form a cloudy solution was evident, which also suggests loss of antimicrobial activity However, the medium with AgNPs$_{10}$/*c*-PEG$_{9k}$ was transparent and remained brownish in color even after 24 h, showing inhibited growth of *E. coli*. Furthermore, UV–Vis spectra were recorded to show transparency of the AgNPs$_{10}$/*c*-PEG$_{9k}$ specimen with a clearly observable SPR absorption peak, while the other specimens were turbid with a considerably increased baseline through scattering by grown *E. coli* (Fig. 2.14b). The growth of *E. coli* was quantified by optical density at 600 nm (OD_{600}): AgNPs$_{10}$/No PEG, 0.79; AgNPs$_{10}$/HO–PEG$_{9k}$–OH, 0.63; AgNPs$_{10}$/MeO–PEG$_{9k}$–OMe, 0.82; AgNPs$_{10}$/HS–PEG$_{9k}$–OMe, 0.86; AgNPs$_{10}$/*c*-PEG$_{9k}$, 0.08. This revealed that the antimicrobial efficacy was preserved in AgNPs$_{10}$/*c*-PEG$_{9k}$ but lost in all other specimens. Because HO–PEG$_{9k}$–OH and MeO–PEG$_{9k}$–OMe could not maintain the

dispersibility of AgNPs in PBS, the antimicrobial potency was quenched before the addition to *E. coli*. In the case of, although AgNPs$_{10}$/HS–PEG$_{9k}$–OMe did not form precipitates, the sulfidation of AgNPs nullified the antimicrobial efficacy. In contrast, physisorption of *c*-PEG exhibited an improved dispersion stability of AgNPs and evidently kept the antimicrobial efficacy.

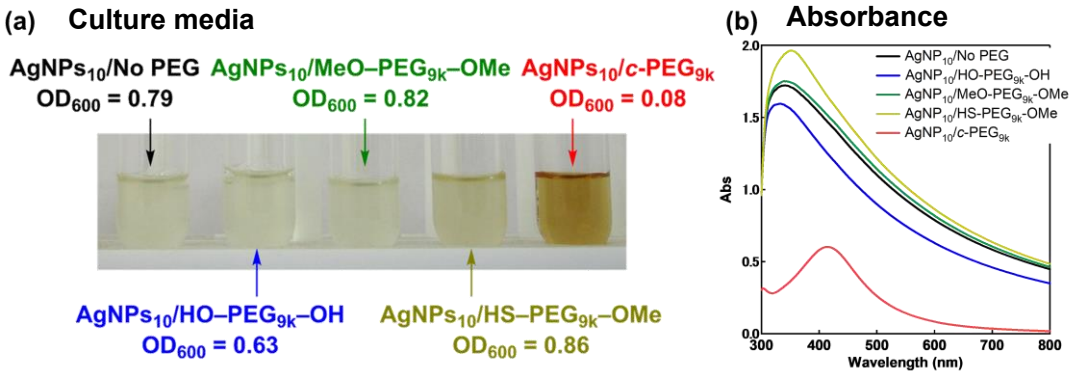

Fig. 2.14 (a) A photograph and (b) UV–Vis spectra of the antimicrobial efficacy test against *E. coli* after 24 h of incubation with AgNP$_{10}$/No PEG, AgNP$_{10}$/HO–PEG$_{9k}$–OH, AgNP$_{10}$/MeO–PEG$_{9k}$–OMe, AgNP$_{10}$/HS–PEG$_{9k}$–OMe, and AgNP$_{10}$/*c*-PEG$_{9k}$. UV–Vis spectra of the incubated specimens subtracted by that of the medium are shown.

Following the various dispersion stability and antimicrobial activity experiments, further evaluation on the biological properties of AgNPs/*c*-PEG by cytotoxicity and scratch assay experiments using HeLa cells were performed. Fig. 2.15 shows the result of cytotoxicity of AgNPs$_{10}$/No PEG, AgNPs$_{10}$/HO–PEG$_{9k}$–OH, AgNPs$_{10}$/MeO–PEG$_{9k}$–OMe,

$AgNPs_{10}$/HS–PEG_{9k}–OMe, and $AgNPs_{10}$/*c*-PEG_{9k} after incubation with HeLa cells in a DMEM medium for 24 h. $AgNPs_{10}$/*c*-PEG_{9k} had the lowest cell viability of 79% which was statistically significant ($p < 0.05$) from $AgNPs_{10}$/No PEG with a viability of 85% with sextuplicate experiments. This suggests that *c*-PEG helps AgNPs dispersed in the medium and preserve the cytotoxicity. On the other hand, no cytotoxicity was seen in $AgNPs_{10}$/HO–PEG_{9k}–OH, $AgNPs_{10}$/MeO–PEG_{9k}–OMe, and $AgNPs_{10}$/HS–PEG_{9k}–OMe likely due to precipitation in the condition.

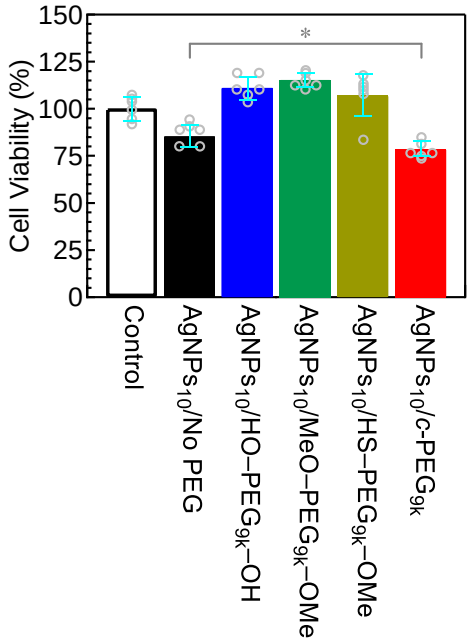

Fig. 2.15 Cell viability for $AgNPs_{10}$/No PEG, $AgNPs_{10}$/HO–PEG_{9k}–OH, $AgNPs_{10}$/MeO–PEG_{9k}–OMe, $AgNPs_{10}$/HS–PEG_{9k}–OMe, and $AgNPs_{10}$/*c*-PEG_{9k}. Data represent mean ± s.e. from measurements of six wells. *$p < 0.05$.

In addition, migration and recovery of HeLa cells were evaluated by a cell scratch assay. A confluent monolayer was scratched on AgNPs$_{10}$/No PEG, AgNPs$_{10}$/HO–PEG$_{9k}$–OH, AgNPs$_{10}$/MeO–PEG$_{9k}$–OMe, AgNPs$_{10}$/HS–PEG$_{9k}$–OMe, and AgNPs$_{10}$/*c*-PEG$_{9k}$ after 2 h of incubation (Fig. 2.16). The scratches in AgNPs$_{10}$/No PEG, AgNPs$_{10}$/HO–PEG$_{9k}$–OH, AgNPs$_{10}$/MeO–PEG$_{9k}$–OMe, and AgNPs$_{10}$/HS–PEG$_{9k}$–OMe specimens were recovered to some extent after 22 h. However, most of the HeLa cells in AgNPs$_{10}$/*c*-PEG$_{9k}$ were stripped off from the plates upon scratching, and basically no recovery was observed. This could be explained by that AgNPs$_{10}$/*c*-PEG$_{9k}$ leads to cell death in the large area, thereby inhibiting adhesion of the cells. These results further confirmed the cytotoxicity through the enhanced dispersion stability of AgNPs by *c*-PEG.

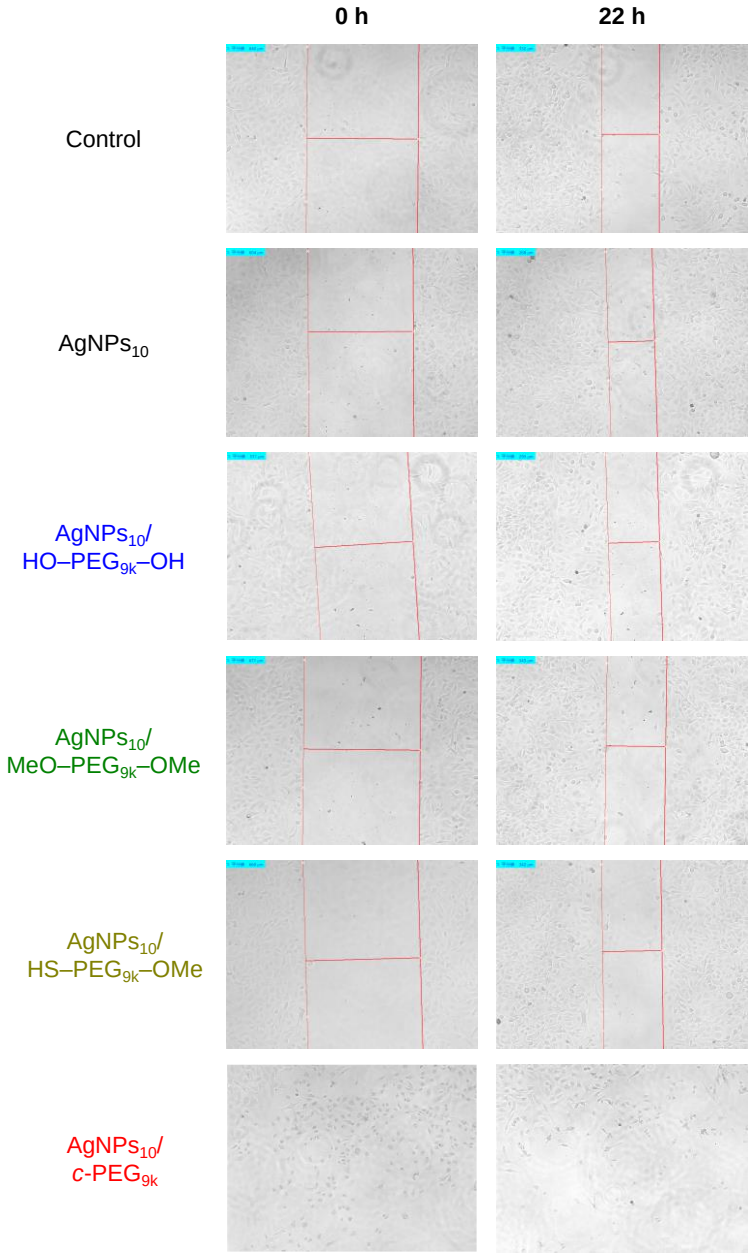

Fig. 2.16 Scratch assay test for $AgNPs_{10}$/No PEG, $AgNPs_{10}$/HO–PEG_{9k}–OH, $AgNPs_{10}$/MeO–PEG_{9k}–OMe, $AgNPs_{10}$/HS–PEG_{9k}–OMe, and $AgNPs_{10}$/*c*-PEG_{9k}. The pictures were taken at 0 and 22 h after scratching. Migration of the cells into the scratched area was observed in all the specimens except for $AgNPs_{10}$/*c*-PEG_{9k}. Most of the cells in $AgNPs_{10}$/*c*-PEG_{9k} were stripped from the plate upon scratching.

2.4. Conclusions

My research has shown the first steady PEGylation method for AgNPs conferred by physisorption of *c*-PEG, which cannot be attained with HS–PEG–OMe due to the formation of silver sulfide. Physisorption of *c*-PEG provided outstanding dispersion stability to AgNPs, against a physiological condition, white light, and high temperature, whereas HO–PEG–OH or MeO–PEG–OMe did not provide such dispersion stability. This method further exhibited persistent antimicrobial activity and cytotoxicity, which are ones of the most important properties of AgNPs. Coupled with the excellent biocompatibility of PEG and the simple physisorption method, *c*-PEG would pave the way and broaden the uses of AgNPs especially in biological and medicinal fields. Moreover, as I previously proved that the physisorption of *c*-PEG can also enhance the dispersion stability of AuNPs,[43] the present method has a great potential of application in a wide variety of metal nanoparticles.

2.5. REFERENCES

1. M. Larguinho and P. V. Baptista, *J. Proteomics*, 2012, **75**, 2811-2823.
2. L. Xu, Y. Y. Wang, J. Huang, C. Y. Chen, Z. X. Wang and H. Xie, *Theranostics*, 2020, **10**, 8996-9031.
3. A. Singh, M. Y. Dar, B. Joshi, B. Sharma, S. Shrivastava and S. Shukla, *Toxicol. Rep.*, 2018, **5**, 333-342.
4. F. Saadmim, T. Forhad, A. Sikder, W. Ghann, M. M. Ali, V. Sitther, A. J. S. Ahammad, M. A. Subhan and J. Uddin, *Molecules*, 2020, **25**, 4021.
5. H. K. A. Elhakim, S. M. Azab and A. M. Fekry, *Mat. Sci. Eng. C-Mater.*, 2018, **92**, 489-495.
6. T. Q. Huy, P. T. M. Huyen, A. T. Le and M. Tonezzer, *Anticancer Agents Med. Chem.*, 2020, **20**, 1276-1287.
7. N. Pandian and S. Chidambaram, *Int. J. Pharm. Sci. Res.*, 2017, **8**, 1633-1641.
8. G. Bagherzade, M. M. Tavakoli and M. H. Namaei, *Asian Pac. J. Trop. Biomed.*, 2017, **7**, 227-233.
9. R. A. Sperling and W. J. Parak, *Philos. Trans. R. Soc. London, Ser. A*, 2010, **368**, 1333-1383.

10. E. Bae, H. J. Park, J. Park, J. Yoon, Y. Kim, K. Choi and J. Yi, *Bull. Korean Chem. Soc.*, 2011, **32**, 613-619.

11. A. B. Albeladi, S. A. Al-Thabaiti and Z. Khan, *J. Mol. Liq.*, 2020, **302**, 112565.

12. R. A. Hamouda, M. Abd El-Mongy and K. F. Eid, *Microb. Pathogen.*, 2019, **129**, 224-232.

13. A. Abuchowski, J. R. McCoy, N. C. Palczuk, T. Vanes and F. F. Davis, *J. Biol. Chem.*, 1977, **252**, 3582-3586.

14. A. Kolate, D. Baradia, S. Patil, I. Vhora, G. Kore and A. Misra, *J. Controlled Release*, 2014, **192**, 67-81.

15. D. Curry, H. Scheller, M. S. Lu, M. Mkandawire, M. R. Servos, S. F. Cui, X. Zhang and K. D. Oakes, *RSC Adv.*, 2015, **5**, 25693-25698.

16. A. A. D'Souza and R. Shegokar, *Expert Opin. Drug Deliv*., 2016, **13**, 1257-1275.

17. J. Manson, D. Kumar, B. J. Meenan and D. Dixon, *Gold Bull.*, 2011, **44**, 99-105.

18. M. Marchioni, C. Battocchio, Y. Joly, C. Gateau, S. Nappini, I. Pis, P. Delangle, I. Michaud-Soret, A. Deniaud and G. Veronesi, *J. Phys. Chem. C*, 2020, **124**, 13467-13478.

19. L. Liu, C. A. Burnyeat, R. S. Lepsenyi, I. O. Nwabuko and T. L. Kelly, *Chem. Mater.*,

2013, **25**, 4206-4214.

20. J. S. Lee, H. Kim and W. R. Algar, *J. Phys. Chem. C*, 2017, **121**, 28566-28575.

21. S. Nam, D. V. Parikh, B. D. Condon, Q. Zhao and M. Yoshioka-Tarver, *J. Nanoparticle Res.*, 2011, **13**, 3755-3764.

22. K. Shameli, M. Bin Ahmad, S. D. Jazayeri, S. Sedaghat, P. Shabanzadeh, H. Jahangirian, M. Mahdavi and Y. Abdollahi, *Int. J. Mol. Sci.*, 2012, **13**, 6639-6650.

23. A. Fahmy, A. El-Zomrawy, A. M. Saeed, A. Z. Sayed, M. A. E. El-Arab, H. A. Shehata and J. Friedrich, *J. Adhes. Sci. Technol.*, 2017, **31**, 1422-1440.

24. J. Roh, H. N. Umh, J. Sim, S. Park, J. Yi and Y. Kim, *Korean J. Chem. Eng.*, 2013, **30**, 671-674.

25. D. Bhatia, A. Mittal and D. K. Malik, *3 Biotech*, 2016, **6**, 196.

26. D. Bhatia, A. Mittal and D. K. Malik, *Microbiology*, 2017, **86**, 602-609.

27. Y. Tezuka, *Acc. Chem. Res.*, 2017, **50**, 2661-2672.

28. G. Polymeropoulos, G. Zapsas, K. Ntetsikas, P. Bilalis, Y. Gnanou and N. Hadjichristidis, *Macromolecules*, 2017, **50**, 1253-1290.

29. H. R. Kricheldorf, *J. Polym. Sci., Part A: Polym. Chem.*, 2010, **48**, 251-284.

30. T. Yamamoto and Y. Tezuka, *Polym. Chem.*, 2011, **2**, 1930-1941.

31. Z. Jia and M. J. Monteiro, *J. Polym. Sci., Part A: Polym. Chem.*, 2012, **50**, 2085-2097.

32. R. J. Williams, A. P. Dove and R. K. O'Reilly, *Polym. Chem.*, 2015, **6**, 2998-3008.

33. G. Morgese, L. Trachsel, M. Romio, M. Divandari, S. N. Ramakrishna and E. M. Benetti, *Angew. Chem., Int. Ed.*, 2016, **55**, 15583-15588.

34. F. M. Haque and S. M. Grayson, *Nat. Chem.*, 2020, 433-444.

35. C. Booth and C. Price, In *Cyclic Polymers*, 2nd ed, ed. J. A. Semlyen, Kluwer Academic Publishers, 2002; pp 229-270.

36. M. A. Cortez, W. T. Godbey, Y. L. Fang, M. E. Payne, B. J. Cafferty, K. A. Kosakowska and S. M. Grayson, *J. Am. Chem. Soc.*, 2015, **137**, 6541-6549.

37. M. E. Fox, F. C. Szoka and J. M. J. Fréchet, *Acc. Chem. Res.*, 2009, **42**, 1141-1151.

38. N. Nasongkla, B. Chen, N. Macaraeg, M. E. Fox, J. M. J. Frechet and F. C. Szoka, *J. Am. Chem. Soc.*, 2009, **131**, 3842-3843.

39. X. Y. Tu, M. Z. Liu and H. Wei, *J. Polym. Sci., Part A: Polym. Chem.*, 2016, **54**, 1447-1458.

40. H. T. Zhang, X. D. Fan, R. T. Suo, H. Li, Z. Yang, W. B. Zhang, Y. Bai, H. Yao and W. Tian, *Chem. Commun.*, 2015, **51**, 15366-15369.

41. S. Honda, T. Yamamoto and Y. Tezuka, *J. Am. Chem. Soc.*, 2010, **132**, 10251-10253.

42. S. Honda, T. Yamamoto and Y. Tezuka, *Nat. Commun.*, 2013, **4**, 1574.

43. Y. Wang, J. E. Q. Quinsaat, T. Ono, M. Maeki, M. Tokeshi, T. Isono, K. Tajima, T. Satoh, S. Sato, Y. Miura and T. Yamamoto, *Nat. Commun.*, 2020, **11**, 6089.

44. O. J. Oziri, M. Maeki, M. Tokeshi, T. Isono, K. Tajima, T. Satoh, S. Sato and T. Yamamoto, unpublished work.

45. A. Patel, T. Cosgrove and J. A. Semlyen, *Polymer*, 1991, **32**, 1313-1317.

46. Y. Wang, W. Qin and D. Qiu, *Langmuir*, 2014, **30**, 5170-5175.

47. G. K. Stratouras and M. K. Kosmas, *Macromolecules*, 1991, **24**, 6754-6758.

48. G. Stratouras and M. Kosmas, *Macromolecules*, 1992, **25**, 3307-3308.

49. L. Zhang, A. Xia and Y. Xu, *Eur. Polym. J.*, 2000, **36**, 847-850.

50. A. Sikorski, *Macromol. Theory Simul.*, 2001, **10**, 38-45.

51. B. van Lent, J. Scheutjens and T. Cosgrove, *Macromolecules*, 1987, **20**, 366-370.

52. J. Cooke, K. Viras, G.-E. Yu, T. Sun, T. Yonemitsu, A. J. Ryan, C. Price and C. Booth, *Macromolecules*, 1998, **31**, 3030-3039.

53. P. Wulandari, T. Nagahiro, N. Fukada, Y. Kimura, M. Niwano and K. Tamada, *J. Colloid Interface Sci.*, 2015, **438**, 244-248.

54. E. Boisselier and D. Astruc, *Chem. Soc. Rev.*, 2009, **38**, 1759-1782.

55. K. A. Huynh and K. L. Chen, *Sci. Total Environ.*, 2011, **45**, 5564-5571.

56. M. Baalousha, Y. Nur, I. Romer, M. Tejamaya and J. R. Lead, *Sci. Total Environ.*, 2013, **454**, 119-131.

57. H. Wang, X. L. Zhao, X. J. Han, Z. Tang, S. S. Liu, W. J. Guo, C. B. Deng, Q. W. Guo, H. H. Wang, F. C. Wu, X. G. Meng and J. P. Giesy, *Sci. Total Environ.*, 2017, **586**, 817-826.

58. W. Zhou, Y. L. Liu, A. M. Stallworth, C. Ye and J. J. Lenhart, *Environ. Sci. Technol.*, 2016, **50**, 12214-12224.

59. J. P. Shi, C. Y. Ma, B. Xu, H. W. Zhang and C. P. Yu, *Environ. Toxicol. Chem.*, 2012, **31**, 1630-1638.

60. J. P. Shi, B. Xu, X. Sun, C. Y. Ma, C. P. Yu and H. W. Zhang, *Aquat. Toxicol.*, 2013, **132**, 53-60.

61. Y. W. Cheng, L. Y. Yin, S. H. Lin, M. Wiesner, E. Bernhardt and J. Liu, *J. Phys. Chem. C*, 2011, **115**, 4425-4432.

62. M. B. R. Aiello, J. C. Azcarate, E. Zelaya, P. D. Gara, G. N. Bosio, T. Gensch and D. O. Martire, *Biomater. Sci.*, 2021, **9**, 2608-2619.

63. D. Kim, R. Amatya, S. Hwang, S. Lee, K. A. Min and M. C. Shin, *Pharmaceutics*, 2021, **13**, 575.

Chapter 3

Topology-Dependent Interaction of Cyclic Poly(Ethylene Glycol) Complexed with Gold Nanoparticles against Bovine Serum Albumin for a Colorimetric Change

3.1 INTRODUCTION

Over the years, influence of polymer topology has been utilized in various applications, which cannot be overemphasized.[1, 2] Among the polymer topologies, cyclic polymers have found various applications because of their unique physical and chemical properties such as salt and thermal stabilities, increased glass transition temperature, higher refractive index, slow hydrolytic degradation, and less entanglement, etc.[3-7] Cyclic polymers also have promising potentials in biomedical applications because of their biological properties such as higher gene transfection,[8] longer circulation time in vivo,[9] controlled release of drugs,[10] etc.

In the meantime, polymer–nanoparticle complexes are often employed in biomedical applications.[11, 12] Among those, gold nanoparticles (AuNPs) are one of the most attractive nanomaterials due to their unique optical properties, chemical stability, and biocompatibility.[13, 14, 15] Especially, AuNPs are used as a probe for biological processes,[16, 17] diagnostic and therapeutic applications,[18, 19] and detection of proteins[20] and DNAs.[21-24] Concerning biological uses of AuNPs, functionalization of the surface with poly(ethylene glycol) (PEG), namely PEGylation, is indispensable. PEG is an excellent polymer for AuNPs and other nanoparticles owing to their biocompatibility and significant stability conferred to

the nanomaterials.[25]

In relation to cyclic polymers on nanoparticles, dithiolated PEG (HS–PEG–SH) is reportedly attached to AuNPs at both chain ends to form a loop on the surface, and the resulting PEG layer is much thicker and denser than that of a linear counterpart.[26] Moreover, cyclic polyoxazoline grafted by nitrocatechol to a Fe_3O_4 nanoparticle surface composes a dense and compact shell.[27] Previously it was reported that cyclized PEG (*c*-PEG), without inhomogeneity in the chemical structure can strongly interact with AuNPs by physisorption,[13] as well as with silver nanoparticles (AgNPs),[28] and form a PEG layer on the surface to drastically enhances the dispersion stability. In the meantime, it was reported that PEG with a discrete triangular structure interacts with lysozyme to help maintaining the higher order structure even at high temperature to avoid aggregation.[29] Bearing these two polymer topology-based interactions of PEG–AuNPs and PEG–protein in mind, here I investigate the unique influence of *c*-PEG in a mixture containing BSA, AuNPs, and PEG (Figure 3.1). In this regard, BSA was selected by the medical significance,[30, 31] structural homology to human serum albumin (HSA),[32] and importance immunological and bioanalytical researches.[33, 34]

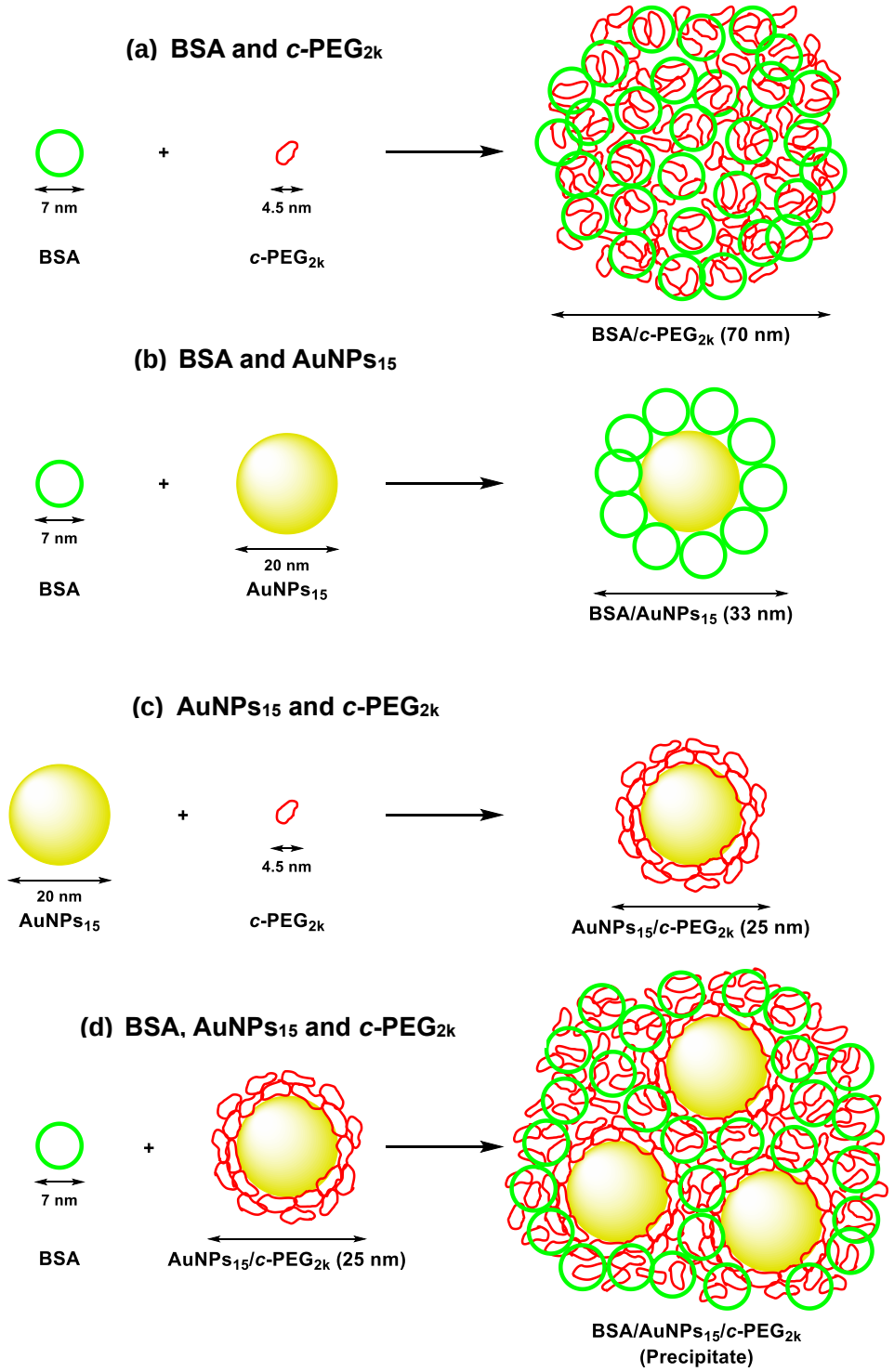

Figure 3.1 Schematic illustrations of complex formation by (a) BSA and *c*-PEG$_{2k}$, (b) BSA and AuNPs$_{15}$, (c) AuNPs$_{15}$ and *c*-PEG$_{2k}$, and (d) BSA and *c*-PEG$_{2k}$-adsorbed AuNPs$_{15}$.

3.2 EXPERIMENTAL SECTION

3.2.1 Materials. Citrate-capped AuNPs with a size of 10, 15, 20, 30, 40, and 50 nm ($AuNPs_{10}$, $AuNPs_{15}$, $AuNPs_{20}$, $AuNPs_{30}$, $AuNPs_{40}$, and $AuNPs_{50}$, respectively) dispersed in a 2 mM sodium citrate solution with a gold mass concentration of 0.05 mg/mL were purchased from nanoComposix, USA and used as received. Poly(ethylene glycol) 2,000 (HO–PEG_{2k}–OH) (Sigma–Aldrich, Japan) was purified by passing through a silica gel column using chloroform/methanol (90/10, v/v) as an eluent. The AuNPs' and PEGs' names in the parentheses above are the ones used in the paper. Bovine serum albumin (Sigma–Aldrich, Japan), NaCl (>99.0%, Kanto Chemicals Co., Japan), Na_2HPO_4 (>99.0%, FUJIFILM Wako Pure Chemical Co., Japan), NaH_2PO_4 (>99.0 %, FUJIFILM Wako Pure Chemical Co., Japan), KCl (>99.0%, Kanto Chemicals Co., Japan), Wakosil C-300 (FUJIFILM Wako Pure Chemical Co., Japan) were used as received. HS–PEG_{2k}–OMe, (>98.0%, Junsei Chemical Co., Ltd.) was purified by recycling preparative SEC. A PBS solution (pH 7.4; NaCl, 137 mM; Na_2HPO_4, 10 mM; NaH_2PO_4, 1.8 mM; KCl 2.7 mM) was prepared by dissolving NaCl (8.0 g), Na_2HPO_4, (1.44 g), NaH_2PO_4 (245 mg), and KCl (200 mg) in deionized water (1000 mL). BSA (1.32 mg, 20 nmol) was dissolved in the PBS solution (1.0 mL) to form a BSA solution (20 μM).

3.2.2 UV–Vis Spectroscopy. UV–Vis spectra were recorded using a JASCO Ubset V–670 Spectrophotometer at 25 °C in a micro quartz cuvette (M25-UV2, GL Science Inc, Japan) with a path length of 10 mm. Deionized water was used as a blank, and spectra were acquired at a wavelength range of 200–800 nm.

3.2.3 Fluorescence Spectroscopy. Fluorescence spectra were acquired at an emission wavelength range of 290–500 nm with an excitation wavelength of 280 nm using 5 nm/5 nm slit widths. Synchronous fluorescence was measured using an emission and excitation wavelength difference ($\lambda_{em} - \lambda_{ex}$) fixed at either 60 or 15 nm.

3.2.4 DLS. Zetasizer Nano ZS (He–Ne laser, 633 nm, Max 4 mW, Malvern Panalytical Ltd.) and a high precision micro quartz cuvette (ZEN2112, Hellma Analytics) were used to measure DLS size. The measurements were performed at 25 °C with an equilibration time of 120 s. A cumulants analysis provided in software built into the instrument was used to determine the z-average size.

3.2.5 Preparation of a Mixture of BSA and PEG (BSA/PEG). HO–PEG_{2k}–OH, MeO–PEG_{2k}–OMe, HS–PEG_{2k}–OMe, or *c*-PEG_{2k} (1.5 or 2.5 mg) was dissolved in PBS (0.9 mL). BSA (20 μM, 0.1 mL) was added to the PEG solution, and the resulting mixture (1.0 mL) contained BSA (2.0 μM) and PEG (0.15 or 0.25 wt%). BSA/No PEG was analogously

prepared without PEG. The mixture was incubated for 2 h at 25 °C using a mixer equipped in an incubator. UV–Vis and fluorescence spectra were recorded.

3.2.6 NMR of BSA/PEG. HO–PEG_{2k}–OH, MeO–PEG_{2k}–OMe, HS–PEG_{2k}–OMe, or *c*-PEG_{2k} (1.5 mg) was dissolved in PBS (0.9 mL). BSA (20 μM, 0.1 mL) was added to the PEG solution, and the resulting mixture (1.0 mL) contained BSA (2.0 μM) and PEG (0.15 wt%). BSA/No PEG was analogously prepared without PEG. The mixture was incubated for 2 h at 25 °C using a mixer equipped in an incubator, lyophilized, and dissolved in D_2O. ^1H NMR spectra were recorded on a JEOL JNM-ESC600 instrument at 25 °C.

3.2.7 Preparation of a Mixture of BSA, AuNPs, and PEG (BSA/AuNPs/PEG). To an aqueous dispersion of $AuNPs_{15}$ (0.9 mL, 0.05 mg/mL), HO–PEG_{2k}–OH, MeO–PEG_{2k}–OMe, HS–PEG_{2k}–OMe, or *c*-PEG_{2k} (1.5 mg) was added, and PEG was dissolved by vortex mixing for 1 min to form $AuNPs_{15}$/HO–PEG_{2k}–OH, $AuNPs_{15}$/MeO–PEG_{2k}–OMe, $AuNPs_{15}$/HS–PEG_{2k}–OMe, or $AuNPs_{15}$/*c*-PEG_{2k}, respectively. BSA (20 μM, 0.1 mL) was added to the dispersions, and the resulting mixtures (1.0 mL) contained BSA (2.0 μM), $AuNPs_{15}$ (0.045 mg/mL), and PEG_{2k} (0.15 wt%). BSA/$AuNPs_{15}$/No PEG was analogously prepared without PEG. The mixture was incubated for 2 h at 25 °C using a mixer equipped in an incubator, and UV–Vis, fluorescence, and synchronous florescence spectra were recorded.

3.2.8 Transmission Electron Microscopy (TEM). A few drops of BSA/AuNPs$_{15}$/No PEG, BSA/AuNPs$_{15}$/HS–PEG$_{2k}$–OMe, or BSA/AuNPs$_{15}$/*c*-PEG$_{2k}$ after 2 h of incubation at 25 °C were placed on a carbon coated Formvar TEM grid and blown away with a blower. Japan Electron Optics Laboratory JEM-2010 operated at 200 kV was used for measurement.

3.2.9 Incubation Time Dependence for BSA/AuNPs/PEG. BSA (20 μM, 0.1 mL) was added to AuNPs$_{15}$/HO–PEG$_{2k}$–OH, AuNPs$_{15}$/MeO–PEG$_{2k}$–OMe, AuNPs$_{15}$/HS–PEG$_{2k}$–OMe, or AuNPs$_{15}$/*c*-PEG$_{2k}$ (0.9 mL), and the resulting mixtures (1.0 mL) contained BSA (2.0 μM), AuNPs (0.045 mg/mL), and PEG (0.15 wt%). BSA/AuNPs$_{15}$/No PEG was analogously prepared without PEG. The mixture was incubated at 25 °C. At incubation time of 10, 30, 60, 90, 120, 150, and 180 min, a small amount of the mixture was taken for UV–Vis, florescence, and synchronous fluorescence measurements and was not returned to the mother liquor.

3.2.10 BSA's Concentration Dependence for BSA/AuNPs/PEG. BSA (20 μM, 0.01, 0.025, 0.05, 0.075, or 0.1 mL) and a complementary amount of PBS (0.99, 0.075, 0.05, 0.025, or 0 mL, respectively) were added to AuNPs$_{15}$/No PEG, AuNPs$_{15}$/HO–PEG$_{2k}$–OH, AuNPs$_{15}$/MeO–PEG$_{2k}$–OMe, AuNPs$_{15}$/HS–PEG$_{2k}$–OMe, and AuNPs$_{15}$/*c*-PEG$_{2k}$ (0.9 mL). The resulting mixture (1.0 mL) contained BSA (0.2, 0.5, 1.0, 1.5, or 2.0 μM), AuNPs (0.045 mg/mL), and PEG (0.15 wt%). The mixture was incubated for 2 h at 25 °C using a mixer

equipped in an incubator, and UV–Vis and fluorescence spectra were recorded.

3.2.11 AuNPs' Concentration Dependence for BSA/AuNPs/PEG. An aqueous dispersion of $AuNPs_{15}$ (0.5 mg/mL, 0.1, 0.3, 0.5, or 0.7 mL) was diluted with a complementary amount of water (0.8, 0.6, 0.4, or 0.2 mL, respectively). HO–PEG_{2k}–OH, MeO–PEG_{2k}–OMe, HS–PEG_{2k}–OMe, or *c*-PEG_{2k} (1.5 mg) was dissolved in the diluted or undiluted AuNPs dispersion (0.9 mL), and the mixture was vortexed for 1 min to form $AuNPs_{15}$/HO–PEG_{2k}–OH, $AuNPs_{15}$/MeO–PEG_{2k}–OMe, $AuNPs_{15}$/HS–PEG_{2k}–OMe, or $AuNPs_{15}$/*c*-PEG_{2k}, respectively, with a varied AuNPs concentration. BSA (20 μM, 0.1 mL) was added to the dispersion, and the resulting mixture (1.0 mL) contained BSA (2.0 μM), $AuNPs_{15}$ (0.005, 0.015, 0.025, 0.035, or 0.045 mg/mL), and PEG (0.15 wt%). BSA/$AuNPs_{15}$/No PEG was analogously prepared without PEG. The mixture was incubated for 2 h at 25 °C using a mixer equipped in an incubator, and UV–Vis and fluorescence spectra were recorded.

3.2.12 AuNPs' Size Dependence for BSA/AuNPs/*c*-PEG. *c*-PEG_{2k} (1.5 mg) was added to an aqueous dispersion of AuNPs (0.9 mL, 0.05 mg/mL) with a varied size (10, 15, 20, 30, 40, or 50 nm), and the mixture was vortexed for 1 min. BSA (20 μM, 0.1 mL) was added, and the resulting mixture (1.0 mL) contained BSA (2.0 μM), AuNPs (0.045 mg/mL), and *c*-PEG_{2k} (0.15 wt%). BSA/AuNPs/No PEG was analogously prepared without *c*-PEG_{2k}. The mixture

was incubated for 2 h at 25 °C using a mixer equipped in an incubator, and UV–Vis and fluorescence spectra were recorded.

3.2.13 *c*-PEG's Concentration Dependence for BSA/AuNPs/*c*-PEG. *c*-PEG_{2k} (1.5 or 2.5 mg) was added to an aqueous dispersion of $AuNPs_{15}$ (0.9 mL, 0.05 mg/mL), and the mixture was vortexed for 1 min. BSA (20 μM, 0.1 mL) was added to the dispersion, and the resulting mixture (1.0 mL) contained BSA (2.0 μM), $AuNPs_{15}$ (0.045 mg/mL), and PEG (0.15 or 0.25 wt%). The mixture was incubated for 2 h at 25 °C using a mixer equipped in an incubator, and UV–Vis and fluorescence spectra were recorded.

3.3 RESULTS AND DISSCUSSION

3.3.1Complexation of *c*-PEG and BSA. *c*-PEG was simply dissolved into a PBS solution of BSA and compared with those of its linear counterparts having various chain end functionalities. The properties of the PEG determined by SEC are listed in Table 3.1. The expected diameter of *c*-PEG_{2k} was 4.5 nm, when the polymer forms an ideal right circular conformation.

Table 3.1 Properties of PEG by SEC

	$M_{n,SEC}$[a] (g mol^{-1})	$M_{p,SEC}$[a] (g mol^{-1})	M_w/M_n	ideal diameter of *c*-PEG (nm)
HO–PEG$_{2k}$–OH	1740	1760	1.05	–
MeO–PEG$_{2k}$–OMe	1780	1760	1.05	–
HS–PEG$_{2k}$–OMe	1690	1760	1.05	–
c-PEG$_{2k}$	1170	1170	1.04	4.5

[a]Determined by SEC in THF using PEG standards.

The fluorescence spectra of BSA before and after the addition of HO–PEG$_{2k}$–OH, MeO–PEG$_{2k}$–OMe, HS–PEG$_{2k}$–OMe, or *c*-PEG$_{2k}$ at a PEG concentration of 0.15 or 0.25 wt% are shown in Figure 3. No significant change in the spectral profile was seen upon the addition of HO–PEG$_{2k}$–OH (Figure 3.2a), MeO–PEG$_{2k}$–OMe (Figure 3.2b), or HS–PEG$_{2k}$–OMe (Figure 3.2c). On the other hand, the addition of *c*-PEG$_{2k}$ to BSA gave a shouldering effect at around 370 nm and longer wavelengths (Figure 3.2d). This effect could be because of a unique interaction between *c*-PEG and BSA.

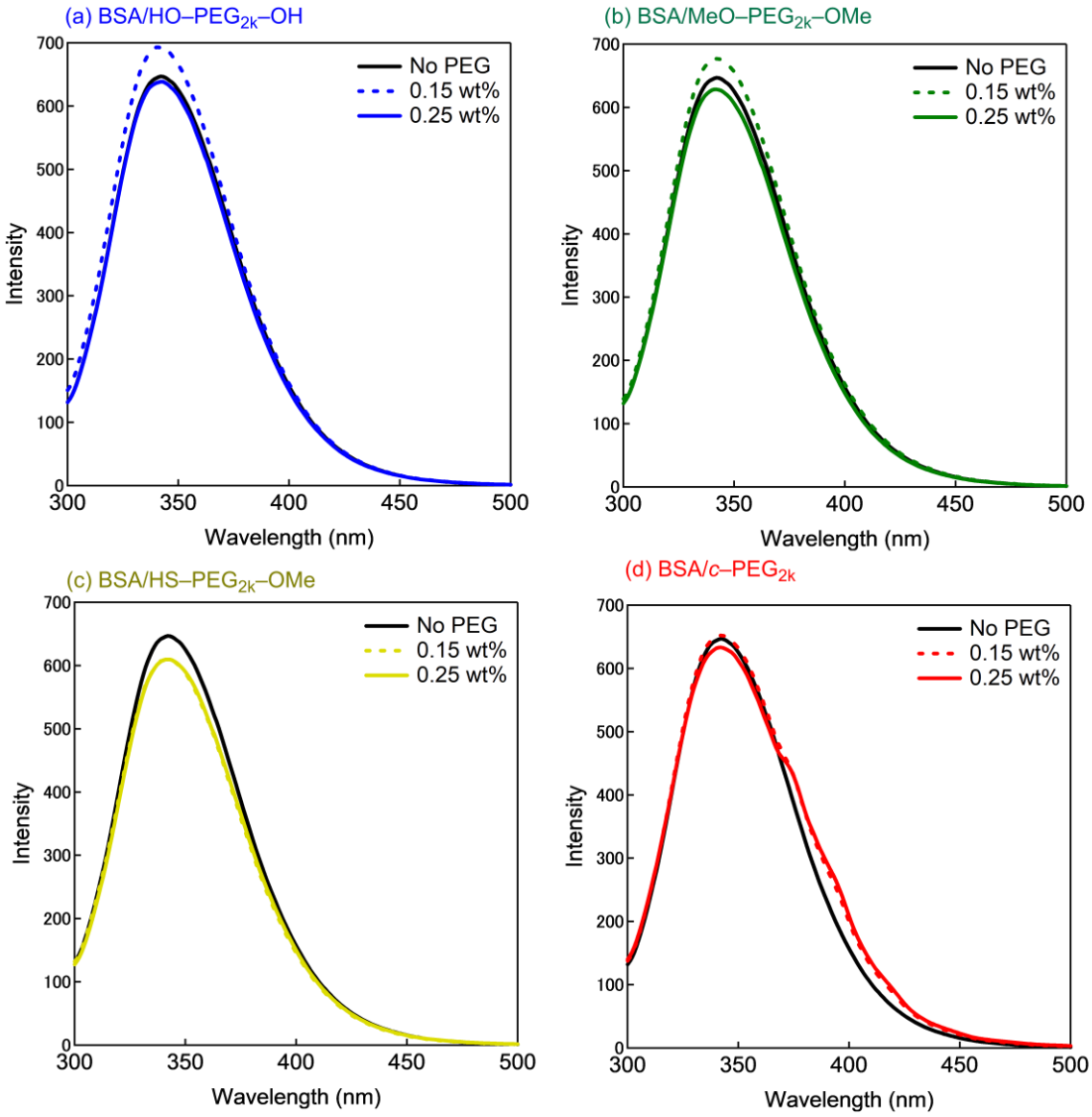

Figure 3.2. Fluorescence spectra of (a) BSA/HO–PEG_{2k}–OH (b) BSA/MeO–PEG_{2k}–OMe, (c) BSA/HS–PEG_{2k}–OMe, (d) BSA/*c*-PEG_{2k} at a BSA concentration of 2.0 μM and PEG concentrations of 0.15 and 0.25 wt%.

Further examination was carried out with DLS to analyze the extent of complex formation between *c*-PEG and BSA. The result in Table 3.2 shows that BSA/No PEG has a size of 7 nm, which on the addition of HO–PEG_{2k}–OH or MeO–PEG_{2k}–OMe does not change significantly. However, the addition of *c*-PEG_{2k} drastically increased the size to 70 ± 20 nm, suggesting complex formation between *c*-PEG and BSA.

Table 3.2. DLS Size of BSA/No PEG, BSA/HO–PEG_{2k}–OH, BSA/MeO–PEG_{2k}–OMe, and BSA/*c*-PEG_{2k}

	size (nm)
BSA/No PEG	7 ± 1
BSA/HO–PEG_{2k}–OH	6 ± 1
BSA/MeO–PEG_{2k}–OMe	5 ± 1
BSA/*c*-PEG_{2k}	70 ± 20

Furthermore, ^{1}H NMR was used for detection of the BSA–PEG interaction by examination of the spectral changes. BSA/*c*-PEG_{2k} shows new peaks at around 1.9 ppm in contrast to BSA/HO–PEG_{2k}–OH, BSA/MeO–PEG_{2k}–OMe, and BSA/HS–PEG_{2k}–OMe, suggesting a significant interaction between *c*-PEG_{2k} and BSA (Fig 3.3). This result, in tandem with the

fluorescence spectroscopy and DLS measurement, indicates complex formation between BSA and *c*-PEG.

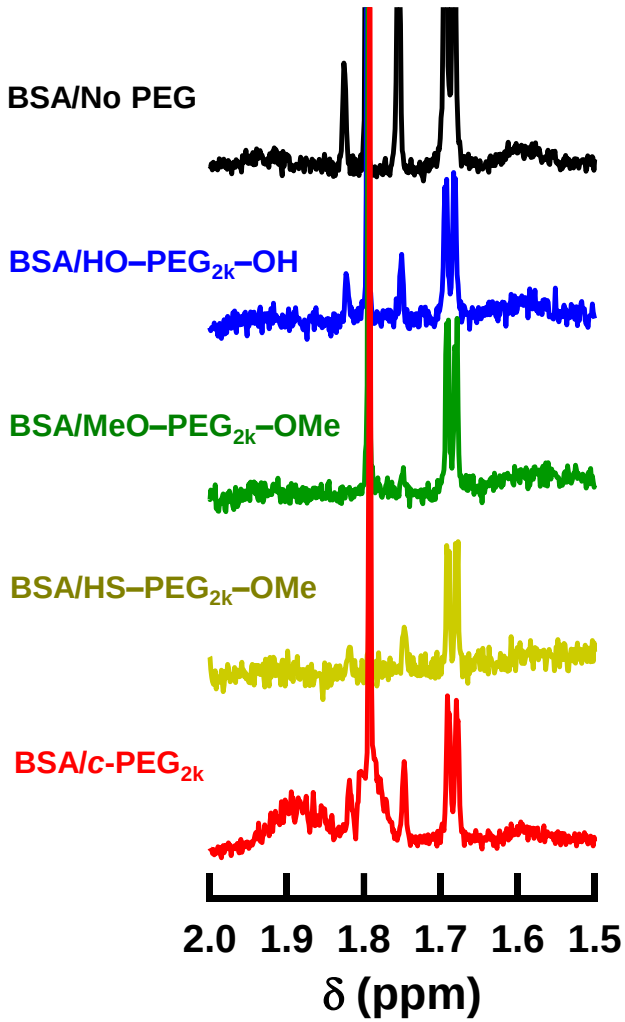

Figure 3.3. ^{1}H NMR spectra of BSA/No PEG (black), BSA/HO–PEG_{2k}–OH (blue), BSA/MeO–PEG_{2k}–OMe (green), BSA/HS–PEG_{2k}–OMe (yellow), and BSA/*c*-PEG_{2k} (red) in D_2O.

3.3.2 **Complexation of BSA/AuNPs/PEG.** Several works abound in the literature on the interaction mechanism and behavior of metal nanoparticles and BSA.[35-40] BSA has also been used to provide stability to metal nanoparticles.[41] Previously it was reported that *c*-PEG strongly adsorbs to AuNPs[13] and now I found above that *c*-PEG also interacts with BSA evident from the results of DLS (Table 3.1), fluorescence spectra (Figure 3.2), and NMR (Figure 3.3). Based on these, I investigated the multiple interactions among BSA, AuNPs, and *c*-PEG (Figure 3.1d).

Thus, BSA was added into $AuNPs_{15}$/No PEG, $AuNPs_{15}$/HO–PEG_{2k}–OH, $AuNPs_{15}$/MeO–PEG_{2k}–OMe, $AuNPs_{15}$/HS–PEG_{2k}–OMe, or $AuNPs_{15}$/*c*-PEG_{2k}, where the concentrations of BSA, $AuNPs_{15}$, and PEG were 2.0 μM, 0.045 mg/mL, and 0.15 wt%, respectively. For BSA/$AuNPs_{15}$/*c*-PEG_{2k}, the red color of the dispersion progressively disappeared (Figure 3.4f–m). The fainting of the red color was evident even at 10 min (Figure 3.4g) and became nearly colorless approximately after 90 min (Figure 3.4j). By taking a careful look, a small amount of the red precipitate formed on the surface of the glass vial. Thus, this suggests that formation of non-dispersible aggregates when BSA, $AuNPs_{15}$, and *c*-PEG_{2k} coexisted. Aggregation of AuNPs often causes a change in the color due to the surface plasmon resonance coupling. However, fainting in the red color without a shift in the

absorption wavelength was reported in thyroxine hormone detection by antibody-labeled AuNPs.[42] This was likely caused by the sufficient separation of each AuNP by the antibody and antigen even in the aggregates. Expect that a similar phenomenon takes place in my case with BSA/AuNPs/*c*-PEG. In the meantime, no significant change was observed for any of BSA/AuNPs$_{15}$/No PEG, BSA/AuNPs$_{15}$/HO–PEG$_{2k}$–OH, BSA/AuNPs$_{15}$/MeO–PEG$_{2k}$–OMe, and BSA/AuNPs$_{15}$/HS–PEG$_{2k}$–OMe. This clearly suggests that the cyclic topology of PEG plays a significant role in the formation of the precipitate. The UV–Vis spectra showed an unambiguous decrease in the absorption from the SPR of BSA/AuNPs$_{15}$/*c*-PEG (Figure 3.4e) with an increase in time, whereas BSA/AuNPs$_{15}$/No PEG (Figure 3.4a), BSA/AuNPs$_{15}$/HO–PEG$_{2k}$–OH (Figure 3.4b), BSA/AuNPs$_{15}$/MeO–PEG$_{2k}$–OMe (Figure 3.4c), and BSA/AuNPs$_{15}$/HS–PEG$_{2k}$–OMe (Figure 3.4d) remained nearly unchanged for 180 min. The absorption peak at 280 nm arose from the aromatic amino acids present in BSA, while the one at 520 nm was from the SPR of AuNPs.

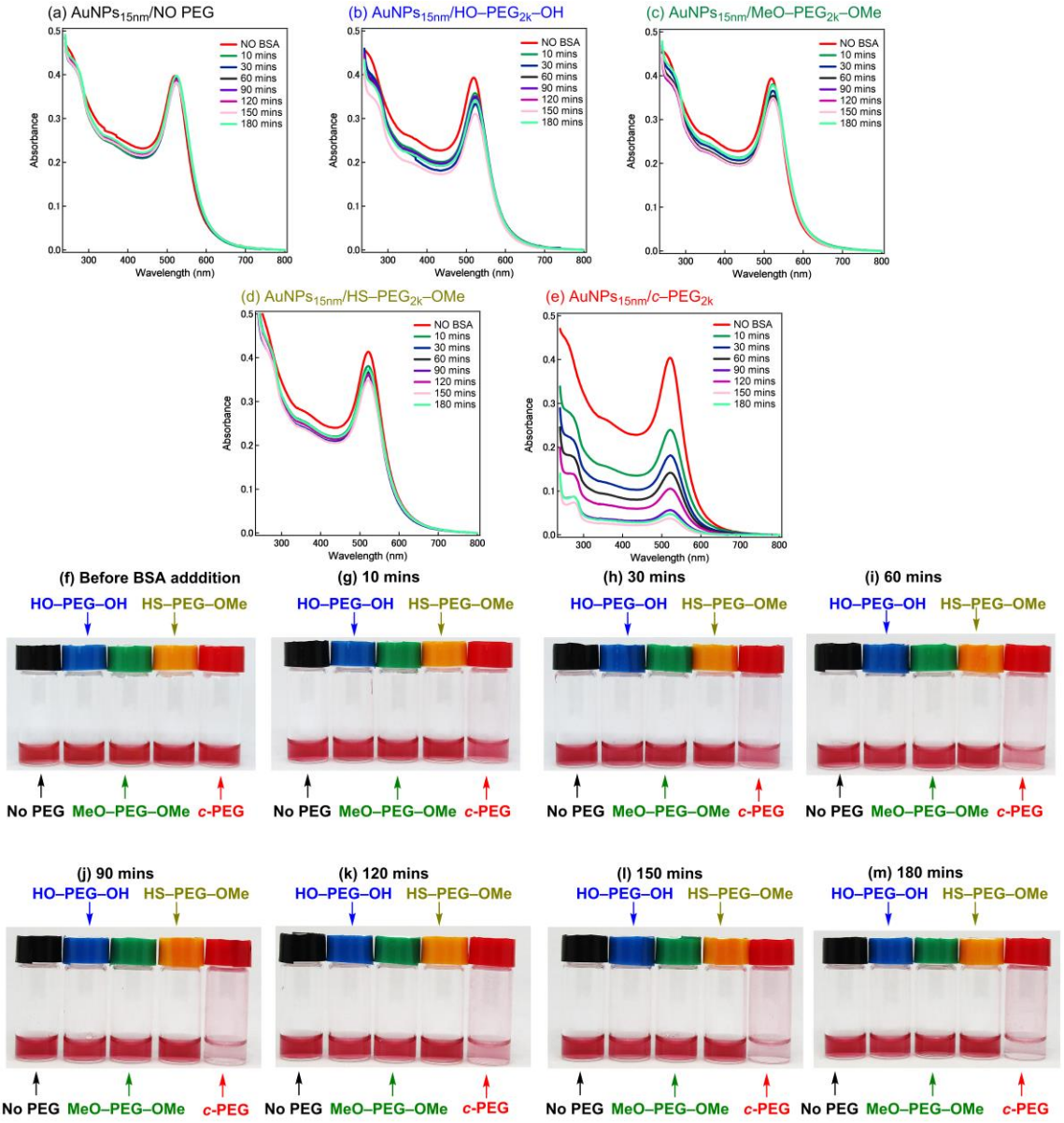

Figure 3.4 Time course UV–Vis spectra and photographs of mixtures of BSA (2.0 μM) and $AuNPs_{15}$ (0.045 mg/mL) with or without various PEG (0.15 wt%). (a) BSA/$AuNPs_{15}$/No PEG, (b) BSA/$AuNPs_{15}$/HO–PEG_{2k}–OH, (c) BSA/$AuNPs_{15}$/MeO–PEG_{2k}–OMe, (d) BSA/$AuNPs_{15}$/HS–PEG_{2k}–OMe, and (e) BSA/$AuNPs_{15}$/*c*-PEG_{2k}. Pictures taken (f) before adding BSA, (g) 10, (h) 30, (i) 60, (j) 90, (k) 120, (l) 150, and (m) 180 min after adding BSA.

Fluorescence spectra were also recorded during the same time course. An decrease in the intensity upon the addition of BSA was observed for BSA/AuNPs$_{15}$/No PEG (Figure 3.5a), BSA/AuNPs$_{15}$/HO–PEG$_{2k}$–OH (Figure 3.5b), BSA/AuNPs$_{15}$/MeO–PEG$_{2k}$–OMe (Figure 3.5c), and BSA/AuNPs$_{15}$/HS–PEG$_{2k}$–OMe (Figure 3.5d) due to the quenching of BSA fluorescence by AuNPs as in literature.[43] Moreover, a slight decrease in the intensity was observed as the time for these four specimens. DLS showed an increase in the size by approximately 10–20 nm, which is consistent with that AuNPs$_{15}$ interact with BSA (Table 3.3).

Table 3.3 DLS Size of AuNPs$_{15}$/No PEG, AuNPs$_{15}$/HO–PEG$_{2k}$–OH, AuNPs$_{15}$/MeO–PEG$_{2k}$–OMe, and AuNPs$_{15}$/*c*-PEG$_{2k}$ Before and After Adding BSA[a]

	before adding BSA	after adding BSA
AuNPs$_{15}$/No PEG	20 ± 1	33 ± 1
AuNPs$_{15}$/HO–PEG$_{2k}$–OH	21 ± 1	33 ± 1
AuNPs$_{15}$/MeO–PEG$_{2k}$–OMe	20 ± 1	39 ± 1
AuNPs$_{15}$/*c*-PEG$_{2k}$	25 ± 1	precipitated

[a]Units are in nm.

On the other hand, the fluorescence intensity of BSA/AuNPs$_{15}$/*c*-PEG$_{2k}$ similarly decreased upon the addition of BSA but later increased (Figure 3.5e). The initial decrease in fluorescence intensity upon the addition of BSA was caused by quenching with AuNPs without precipitate formation.[44] Later, the complexed BSA molecules in dispersing BSA/AuNPs/*c*-PEG was likely replaced with uncomplexed *c*-PEG to be released into the solution, resulting in the increase in the concentration of BSA in the solution and simultaneous precipitation of BSA/AuNPs/*c*-PEG. Thus, it seems that the interaction between BSA and AuNPs is faster but weaker, and that between *c*-PEG and BSA is slower but stronger. By comparing the fluorescence intensity of BSA only and that of 180 min after mixing with AuNPs$_{15}$/*c*-PEG$_{2k}$, most of the BSA molecules was likely released.

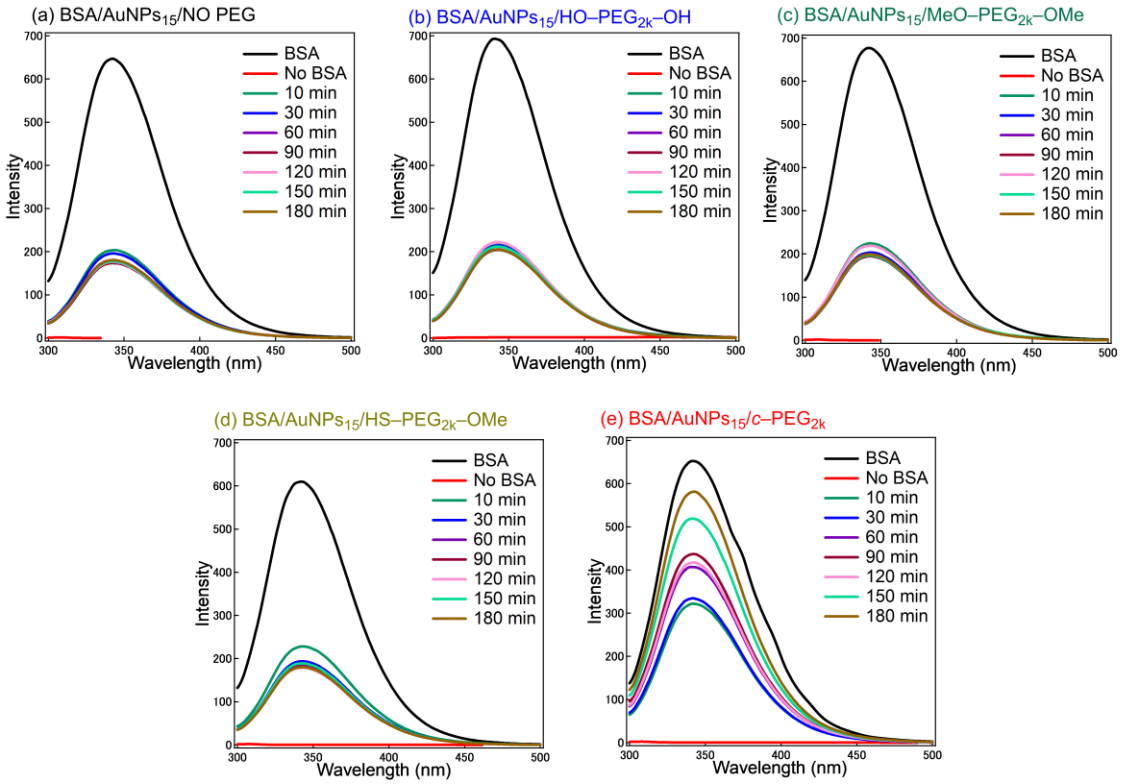

Figure 3.5 Time course fluorescence spectra of mixtures of BSA (2.0 μM) and $AuNPs_{15}$ (0.045 mg/mL) with or without various PEG (0.15 wt%). (a) BSA/$AuNPs_{15}$/No PEG, (b) BSA/$AuNPs_{15}$/HO–PEG_{2k}–OH, (c) BSA/$AuNPs_{15}$/MeO–PEG_{2k}–OMe, (d) BSA/$AuNPs_{15}$/HS–PEG_{2k}–OMe, and (e) BSA/$AuNPs_{15}$/*c*-PEG_{2k}.

The driving force to induce the interaction among BSA/AuNPs/*c*-PEG was expected to be the presence of *c*-PEG, which interacts with both BSA and AuNPs likely due to an entropic effect. Because of the smaller number of the *c*-PEG's conformations in the uncomplexed state compared to that of HO–PEG–OH and MeO–PEG–OMe, the smaller entropic penalty upon the complexation is anticipated.[45, 46] This phenomenon was also reported in theoretical and computational studies.[47-51]

It was reported that the microenvironment of the tyrosine and tryptophan residues in BSA can be evaluated by synchronous fluorescence spectroscopy with $\Delta\lambda$ = 15 and 60 nm, respectively.[43] The result shows no shift in wavelength for both $\Delta\lambda$ = 15 and 60 nm, suggesting no significant environmental change for the tyrosine or tryptophan residues upon mixing with $AuNPs_{15}$/No PEG, $AuNPs_{15}$/HO–PEG_{2k}–OH, $AuNPs_{15}$/MeO–PEG_{2k}–OMe, $AuNPs_{15}$/HS–PEG_{2k}–OMe, and even $AuNPs_{15}$/*c*-PEG_{2k} (Figure 3.6). The change in the intensity of the synchronous fluorescence spectroscopy was essentially the same as that of

the fluorescence spectroscopy with a fix excitation wavelength at 280 nm (Figure 3.6).

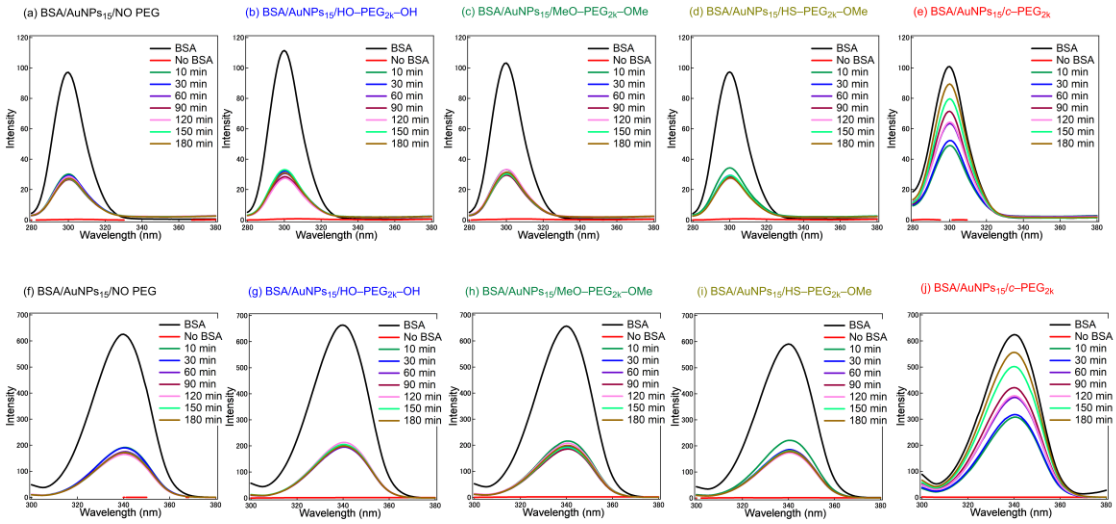

Figure 3.6 Time course synchronous fluorescence spectra of mixtures of BSA (2.0 μM) and $AuNPs_{15}$ (0.045 mg/mL) with or without various PEG (0.15 wt%). (a) BSA/$AuNPs_{15}$/No PEG with $\Delta\lambda$ = 60 nm, (b) BSA/$AuNPs_{15}$/HO–PEG_{2k}–OH with $\Delta\lambda$ = 60 nm, (c) BSA/$AuNPs_{15}$/MeO–PEG_{2k}–OMe with $\Delta\lambda$ = 60 nm, (d) BSA/$AuNPs_{15}$/HS–PEG_{2k}–OMe with $\Delta\lambda$ = 60 nm, (e) BSA/$AuNPs_{15}$/*c*-PEG_{2k} with $\Delta\lambda$ = 60 nm, (f) BSA/$AuNPs_{15}$/No PEG with $\Delta\lambda$ = 15 nm, (g) BSA/$AuNPs_{15}$/HO–PEG_{2k}–OH with $\Delta\lambda$ = 15 nm, (h) BSA/$AuNPs_{15}$/MeO–PEG_{2k}–OMe with $\Delta\lambda$ = 15 nm, (i) BSA/$AuNPs_{15}$/HS–PEG_{2k}–OMe with $\Delta\lambda$ = 15 nm, and (j) BSA/$AuNPs_{15}$/*c*-PEG_{2k} with $\Delta\lambda$ = 15 nm.

TEM measurements of BSA/AuNPs$_{15}$/No PEG, AuNPs$_{15}$/HS–PEG$_{2k}$–OMe, and BSA/AuNPs$_{15}$/*c*-PEG$_{2k}$ were carried out to observe the structure of the dispersion and aggregate (Figure 3.7). The TEM photograph of AuNPs$_{15}$/*c*-PEG$_{2k}$ showed aggregated AuNPs$_{15}$, which resulted from the cooperative binding among BSA, AuNPs$_{15}$, and *c*-PEG$_{2k}$ (Figure 3.7c). On the other hand, AuNPs in BSA/AuNPs$_{15}$/No PEG (Figure 3.7a) and BSA/AuNPs$_{15}$/HS–PEG$_{2k}$–OMe (Figure 3.7b) were still dispersed. These further demonstrated the sensitivity of AuNPs$_{15}$/*c*-PEG toward BSA.

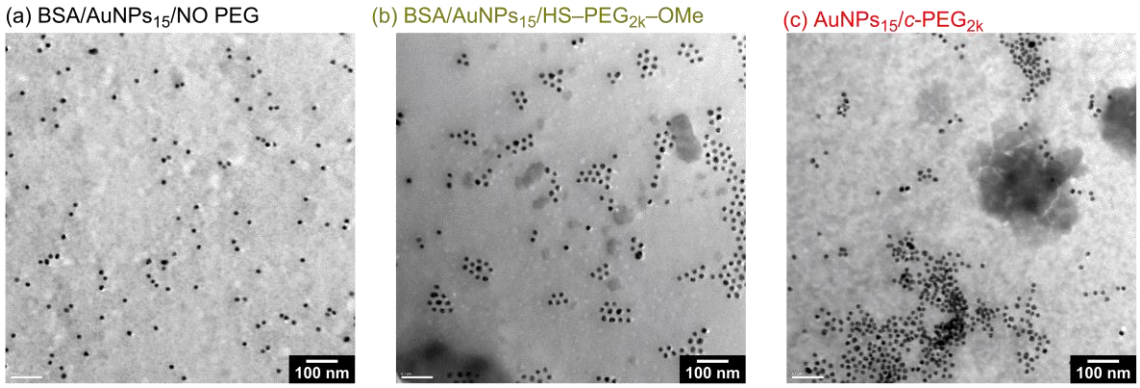

Figure 3.7. TEM photographs of (a) BSA/AuNP$_{15}$/No PEG, (b) BSA/AuNP$_{15}$/HS–PEG$_{2k}$–OMe, and (c) BSA/AuNP$_{15}$/*c*-PEG$_{2k}$. Scale bar: 100 nm.

3.3.3 BSA's Concentration Dependence. The BSA concentration was varied from 0.2 to 2.0 μM for BSA/AuNP$_{15}$/No PEG, BSA/AuNP$_{15}$/HO–PEG$_{2k}$–OH, BSA/AuNP$_{15}$/MeO–PEG$_{2k}$–OMe, BSA/AuNP$_{15}$/HS–PEG$_{2k}$–OMe and BSA/AuNP$_{15}$/*c*-PEG$_{2k}$ as shown in Figure 3.8. Changing the concentration of BSA had no significant effect on BSA/AuNP$_{15}$/No PEG (Figure 3.8a), BSA/AuNP$_{15}$/HO–PEG$_{2k}$–OH (Figure 3.8b), BSA/AuNP$_{15}$/MeO–PEG$_{2k}$–OMe (Figure 3.8c), and BSA/AuNP$_{15}$/HS–PEG$_{2k}$–OMe (Figure 3.8d) evident from the absorption spectra. On the other hand, the increase in the BSA concentration resulted in a decrease in the absorbance for BSA/AuNP$_{15}$/*c*-PEG$_{2k}$ (Figure 3.8e). The fainting in the red color can be visually observed (Figure 3.8g–6l). Figure 6f shows a decrease in the absorption from the AuNPs$_{15}$ as the BSA concentration increases in the presence of *c*-PEG.

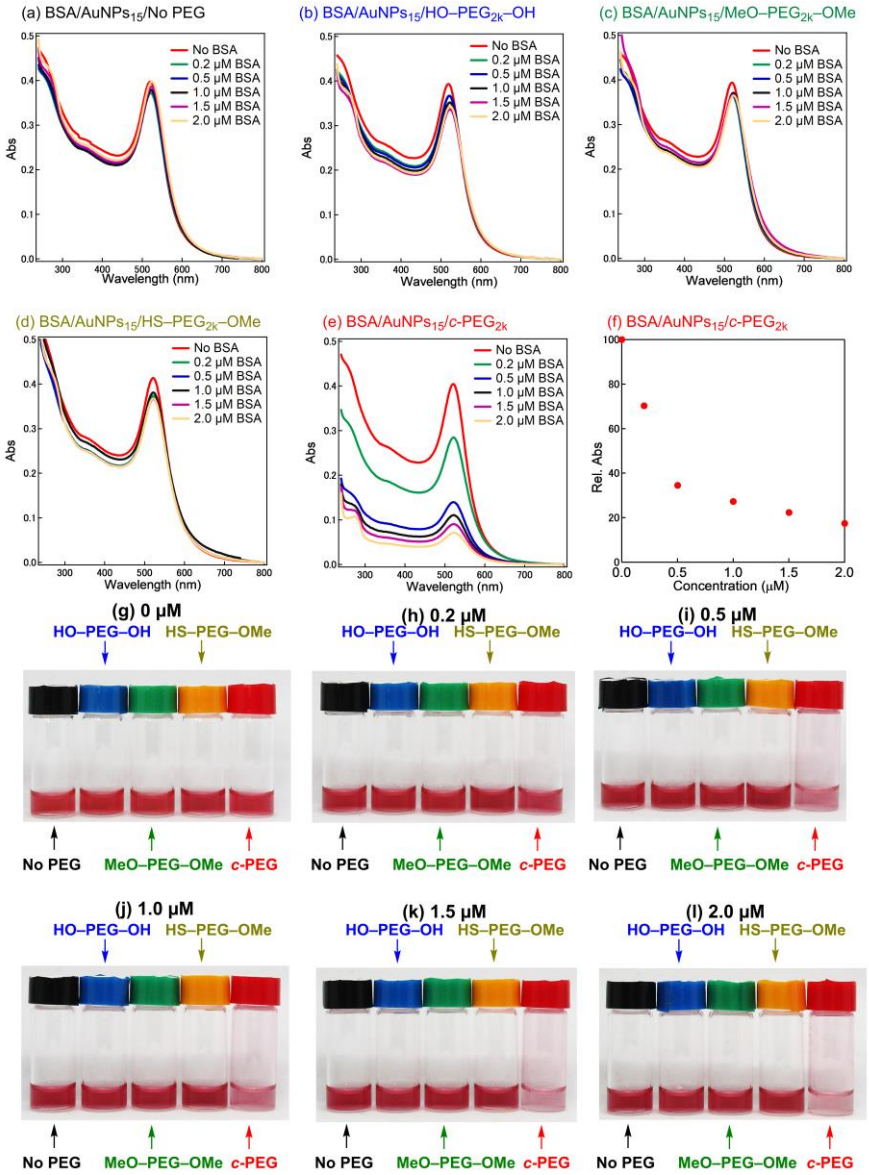

Figure 3.8. BSA's concentration-dependent absorption. UV–Vis spectra and photographs of mixtures of BSA (0–2.0 μM) and $AuNPs_{15}$ (0.045 mg/mL) with or without various PEG (0.15 wt%). (a) BSA/$AuNPs_{15}$/No PEG, (b) BSA/$AuNPs_{15}$/HO–PEG_{2k}–OH, (c) BSA/$AuNPs_{15}$/MeO–PEG_{2k}–OMe, (d) BSA/$AuNPs_{15}$/HS–PEG_{2k}–OMe, and (e) BSA/$AuNPs_{15}$/*c*-PEG_{2k}. (f) Rel. Abs versus concentration of BSA for BSA/$AuNPs_{15}$/*c*-PEG_{2k}. Pictures of BSA/$AuNPs_{15}$/PEG with a BSA concentration of (g) 0, (h) 0.2, (i) 0.5, (j) 1.0, (k) 1.5, and (l) 2.0 μM.

3.3.4 AuNPs' Concentration Dependence. Furthermore, quenching of the absorption and fluorescence depending on the concentration of AuNPs was evaluated. Thus, BSA was added into $AuNPs_{15}$/No PEG, $AuNPs_{15}$/HO–PEG_{2k}–OH, $AuNPs_{15}$/MeO–PEG_{2k}–OMe, $AuNPs_{15}$/HS–PEG_{2k}–OMe, or $AuNPs_{15}$/*c*-PEG_{2k}, where the concentrations of BSA, $AuNPs_{15}$, and PEG were 2.0 μM, 0.005–0.045 mg/mL, and 0.15 wt%, respectively. The mixture was stirred for 2 h at 25 °C, resulting in a different spectral change shown in Figures 3.9 and 3.9 based on the concentration of AuNPs and the topology of PEG. Although an increase in the absorption was seen in all the specimens by increasing the concentration of $AuNPs_{15}$ (Figure 3.9), BSA/$AuNPs_{15}$/*c*-PEG_{2k} exhibited a suppressed absorption in all the concentrations (Figure 3.9e). On the other hand, fluorescence spectroscopy showed that the magnitude in the decreasing intensity in BSA/$AuNPs_{15}$/*c*-PEG_{2k} (Figure 3.10e) was smaller upon increasing the AuNPs concentration compared to the other specimens with and without linear PEG (Figure 3.10). The result of the less reduced fluorescence intensity suggests the presence of a larger number of free BSA molecules in BSA/$AuNP_{15}$/*c*-PEG_{2k} compared to the others.

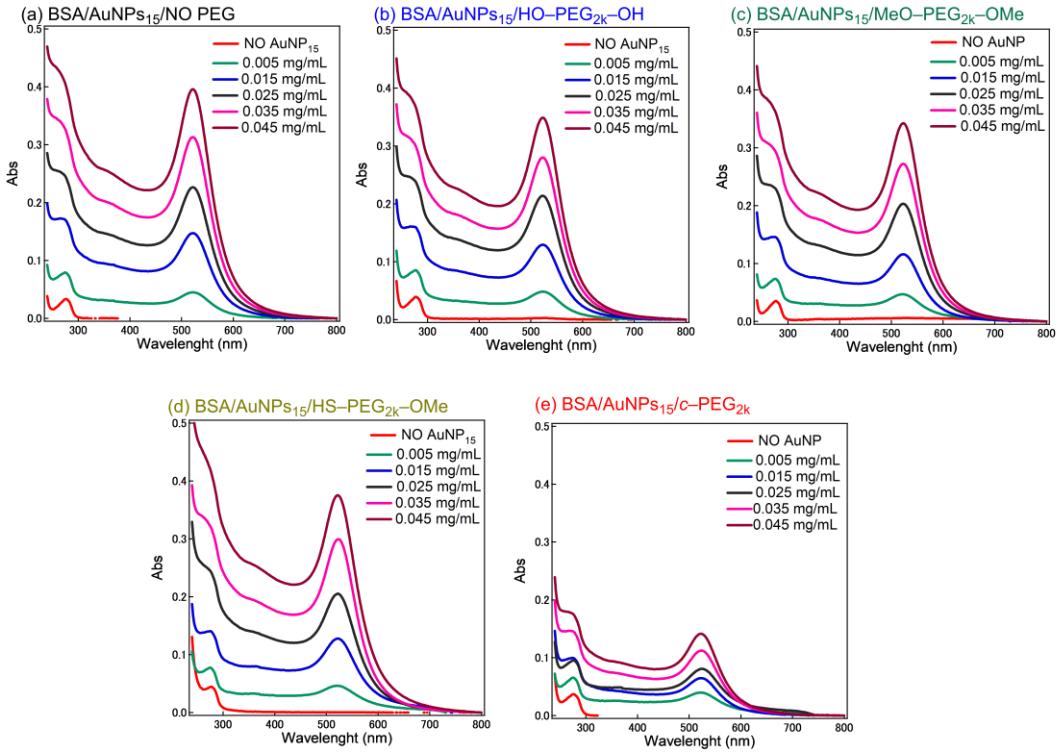

Figure 3.9 AuNPs' concentration-dependent absorption. UV–Vis spectra of mixtures of BSA (2.0 μM) and $AuNPs_{15}$ (0.005–0.045 mg/mL) with or without various PEG (0.15 wt%). (a) BSA/$AuNPs_{15}$/No PEG, (b) BSA/$AuNPs_{15}$/HO–PEG_{2k}–OH, (c) BSA/$AuNPs_{15}$/MeO–PEG_{2k}–OMe, (d) BSA/$AuNPs_{15}$/HS–PEG_{2k}–OMe, and (e) BSA/$AuNPs_{15}$/*c*-PEG_{2k}.

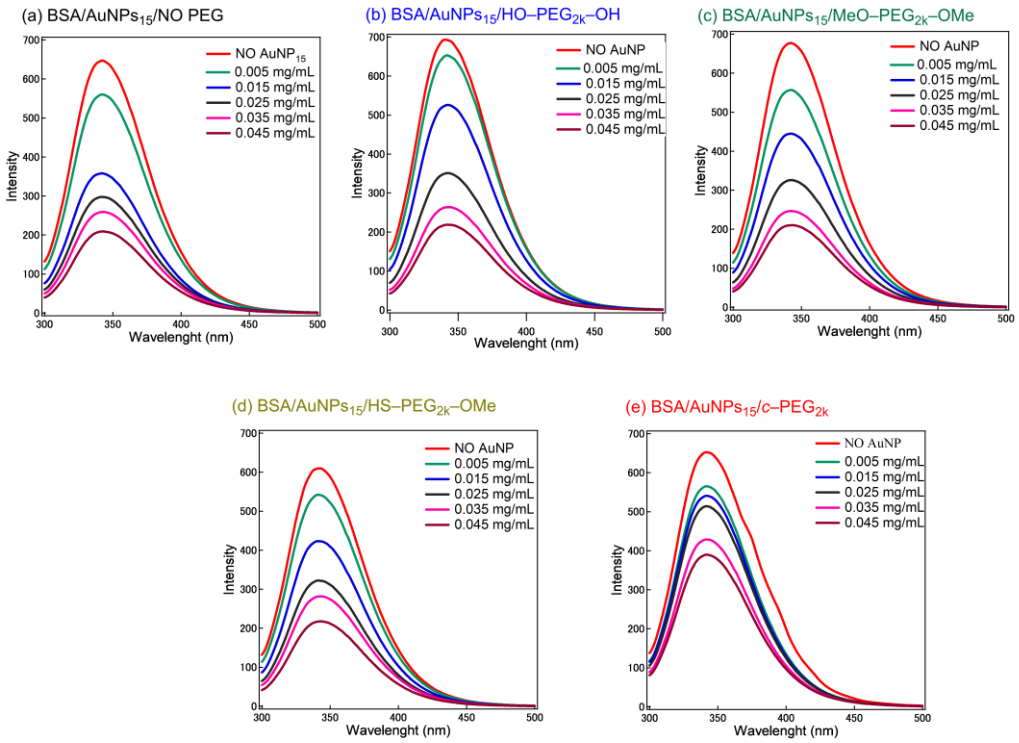

Figure 3.10 AuNPs' concentration-dependent fluorescence. Fluorescence spectra of mixtures of BSA (2.0 μM) and $AuNPs_{15}$ (0.005–0.045 mg/mL) with or without various PEG (0.15 wt%). (a) BSA/$AuNPs_{15}$/No PEG, (b) BSA/$AuNPs_{15}$/HO–PEG_{2k}–OH, (c) BSA/$AuNPs_{15}$/MeO–PEG_{2k}–OMe, (d) BSA/$AuNPs_{15}$/HS–PEG_{2k}–OMe, and (e) BSA/$AuNPs_{15}$/*c*-PEG_{2k}.

3.3.5AuNPs' Size Dependence. The size effect of AuNPs was also investigated by using BSA (2.0 μM) against AuNPs with a size of 10, 15, 20, 30, 40, and 50 nm (0.045 mg/mL) at a *c*-PEG concentration of 0.15 wt% (Figure 3.11). The result shows a general trend of a better sensing ability of AuNP with smaller sizes in the presence of *c*-PEG$_{2k}$. This can be explained by an increase in the surface area with reduction in particle sizes, leading to accommodation of a larger number of BSA molecules around AuNPs.[37]

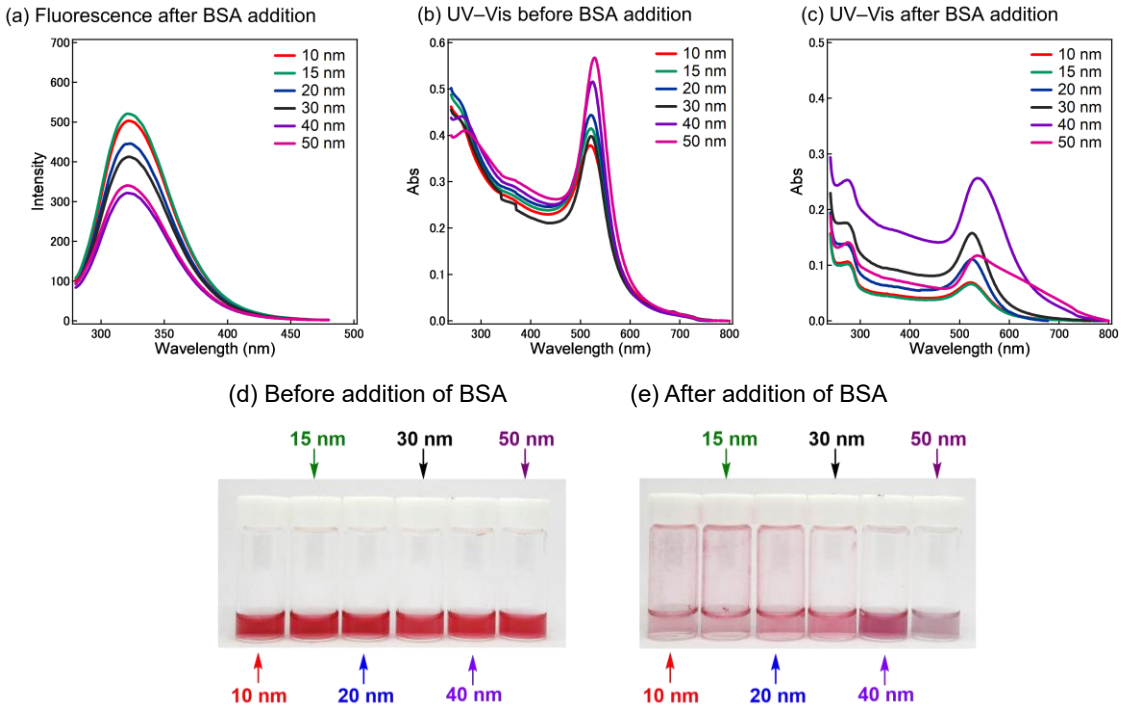

Figure 3.11. AuNPs' size dependence (10, 15, 20, 30, 40, and 50 nm) for mixtures of BSA (2.0 μM), AuNPs (0.045 mg/mL), and *c*-PEG$_{2k}$ (0.15 wt%). (a) Fluorescence spectra of AuNPs/*c*-PEG$_{2k}$ after adding BSA. UV–Vis spectra of AuNPs/*c*-PEG$_{2k}$ (b) before and (c) after adding BSA. Photographs of AuNPs/*c*-PEG$_{2k}$ (d) before and (e) after adding BSA.

3.3.6 *c*-PEG's Concentration Dependence. The concentration of PEG was increased to 0.25 wt% with BSA (2.0 μM) and $AuNPs_{15}$ (0.045 mg/mL), and the results are shown in Figure 12. A significant change was seen evident in the appearance and absorption spectra of BSA/$AuNPs_{15}$/*c*-PEG. Thus, less color change or precipitation was observed for the specimen with 0.25 wt% of *c*-PEG unlike that of 0.15 wt% (Figure 3.12b). Moreover, the absorption intensity of 0.25 wt% of *c*-PEG was substantially higher than that of 0.15 wt% (Figure 3.12a). This seems to be counterintuitive, however, the increase in the *c*-PEG concentration likely leads to saturation of both BSA and AuNPs surfaces with *c*-PEG. Thereby, the competitive interactions between BSA, AuNPs, and *c*-PEG were relieved and tend not to bind to each other. In this regard, *c*-PEG's ability in recognizing BSA is concentration dependent.

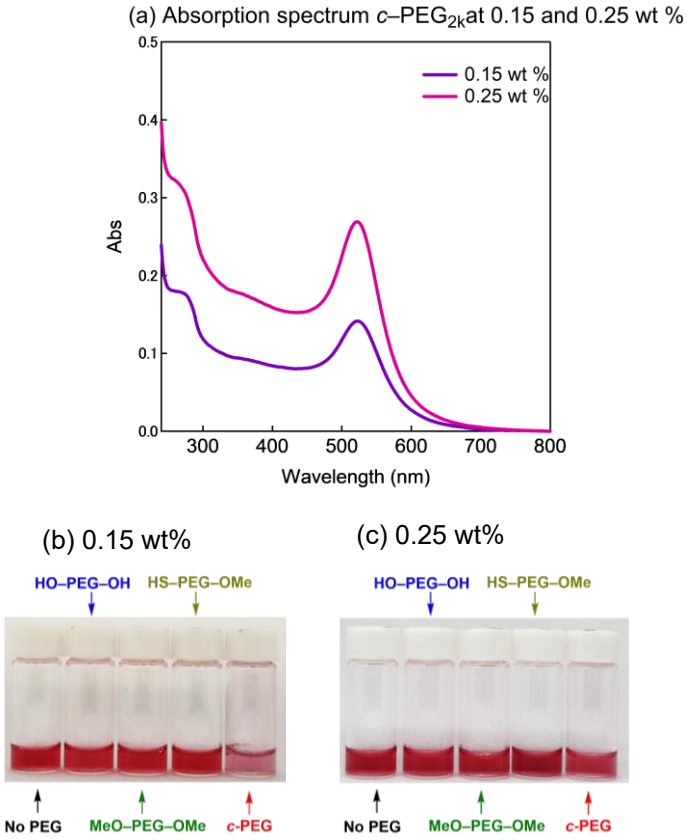

Figure 3.12 *c*-PEGs' concentration dependence. (a) UV–Vis spectra of mixtures

3.4 CONCLUSIONS

My research has shown the unique sensitivity of *c*-PEG to BSA. Moreover, in the presence of AuNPs, a colorimetric change was clearly observed. The interaction of *c*-PEG arose from the topology and was not attainable by the linear counterparts. The concentration effect of each of BSA, AuNPs, and *c*-PEG was also evident as well as the incubation time for the interacting properties. This research would give an insight into a new topology effect of *c*-PEG.

3.5 REFERENCES

1. Matyjaszewski, K.; Xia, J. *Chem. Rev.* **2001,** *101*, 2921-2990.

2. Haque, F. M.; Grayson, S. M. *Nat. Chem.* **2020**, 433-444.

3. Williams,R. J.; Dove, A. P.; O'Reilly, R. K. *Polym. Chem.* **2015,** *6*, 2998-3008.

4. Kricheldorf, H. R. *J. Polym. Sci. A Polym. Chem.* **2010,** *48*, 251-284.

5. Yamamoto, T.; Tezuka, Y. *Polym. Chem.* **2011,** *2*, 1930-1941.

6. Yamamoto, T.; Tezuka, Y. *Soft Matter* **2015,** *11*, 7458-7468.

7. Jia, Z.; Monteiro, M. J. *J. Polym. Sci., Part A: Polym. Chem.* **2012,** *50*, 2085-2097.

8. Cortez, M. A.; Godbey, W. T.; Fang, Y. L.; Payne, M. E.; Cafferty, B. J.; Kosakowska, K. A.; Grayson, S. M. *J. Am. Chem. Soc.* **2015,** *137*, 6541-6549.

9. Nasongkla, N.; Chen, B.; Macaraeg, N.; Fox, M. E.; Fréchet, J. M. J.; Szoka, F. C. *J. Am. Chem. Soc.* **2009,** *131*, 3842-3843.

10. Wan, X. J.; Liu, T.; Liu, S. Y. *Biomacromolecules* **2011,** *12*, 1146-1154.

11. Gupta, A. K.; Gupta, M. *Biomaterials* **2005,** *26*, 3995-4021

12. Harris, J. M.; Martin, N. E.; Modi, M.. *Clin. Pharmacokinet.* **2001,** *40*, 539-551.

13. Wang, Y.; Quinsaat, J. E. Q.; Ono, T.; Maeki, M.; Tokeshi, M.; Isono, T.; Tajima, K.; Satoh, T.; Sato, S.; Miura, Y.; Yamamoto, T. *Nat. Commun.* **2020,** *11*, 6089.

14. Shukla, R.; Bansal, V.; Chaudhary, M.; Basu, A.; Bhonde, R. R.; Sastry, M. *Langmuir* **2005,** *21*, 10644-10654.

15. Boisselier, E.; Astruc, D. *Chem. Soc. Rev.* **2009,** *38*, 1759-1782.

16. Svard, A.; Neilands, J.; Palm, E.; Svensater, G.; Bengtsson, T.; Aili, D. *ACS Appl. Nano Mater.* **2020,** *3* , 9822-9830.

17. Hu, S. Q.; Huang, P. J. J.; Wang, J. X.; Liu, J. W. *Anal. Biochem.* **2020,** *92*, 13354-13360.

18. Scari, G.; Porta, F.; Fascio, U.; Avvakumova, S.; Dal Santo, V.; De Simone, M.; Saviano, M.; Leone, M.; Del Gatto, A.; Pedone, C.; Zaccaro, L. *Bioconjugate Chem.* **2012,** *23*, 340-349.

19. Wang, G. K.; Papasani, M. R.; Cheguru, P.; Hrdlicka, P. J.; Hill, R. A *Nanomed.: Nanotechnol. Biol. Med.* **2012,** *8* , 822-832.

20. Aslan, K.; Perez-Luna, V. H. *J. Fluoresc.* **2004,** *14*, 401-405.

21. Elghanian, R.; Storhoff, J. J.; Mucic, R. C.; Letsinger, R. L.; Mirkin, C. A. *Science* **1997,** *277*, 1078-1081.

22. Dubertret, B.; Calame, M.; Libchaber, A. J. *Nat. Biotechnol.* **2001,** *19*, 365-370.

23. Maxwell, D. J.; Taylor, J. R.; Nie, S. M. *J. Am. Chem. Soc.* **2002,** *124*, 9606-9612.

24. Kim, C. K.; Kalluru, R. R.; Singh, J. P.; Fortner, A.; Griffin, J.; Darbha, G. K.; Ray, P. C. *Nanotechnol.* **2006,** *17*, 3085-3093.

25. Zhang, G.; Yang, Z.; Lu, W.; Zhang, R.; Huang, Q.; Tian, M.; Li, L.; Liang, D.; Li, C. *Biomater.* **2009,** *30*, 1928-1936.

26. Du, Y.; Jin, J.; Liang, H.; Jiang, W. *Langmuir* **2019,** *35*, 8316-8324.

27. Morgese, G.; Shaghasemi, B. S.; Causin, V.; Zenobi-Wong, M.; Ramakrishna, S. N.; Reimhult, E.; Benetti, E. M. *Angew. Chem., Int. Ed.* **2017,** *56*, 4507-4511.

28. Oziri O. J.; Wang, Y.; Watanabe, T.; Uno, S.; Maeki, M.; Tokeshi, M.; Isono, T.; Tajima, K.; Satoh, T.; Sato, S.; Miura, Y.; Yamamoto, T. *Nanoscale Adv*. **2021,** *3*, in press. DOI: 10.1039/D1NA00720C

29. Muraoka, T.; Adachi, K.; Ui, M.; Kawasaki, S.; Sadhukhan, N.; Obara, H.; Tochio, H.; Shirakawa, M.; Kinbara, K. *Angew. Chem. Int., Ed.* **2013,** *52*, 2430-2434.

30. Tkachenko, A. G.; Xie, H.; Coleman, D.; Glomm, W.; Ryan, J.; Anderson, M. F.; Franzen, S.; Feldheim, D. L. *J. Am. Chem. Soc.* **2003,** *125* , 4700-4701.

31. Jahanban-Esfahlan, A.; Ostadrahimi, A.; Jahanban-Esfahlan, R.; Roufegarinejad, L.; Tabibiazar, M.; Amarowicz, R. *Int J. Biol. Macromol.* **2019,** *138*, 602-617.

32. Steinhardt, J.; Krijn, J.; Leidy, J. G. *Biochem* **1971,** *10*, 4005-4015.

33. Cheng, Z. J.; Liu, R.; Jiang, X. H. *Spectrochim. Acta A Mol. Biomol. Spectrosc.* **2013,** *115*, 92-105.

34. Gelamo, E. L.; Silva, C.; Imasato, H.; Tabak, M. *Biochim Biophys Acta* **2002,** *1594*, 84-99.

35. Lacerda, S. H. D.; Park, J. J.; Meuse, C.; Pristinski, D.; Becker, M. L.; Karim, A.; Douglas, J. F. *ACS Nano* **2010,** *4*, 365-379.

36. Naveenraj, S.; Anandan, S.; Kathiravan, A.; Renganathan, R.; Ashokkumar, M. *J. Pharm. Biomed. Anal.* **2010,** *53*, 804-810.

37. Pramanik, S.; Banerjee, P.; Sarkar, A.; Bhattacharya, S. C. *J. Lumin.* **2008,** *128*, 1969-1974.

38. Kathiravan, A.; Paramaguru, G.; Renganathan, R. *J. Mol. Struct.* **2009,** *934*, 129-137.

39. Kathiravan, A.; Anandan, S.; Renganathan, R. I. *Colloids Surf. A Physicochem. Eng. Asp.* **2009,** *333*, 91-95.

40. Brewer, S. H.; Glomm, W. R.; Johnson, M. C.; Knag, M. K.; Franzen, S. *Langmuir* **2005,** *21*, 9303-9307.

41. Wang, J.; Zhao, J.; Ma, G. *Nano-Struct. Nano-Objects* **2019,** *19*, 100349.

42. Mradula; Raj, R.; Devi, S.; Mishra, S. *Anal. Sci,* **2020,** *36*, 799-806.

43. Wang, G. K.; Yan, C. L.; Gao, S. Y.; Liu, Y. F. *Mater. Sci. Eng. C.* **2019,** *103*, 109856.

44. Ravikumar, S.; Sreekanth, T. V. M.; Eom, I. Y. *J. Nanosci. Nanotechnol.* **2015,** *15*, 9617-9623.

45. Patel, A.; Cosgrove, T.; Semlyen, J. A. *Polymer* **1991,** *32*, 1313-1317.

46. Wang, Y.; Qin, W.; Qiu, D. *Langmuir* **2014,** *30*, 5170-5175.

47. van Lent, B.; Scheutjens, J.; Cosgrove, T. *Macromolecules* **1987,** *20*, 366-370.

48. Stratouras, G. K.; Kosmas, M. K. *Macromolecules* **1991,** *24*, 6754-6758.

49. Stratouras, G.; Kosmas, M. *Macromolecules* **1992,** *25*, 3307-3308.

50. Zhang, L.; Xia, A.; Xu, Y. *Eur. Polym. J.* **2000,** *36*, 847-850.

51. Sikorski, A. *Macromol. Theory Simul.* **2001,** *10*, 38-45.

Chapter 4
conclusion

In this dissertation, the author had successfully documented *c*-PEG interactions with silver nanoparticles (AgNPs) and bovine serum albumin (BSA). This novel interaction is assumed to be based on the entropic penalty on *c*-PEG because of it lacked termini. In addition, the author found an interesting novel method of physisorption as *c*-PEG was not chemically functionalized to AgNPs or BSA to establish it interaction. Physisorption is simply the mixing of *c*-PEG with AgNPs or BSA. The resultant effect of the interaction enhanced the dispersion stability of AgNPs against physiological condition (150 mM NaCl), high temperature and white light. On the other hand, a complex formation between *c*-PEG and BSA was reported which further lead to sensitivity towards BSA and resultant aggregation of AuNPs.

A summary of the important achievements and findings presented in this study as follows.

Chapter two: The author successfully synthesized *c*-PEG from its prepolymer by Williamson etherification method. Methyl terminated PEG was also synthesized. All PEGs were purified and characterized. Thereafter, *c*-PEG and other linear PEGs were subjected to conditions of physiological condition (150 mM NaCl), high temperature and white light. Biological properties of physiosorbed PEGs were evaluated as well. This study revealed enhanced dispersion stability of AgNPs by *c*-PEG and further maintained the biological properties of AgNPs. On the other hand, stability was not obtainable neither was the biological activity of

AgNPs by linear PEGs.

Chapter 3: The author presented a unique kind of interaction seen between *c*-PEG and BSA. First, PEGs were synthesized as state before was added to phosphate buffer solution containing BSA. It is notable that a complex was formed between *c*-PEG and BSA which was significantly different form other linear PEGs. Sequel to my previous report of strong interaction between *c*-PEG and AuNPs or AgNPs, and *c*-PEG and BSA, AuNPs was further introduced to *c*-PEG/BSA system thereby forming *c*-PEG/AuNPs/BSA system. i.e three elements in one system. A series of investigation shows sensitivity of *c*-PEG towards BSA and subsequent aggregation of AuNPs in *c*-PEG/AuNPs/BSA system. *c*-PEG could be said to be the major driving force for this interaction.

In conclusion, the author established, a new possible application of c-PEG in nano biotechnology. Over the years, applications of nanomaterial and biomolecules have encountered several drawbacks owing to their instabilities, biocompatibility, aggregation in various application conditions. This present study has provided an approach to solving these limitations by simply physisorption of *c*-PEG. This study has paved way to applications of *c*-PEG in biomedicine.